Modelling and Optimisation of Free Running Axial Turbine for Flow Measurements

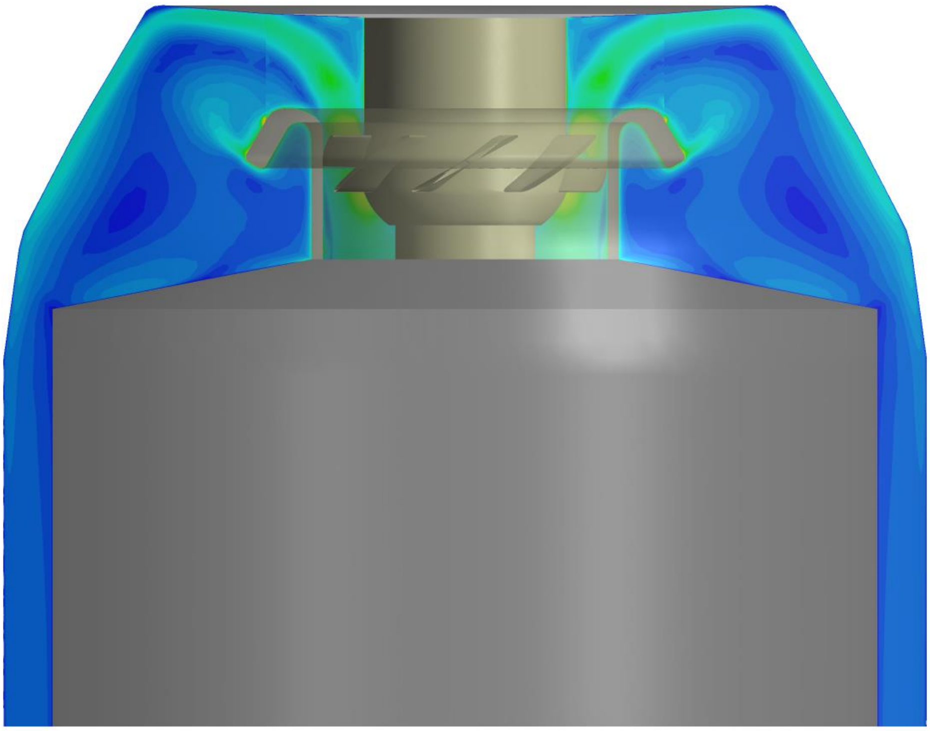

TEPE4-1000: Daniel Villamar Cabezas and Nick Høy Hansen

Master's Thesis Project – Thermal Energy and Process Engineering.

June 2017

Department of Energy Technology

AALBORG UNIVERSITY
DENMARK

Board of Studies of Energy

Title:	Modelling and Optimisation of Free Running Axial Turbine for Flow Measurements
Semester:	4^{th} Semester, Spring 2017
Semester theme:	Master´s Thesis
Project period:	01.02.2017 to 01.06.2017
ECTS:	30
Supervisors:	Lasse Aistrup Rosendahl and Henrik Sørensen
Project group:	TEPE4-1000

Daniel Villamar Cabezas

Nick Høy Hansen

SYNOPSIS:
This project focuses on the creation of a CFD model to simulate the behaviour of a turbine flow meter designed by *Grundfos* to be used in a CR 10 pump. The model is validated with experimental data and used as a tool to optimize the turbine geometry. Additionally, a sensitivity analysis is conducted to determine the robustness of the model to certain parameters variations. The main modification performed on the geometry is a radical reduction of the turbine solidity by decreasing the blade number from 8 to 3. The optimised prototype provided with 3 blades is 3D printed and tested to validate the improvements and to analyse the accuracy of the model. This model exhibits a decrease in head loss across the turbine, but generates a flow separation at the blades. Then, a modification of the blade angle is attempted, showing promising results in the model.

Submission form:	Electronic submission
Pages, total:	92
Supplements:	Data (submitted together with report in Zip-folder)

By signing this document, each member of the group confirms that all group members have participated in the project work, and thereby all members are collectively liable for the contents of the report. Furthermore, all group members confirm that the report does not include plagiarism.

Executive Summary

Modelling of the Rotational Speed

To contribute to the evolution of the turbomachinery industry, this study presents a CFD model capable of predicting the rotational speed and the behaviour of a turbine flow meter (TFM). Earlier studies have mainly focused on the behaviour of the TFM [Zoheir et al., 2014]. For this classical approach the rotational speed was determined experimentally. This new method overcomes that necessity, decreasing the time needed to optimize a TFM design. The main idea behind the simulation is that for each flow rate a constant rotational speed is obtained. Thus, the torques on the turbine comply with Equation 1.

$$\begin{aligned}\textbf{Fluid driving torque} = {} & \textbf{rotor blade surfaces fluid drag torque} + \textbf{rotor hub} \\ & \textbf{and tip clearance fluid drag torque} + \textbf{rotation sensor} \\ & \textbf{drag torque} + \textbf{bearing friction retarding torque}\end{aligned} \tag{1}$$

All the torques from Equation 1 can be found with the CFD model except the bearing friction, for which a separate model was created. By coupling the two models the rotational speed can be obtained.

Validity and Sensitivity of the Model

The coupled model generally proved successful to describe the rotational speed of the TFM but with an error increasing with the flow rate. To investigate the robustness of the model a sensitivity analysis was made using the key parameters affecting the model.
To investigate the model capability to predict the rotational speed, the simulated results including variations from the sensitivity analysis, have been compared to experiments. This comparison is presented in Figure 1.

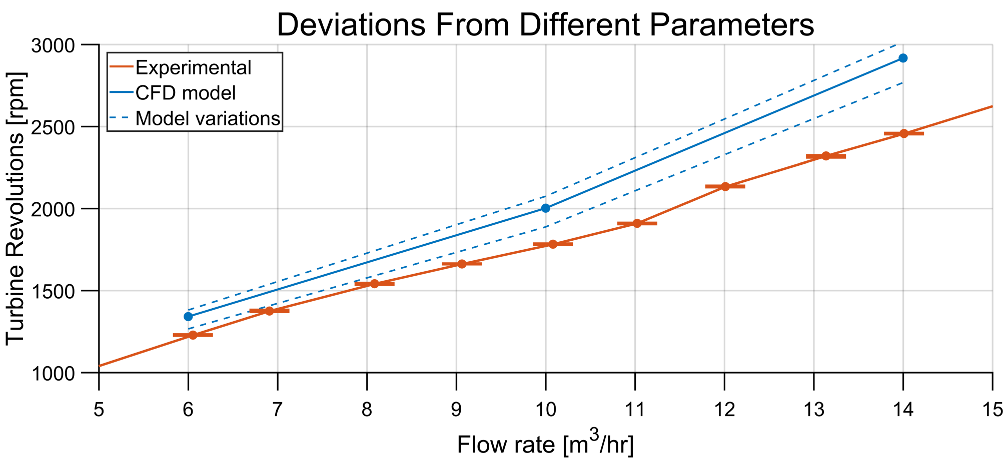

Figure 1. Comparison between the simulated and experimental results.

Figure 1 shows that the model is able to predict the rotational speed, with an error that increasing at higher flow rates.

Geometrical Changes

After the validation of the model, an optimisation of the existing TFM was performed. Simulations with different blade numbers revealed that a smaller number of blades decreases the head loss in the system and a 3 bladed turbine was found the most efficient design. To verify the results, 3 bladed prototype was 3D printed, tested, and compared in performance with the 8 bladed turbine. This comparison is presented in Figure 2.

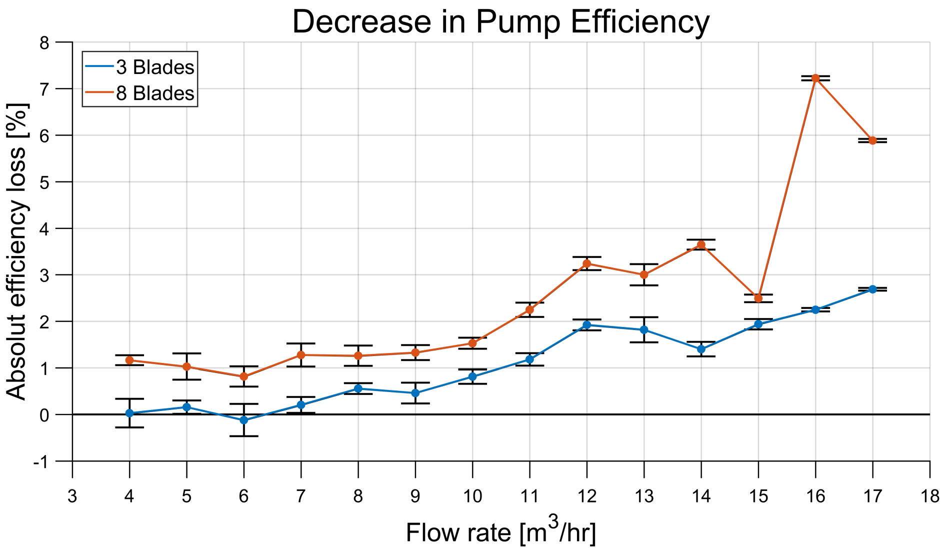

Figure 2. Efficiency drop generated by the 8 and 3 bladed turbine, including the standard deviation generated by the experimental results.

Looking at the overall range from 4 to 17 m^3/hr the 3 bladed turbine have decreased the efficiency loss with an average of 1.49% compared to the 8 bladed, which corresponds to 57.7% of the efficiency loss generated by the 8 bladed turbine.

Conclusions

An extension of the existing modelling framework for turbine flow meters was defined. A way of predicting the rotational speed was developed and the results were validated by experimental work. The model has proven to be a valid design tool to optimize the TFM geometry.

Future work should focus on adjusting different turbine parameters to optimize the angle of attack. Furthermore, an extensive investigation of the flow meter's applicabilities in the whole range of CR pumps should be made.

Preface

This report was carried out by group TEPE4-1000 on 10th semester, at the Department of Energy Technology, Aalborg University.

This project investigates the possibility of performing a Computational Fluid Dynamics (CFD) flow meter model. This study was conducted in collaboration with *Grundfos A/S* as a part of the master's thesis on Energy Department at Aalborg University.

The main purpose of this project is to generate an accurate CFD model able to predict the rotational speed of the flow meter and the pressure drop generated across the flow meter. Additionally, a parametric study have been performed in order to determine the influence on the rotational speed. Furthermore, experimental work is conducted in laboratories located at *Grundfos*

For understanding of the report, basic knowledge of CFD and mechanics is prescribed. In this report the following software packages have been used: *ANSYS CFX*, *ANSYS meshing*, *CATIA V*5 and *Matlab R*2015

Readers Guide

In the start of the report, the nomenclature is included. The nomenclature is listed with the latin and then the Greek alphabet, followed by a list of subcribts and abbreviations.

Through the report, the Harvard method is used as reference style. The Harvard method presents the references as [Author, year, page] and the sources can be found in the end of the report under List of Refereces or as pdf files on the zip file handed in. The list of references is followed by lists of figures and tables present in the report.

At the beginning of the thesis, the investigation of the turbine flow meter used data showing a large deviation in head loss after a flow rate of 12 m^3/hr. These data was proven wrong with new experiments conducted at *Grundfos*. The mistake was found late in the project phase and some of the investigations still maintain the old focus of decreasing the large head losses reported in the old data.

Acknowledgements

Acknowledgements are addressed to supervisors: Professor Lasse Rosendahl (AAU), Associate Professor Henrik Sørensen (AAU), Development Engineer Tobias Randers Olesen (Grundfos) and Internal Consultant Peter Elvekjær (Grundfos), and Søren Kjelden Development Engineer (Grundfos) for helpful supervision and advise.

Contents

Nomenclature

Symbol	**Units**	**Description**
A	$[m^2]$	Area
b	[m]	Axial blade length
AR	$[-]$	Aspect ratio
c	$[m]$	Chord length
c_Θ	$[m/s]$	Tangential velocity
C_D	$[-]$	Drag coefficient
C_F	$[-]$	Lift coefficient
d	$[m]$	Distance between blades
e	$[m]$	clearance space
F	$[N]$	Force
F_c	$[-]$	Friction coefficient
h	$[m]$	Distance between interacting surfaces
L	$[m]$	Length
m	$[kg]$	Mass
$\dot{m}$	$[kg/s]$	Mass flow
N_T	$[N \cdot m]$	Overall retarding torque
n	$[-]$	Number of blades
P	$[Pa]$	Pressure
P_0	$[Pa]$	Stagnation pressure
Q	$[m^3/hr]$	Volumetric flow
r	$[m]$	Radial distance
r_d	$[m]$	Difference between inner and outer blade radius
S	$[-]$	Suction
s	$[m]$	Blade pitch
T_d	$[N \cdot m]$	Driving torque
U	$[m/s]$	Blade speed
K	$[-]$	Meter factor
Y	$[Kg/s^2]$	Tangential blade loading

Greek symbol	Units	Description
α	$[Deg]$	Angle of attack
β	$[Deg]$	Blade angle
γ	$[Deg]$	Flow angle
ΔW	$[J]$	Work variation
θ	$[Deg]$	Swirl or exit angle
μ	$[Pa \cdot s]$	Dynamic viscosity
ρ	$[kg/m^3]$	Fluid density
τ_A	$[kg \cdot m^2/s]$	Angular momentum
τ_s	$[Pa]$	Shear stress
ϕ	$[Deg]$	Angle between real and relative flow
Ψ_T	$[-]$	Ratio between ideal and real tangential blade loading
ω	$[rad/s]$	Angular velocity

Subindex	Description
1	Initial conditions
2	Final conditions
i	Ideal conditions
D	Drag
in	Inlet conditions
L	Lift
out	Outlet conditions
rel	Relative
t	Turbine
x	Axial direction
y	Radial direction

Abbreviations	Description
CFD	Computational Fluid Dynamics
$NACA$	National Advisory Committee for Aeronautics
SST	Shear Stress Transport
TFM	Turbine Flow Meter

1 Introduction

The pump industry is constantly evolving and innovation is vital for companies that want to maintain their leadership. Companies like *Grundfos A/S* are committed with the constant product innovation as a main priority. This is demonstrated in products like the CR 10-4 multi-stage centrifugal pump which is being complemented with a turbine flow meter. By including this device in the pump, real time data would be generated and the performance of the pump could be adjusted according to the process requirements, thereby enhancing the efficiency. A pump capable of receiving instructions from a central module and send feedback from the process will contribute to the automation of the process and allow remote controlled operations. All this characteristics are required in the today's industry. Moreover, the future tendencies aim for smart equipment capable of self-controlled operations [Kagermann et al., 2013], and the incorporated sensors are the first step in that direction.

Different sensors could be used to fulfil the requirement of a flow meter for the CR 10-4 pump. Nevertheless, important characteristics like size, cost, precision, and adaptability to the pump design have to be considered.

A first option is the differential pressure flow meter which employs a flow restriction to force a pressure drop. This pressure variation is measured in order to calculate the flow rate. The accuracy of this apparatus is around $\pm 2\%$ [Thorn, 1998].
If a higher accuracy is required, high precision devices like positive displacement meters could be used. However, this type of meter is less compact compared to other flow meters. Other metering devices like pitot tube or velocity flow meters could also be used, but they require a flow with a fully developed profile, thus a certain pipe length is required prior for the measuring device.
More complex flow meters are also available, for example the calorific or the Doppler flow meters, but their higher complexity is usually accompanied by an increase in size or price. Another type of flow meter, that is the one selected by *Grundfos* for this application, is the turbine flow meter (TFM). The size of the TFM makes it optimal for being incorporated into the existing pump casing. Moreover, only a single sensor is required to determine the flow, combining simplicity and compactness. Additionally, since the pumped fluid is water, no expensive materials are required to build the turbine. Furthermore, the accuracy provided by a TFM ranges between ± 0.1 and $\pm 0.5\%$ [Baker, 1991], with a measurements repeatability of $\pm 0.05\%$ for small turbines (diameters less than 50 mm) and even more precise for bigger turbines [Baker, 1991]. The characteristics enlisted are for high performance metering devices. It is expected that the TFM used in this application exhibits a lower performance due to design restrictions and non optimal operation conditions. On the basis of the given information the TFM has be chosen as the best suitable solution for this specific case.

The turbine flow meter has been used in the industry for more than a century. Its invention is attributed to Reinhard Woltman and dates back to 1790. The original prototype was built for water flow and its working principle is founded on a linear relation between the turbine angular rotation and the flow rate. This relation is maintained for a wide quantity of fluids including gases and liquid flows with kinematic viscosities as high as $10 - 4\ m^2/s$. Besides, this kind of device present high accuracy and repeatability on the readings [Wadlow, 1998]. Due to this characteristic, TFM´s are used on different industries including aeronautics, petroleum and hydraulics. An overview of this technology and its different applications is presented in [Baker, 1991] and [Baker, 1993]

Many studies on the subject have been carried out. Most of the studies include experimental and analytical methods which try to provide empirical relations to predict the behaviour of the turbine at different working conditions. A fundamental study was conducted in the 60´s by the US rocket program [Thompson and Grey, 1967]. This investigation described the behaviour of the TFM according to different parameters like: rotor design, flow characteristics and calibration/installation methods, emphasising the importance of the inlet velocity profile. The capital importance of the inlet flow for the proper behaviour of the device is also shown in [Xu, 1992a], [Stoltenkamp, 2007] and [Salami, 1984]. These studies show the effect of using different velocity profiles or considering the flow swirling in the turbine performance. The swirling could also involve some reading problems as studied in [Venkatesa, 2005].

New designs are not the only innovation of the industry, the analysis methods are evolving as well. Numerical methods complemented by experimental analysis have become a common tool to approach fluid dynamic problems. As an example, the study [Xu, 1992b] can be mentioned, it predicts the behaviour of the blade while including flow detachments on the leading edge and wake formation on the trailing edge.

Other studies uses Computational Fluid Dynamics (CFD), which is a very powerful tool to predict the behaviour of the turbine while minimizing the experimental approach. Different models using this tool appear in new researches. In [Zoheir et al., 2014] the performance of a helical turbine flow meter is predicted using CFD. Another computational study [Tegtmeier, 2015] determines the importance of viscosity in the turbine behaviour and in the calibration of the device. As a final example, the CFD tool could predict the behaviour of a TFM even for abnormal situation like a damaged blade [Hariri et al., 2015].

The variety of studies presented determine the possibility of evaluating the performance of the TFM by using computational methods, but they require experimental data as input for the system. The industry aims for faster methods to improve their equipment and a great interest has been devoted to the usage of CFD as a design tool. By using a CFD model to evaluate the different design parameters, the experimental cost can be reduced avoiding fabrication and tests of different prototypes. The experimental work will be reserved to validate the CFD model and to test the final prototype.

This project investigates the viability of producing a CFD model able to analyse different variations in the pump system without experimental boundary conditions, in order to optimize the existing turbine design. This is done by modelling and simulating the existing turbine within a CFD and a bearing friction study.

1.1 Pump and flow meter description

The following section describes the CR 10-4 pump from *Grundfos A/S* and the associated axial turbine for flow measurements. A technical overview of the pump is presented and the relevant aspects of the equipment are described. This aspects are fundamental for the generation of the computational fluid dynamic (CFD) model.

The CR 10-4 pump is a four-stage centrifugal water pump operating at a rated flow of 10 m^3/hr. The performance of the CR 10-4 pump at a speed of 2896 rpm is presented in Figure 1.1. The rated head of this pump is 31.9 m.

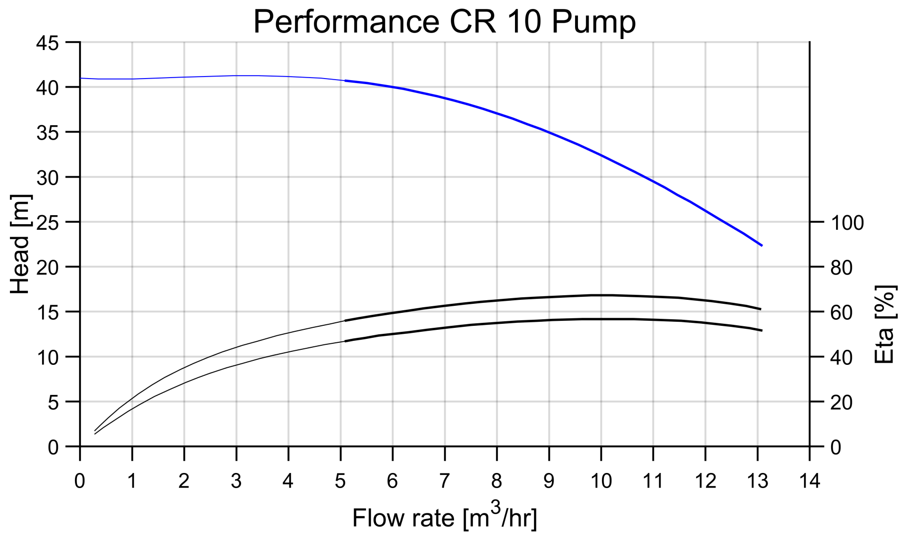

Figure 1.1. Head and efficiency vs flow for the CR 10 pump at 2896 rpm [Grundfos, 2013].

A sensor capable of determining the amount of water flowing through the pump is an important feature that would allow a better control of the machine without the need of an external measuring device. For this reason *Grundfos* studies the possibility of installing a rotational free wheel turbine that measures the pump flow. The usage of this small free wheel turbine, which has a rotational speed proportional to the amount of flow passing through it, is a compact and practical solution for flow measurements.

The location selected for the turbine is at the exit of the last stage of the pump, mounted on the pump shaft. At this place, all the flow will pass through the turbine and the magnetic sensor can be placed in one of the existing sockets of the pump lid. The placement of the turbine and the sensor can be seen in Figure 1.2. The simple installation of the flow meter without requiring any radical change in the pump is one of the major benefits of this device.

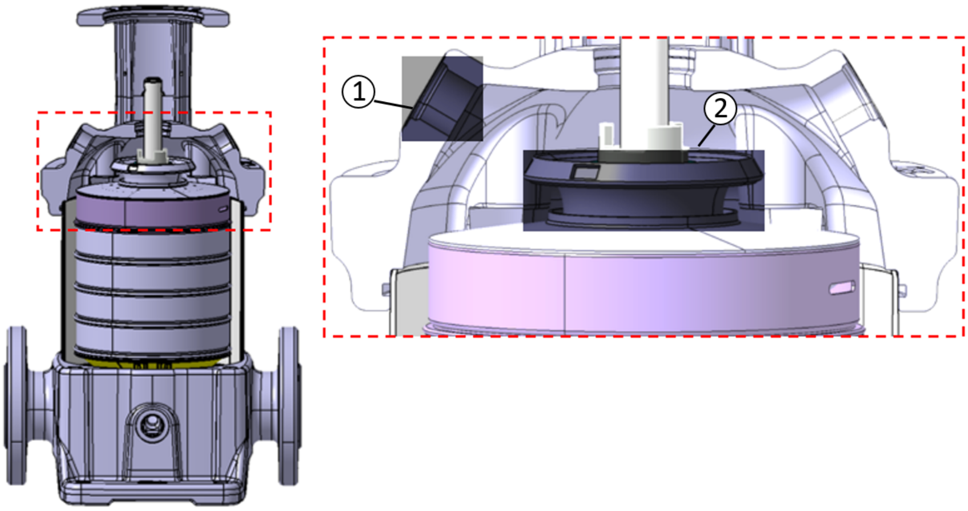

Figure 1.2. Location for the magnetic sensor (1) and the free running wheel (2) in the pump.

The turbine flow meter is designed to run in the opposite direction of the shaft, avoiding wrong measurements related to the main shaft rotation. Furthermore, magnets have been unevenly located in the turbine, as seen in Figure 1.3. This placement permits to evaluate the rotation direction and determine possible co-rotations between the shaft and the turbine.

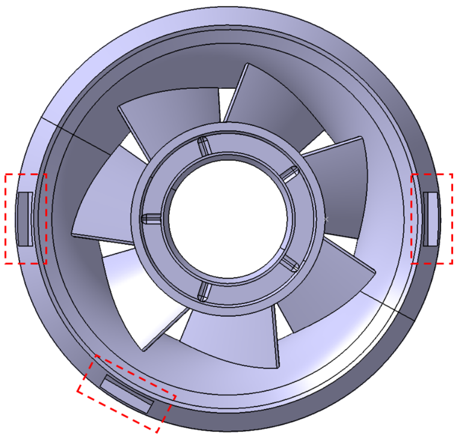

Figure 1.3. Flow meter with placement of magnets. Illustration based on [Grundfos, Blueprints, 2016].

To approach the defined problem in an efficient way a CFD model is implemented.

1.2 CFD as a designing tool

Nowadays, the method used in the industry to improve a design includes the analysis of different prototypes in laboratory tests; big facilities are devoted to this costly endeavour. As an example, the TFM design for the CR 10-4 pump can be mentioned. Its design required multiple prototypes which had underwent laboratory tests. The performance of the last tested prototype can be seen in Figure 1.4.

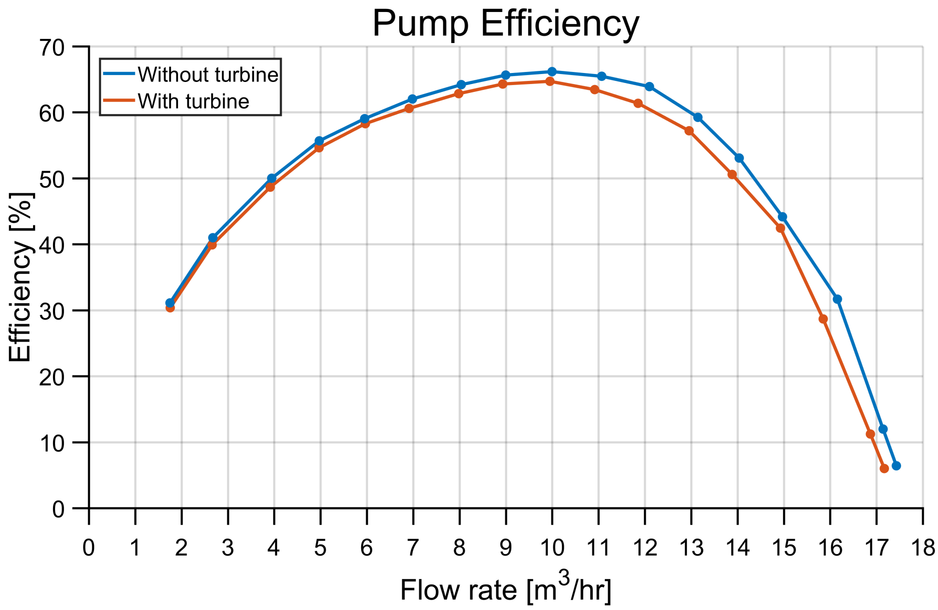

Figure 1.4. Effect of the flow meter in the pump efficiency.

The performance of the pump with and without the flow meter follows a similar tendency. At low flows the efficiency difference depicted by the curves is almost indistinguishable. At middle and high flows a bigger gap is available for improving the actual design. A CFD model capable of improving this prototype will demonstrate that a computational analysis could replace the exhaustive test approach.

In order to validate a CFD model it is only necessary to perform tests to determine the correct performance of the model and also possible deviance between the real and the simulated results. After validating the model, different analyses could be carried out only by simulations.

It has to be considered that a design based only on simulations has to rely on the designer's expertise. Parameters like machinability and wear resistance will not be revealed in a CFD analysis.

2 Problem Formulation and Statement

The main objective of this project is to determine the viability of creating a CFD model capable of mimicking the performance of a turbine flow meter subjected to divers water flows. This model will be complemented by a secondary model that provides the frictional torque on the turbine bearings. The models are used as a tool to define the important parameters affecting the TFM performance. Particular interest is allocated to the understanding of the losses generated by the turbine since an optimisation is intended on this behalf. The studied system is placed at the outlet of the last stage of a CR 10-4 centrifugal pump, manufactured by *Grundfos*. The departure point for the analysis is a flow meter prototype that has been tested by the company showing a reduction in the pump efficiency. This study tends to determine the nature of the losses produced on the turbine and use this understanding to optimise the geometry and thereby its performance. Since this equipment could be applied to the whole range of CR pumps, maintaining the relative simplicity of the measuring device is crucial for the design.

2.1 Problem Statement

This project aims to develop a model using CFD and torque calculations to predict the rotational speed and flow behaviours of a turbine flow meter. This leads to the following statement:

How can a CFD model capable of predicting the rotational speed and losses of a turbine flow meter be developed with the purpose of optimising the performance?

To accomplish this problem the following objectives are analysed:

- Investigate the thermodynamic boundaries linked with the flow meter.
- Develop a model that can simulate the flow meter at different flows.
- Develop a model to calculate the friction at the turbine bearing.
- Perform a sensitivity analysis of the factors that affect the turbine behaviour.
- Conduct flow measurements with the existing flow meter design at *Grundfos*' test facilities in order to verify the CFD model.
- Conduct flow tests with a new flow meter prototypes at *Grundfos*' test facilities in order to validate the new design.

2.2 Methodology

The first step to achieve the objectives of this study is to investigate the literature related with turbine flow meters and the existing CFD models created to simulate the turbine behaviour. The second step is to create a CFD model capable of simulating the fluid flow, complemented by a model that calculates the friction generated on the bearing. The results from this combined model is compared with experimental data in order to validate the simulated results. Then, the validated model is used as a tool to analyse divers modifications on the turbine parameters. This makes it possible to determine the turbine sensitivity to each parameter, as well as their combined effect on the turbine performance. Finally, in order to optimize the existing turbine design, simulations for different modifications on the blades are performed. An optimized design is then defined and a prototype is 3D printed and tested, to confirm the optimised results experimentally.

2.3 Project limitations

The location and the type of flow meter used are parameters stipulated by the company, thus no changes are considered in this regard. Other limitations are related to the software used for the project. The CFD software used by $Grundfos$ is ANSYS CFX and is thereby used in this project. Furthermore, ANSYS CFX produces better convergence than ANSYS Fluent when dealing with turbomachinery. The usage of the same software is vital to avoid incompatibility and also to take advantage of the expertise of $Grundfos'$ personnel. For the grid creation ANSYS Meshing is used instead of GridPro which is the software used in the company. The reason for this choice is the time required to learn the program properly. To reduce the time consumption under the construction of the CFD model, the pump prior to the turbine is not modelled. To reduce the experimental time the experiments are conducted with existing equipment at Grundfos test facilities.

3 Theoretical Background

This chapter describes the theory related to the modelling of the turbine flow meter and the understanding of its modelled behaviour. Firstly, an overview of the driving torques and the counter torques is presented, followed by an explanation of the theory used for determining the frictional torque. Afterwards, the important design parameters of the turbine flow meter are described. Finally, an overview of the CFD validation parameters is presented.

3.1 Determination of the equilibrium torque

When modelling the rotational speed of the turbine flow meter, there are numerous torques of different importance that oppose the driving torque. At steady flows, the rotor speed is assumed constant, satisfying the equilibrium stated in Equation 3.1 .

$$\begin{aligned} Fluid\ driving\ torque = {} & rotor\ blade\ surfaces\ fluid\ drag\ torque + rotor\ hub \\ & and\ tip\ clearance\ fluid\ drag\ torque + rotation\ sensor \\ & drag\ torque + bearing\ friction\ retarding\ torque \end{aligned} \tag{3.1}$$

All the torques from Equation 3.1 can be found either from a CFD or a frictional torque model. The CFD model, presented in Chapter 5, provides the driving torque from the blades and most of the counter torques. The basis for the bearing friction retarding torque calculations are investigated in the following section.

3.2 Friction torque

In this section the two resistance torques acting on the turbine bearing are considered. The first one describes a hydro lubricated surface interaction, while the second considers friction between two solid surfaces. These resistant forces will contribute to the counter torque present on the turbine.

3.2.1 Lubricated friction torque

The friction between the shaft and the hub of the turbine is responsible for one of the torques opposing the rotation of the turbine. For this surface interaction, hydrodynamic lubrication is considered. Due to the high rotational speed existing between the surfaces, a pressurized film is created avoiding direct surface contact [Shigley et al., 2006]. In this scenario, Newton´s viscous law is used to determine the torque generated by the relative movement between the shaft and the hub. As seen in Equation 3.2, the shear stress, τ_s of the fluid is proportional to the velocity change with respect to the plate distance, where the dynamic viscosity μ is the proportionality coefficient.

$$\tau_s = \mu \frac{dv}{dy} \tag{3.2}$$

Considering a Newtonian fluid, which is the case for the present analysis where water is used, the expression can be written as in Equation 3.3, where h is the distance between the surfaces.

$$\tau_s = \mu \frac{v}{h} \tag{3.3}$$

Richard Stribeck theorized about the relation between the friction coefficient and certain characteristics of the hydrodynamic lubrication of the interacting surfaces. The Stribeck curve presented in Figure 3.1 illustrated the three possible regimes that can be found depending on these characteristics.

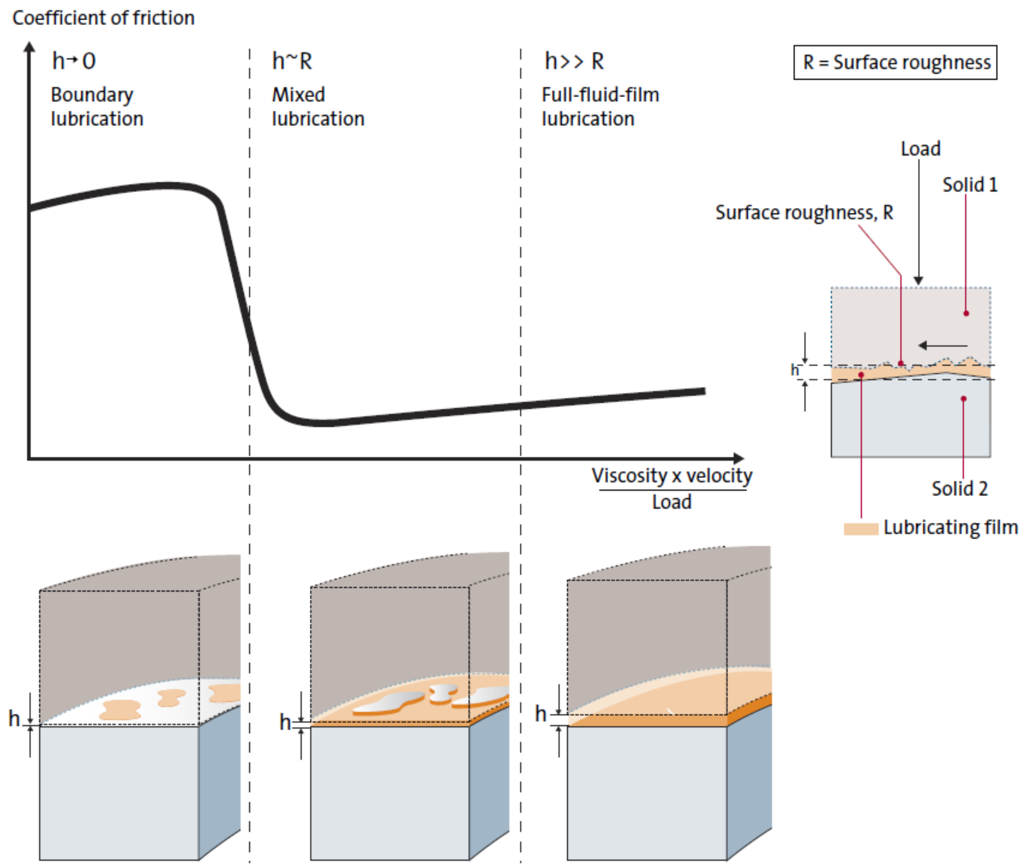

Figure 3.1. Stribeck curve showing different lubrication regimes [GRUNDFOS Management A/S, 2009].

Considering high loads and slow relative movement between the surfaces, the hydrodynamic pressure does not contribute to the surface separation. These characteristics describe a boundary lubrication regime. In this case the friction coefficient is high compared with the other possible scenarios. The two other regimes suppose a better lubrication between surfaces due to lower loads and higher relative speeds between the interacting surfaces. The regime is called mixed if the hydrodynamic pressure contributes to the surfaces separation, even if the surface contact is not fully avoided. A regime where the separating is entirely achieved is called full fluid film lubrication. For the last two scenarios described, a lower friction coefficient is expected.

A full fluid film lubrication regime is considered in this study for the calculations of the torque produced by the journal bearing on the turbine. Under this premise the Petroff´s equation, which complies with the following assumptions, is applicable:

- There is no axial movement between the surfaces.
- The load is small in the radial direction.
- The surface interaction is between two concentric cylinders.
- The clearance space is fully occupied by the lubricant fluid.

These considerations are quite realistic, due to good lubrication generated by the high rotational velocity between the shaft and the hub. Besides, the turbine is very light and the force in the axial direction is presumably well distributed, thereby only small radial forces could be exerted to the shaft.

A scheme representing the journal bearing used in this study is depicted in Figure 3.2. Petroff´s formula will be explained by using this scheme.

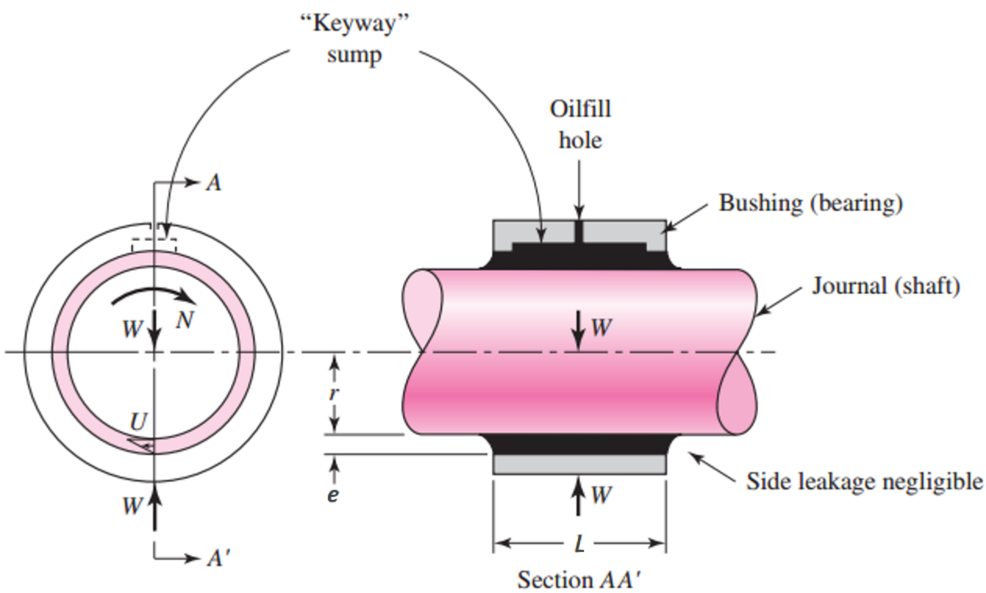

Figure 3.2. Petroff's lightly loaded journal [Shigley et al., 2006].

The torque represented takes into account the force generated from the shear stress over the whole contact area and the radial distance to the clearance space. Equation 3.4 expresses the torque calculation made with the considerations stated before.

$$T = \tau_s A r = \frac{4\pi^2 r^3 L \mu \omega}{e} \tag{3.4}$$

Where τ_s is the shear stress, A the contact area, r the shaft radius, e the clearance space, L the axial length of the bearing, μ the dynamic viscosity and ω the rotational speed. In the studied case, the turbine and the bearing rotate in opposite directions. Thus, the rotational speed is the sum of the two angular velocities.

3.2.2 Contact friction torque

The axial movement of the turbine is restricted by an edge which shares a contact surface with the turbine, this contact is the trust bearing. The friction magnitude on the trust bearing will depend on the following factors:

- The force exerted between the surfaces.
- The size of the contact area.
- The friction coefficient, which depends on materials and roughness of the surfaces.

Due to the lack of information about the material and the coarseness of the surfaces a value of 0.01 is used as friction coefficient (this value is an estimate determined by an expert on the topic [Grann, 2017]). The torque generated by this friction force is calculated using Equation 3.5.

$$T = \frac{2}{3} F_c F \frac{r_{in}^3 - r_{out}^3}{r_{in}^2 - r_{out}^2} \tag{3.5}$$

Where F_c is the friction coefficient, F is the force between the two surfaces, and r_{in} and r_{out} are the inner and outer radius of the annular part of the hub which experiences the frictional torque.

3.3 Design parameters

In this section the geometrical parameters of interest, for the turbine design, are defined including the shape of the blades and the amount of blades in the turbine. The interaction between these parameters and the performance of the turbine is described in order to link these geometrical factors to the losses generated across the turbine.

3.3.1 Blade shape

The blade can be shaped using different profiles. The most basic would consist of a flat rectangular blade that remains invariant all over the turbine, this is approximately the case for the existing blade design from $Grundfos$. Apart from the flow characteristics, the forces acting on the blade depends on the angle of attack and the blade dimensions.

According to an experimental research [Ortiz et al., 2015], the aspect ratio of the blade influences the lift and drag coefficients. This aspect ratio is defined as the spanwise over the blade length. The results obtained by the mentioned research are presented in Figure 3.3.

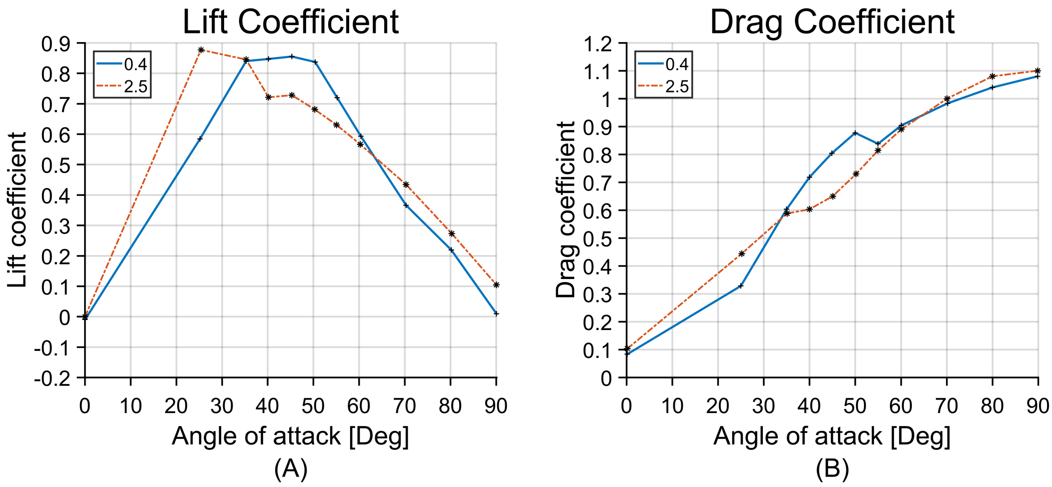

Figure 3.3. Lift and Drag coefficients for a flat blade with different aspect ratios [Ortiz et al., 2015].

In Figure 3.3 (A) the lift coefficient shows two curves with a pick around 45° and 25° for an aspect ratio of 0.4 and 2.5 respectively. The drag coefficient in Figure 3.3 (B) shows a similar tendency for the different aspect ratios, increasing almost linearly with the angle of attack. The aspect ratio for the existing turbine lays around 0.4. The associated lift and drag curves for a ratio of 0.4 will be used to explain some of the phenominomes generated in the CFD model in Chaper 5.

Another factor influencing the lift coefficient is the flow Reynolds number. For flows with a small Reynolds number (under 100000), the lift coefficient is slightly affected by this parameter, obtaining a higher coefficient for higher Reynolds values [Torres, 2002]. This effect is shown in Appendix A.4.

3.3.2 Number of blades

The number of blades is an important issue in the turbine design, it affects the drag and the lift of the turbine. If the flow meter has too few blades, the fluid guidance will not be assured, resulting in high losses from the flow separation [Dixon and Hall, 2010]. These losses could disturb the linear relation between flow quantity and the rotational velocity, reducing the accuracy of the measurement device. On the contrary, by increasing the solidity of the turbine, better flow guidance will be achieved and the rotational speed will increase considerably. Nevertheless, the contact surface between the fluid and the rotor would become larger, increasing the frictional losses. Moreover, interference between the blades could affect the performance of the device [Thompson and Grey, 1967].

An optimal number of blades will ensure accurate readings from the flow meter without increasing the frictional losses unnecessarily. To determine this optimum compared to losses, the Zweifel's criterion is used. It is based on the ratio between a real and an ideal tangential blade loading. The equations representing these loadings are 3.6 and 3.7 respectively.

$$Y = \rho d c_x (c_{y2} + c_{y1}) \tag{3.6}$$

$$Y_i = \frac{1}{2} \rho c_2^2 b \tag{3.7}$$

Where ρ is the fluid density, c_1 and c_2 are the velocities before and after the blade which has an axial length b. The concept of an ideal loading supposes constant pressures along the suction and the pressure side of the blade. This is opposed to a real distribution exemplified in Figure 3.4, where the pressure varies along the blade. P_1 and P_2 are the inlet and outlet pressures.

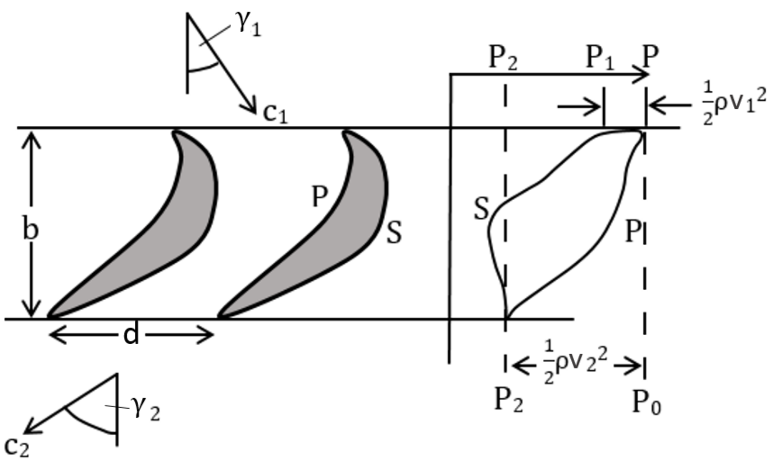

Figure 3.4. Pressure distribution around a turbine, where P is the pressure and S the suction sides on the cascade blade [Dixon and Hall, 2010].

Zweifel has experimentally determined the optimum ratio Ψ_T between the ideal and real tangential blade loadings, which should be around 0.8 in order to minimise the losses. Equation 6.1 presents the optimal tangential blade loading.

$$\Psi_T = \frac{Y}{Y_i} = 2(\frac{d}{b}) cos^2 \alpha_2 (tan\alpha_1 + tan\alpha_2) = 0.8 \tag{3.8}$$

Zweifel's criterion will later on be used in the proses of choosing a blade number for the turbine flow meter.

3.4 CFD validation parameters

In this section a brief explanation of the CFD tool is given, including the indicators of convergence used to guaranty the data reliability.

A CFD model is a powerful software tool utilized to solve complex fluid phenomena problems. The working principle of this tool is to discretize the volume that contains the system of interest. Then, numerical methods and algorithms are applied to evaluate the variables and characterize the flow behaviour. This method applies extensive iterative calculations that will provide a non exact solution to the problem. A solution that depicts the real phenomena accurately is the goal for every CFD simulation. Nevertheless, it is also true that there is a compromise between the accuracy and the calculation time of the model that has to be assessed. The indicators, described below, are used as limiting parameters under which a result is considered reliable.

Residual values:

The solver calculates the root mean square error of the values obtained during the run, the user has to determine the error value deserved. If the allow error is lower, the results will be more accurate. Values above 10^{-4} or even 10^{-5} are considered acceptable.

Solution imbalances:

The physical phenomena represented by the model has to comply with principles like the conservation of mass and energy. Nevertheless, numerical deviances are introduced along the software calculation and an imbalance of these properties is inevitable. An inlet and outlet control of these parameters has to be conducted to avoid that the imbalance surpasses a maximum value that is usually set as 1%

Quantities of interest:

The quantities of interest are the main outputs expected from the simulation model, like forces, torques, pressures or velocities. They have to be monitored during the software calculation. If the model represents a steady state problem and is converging adequately, these variables will reach a stable value. For a not stabilized value, different results will be obtained depending on the number of iterations.

The values for the convergence criteria presented are more a general guide than a rule. It is the users criteria, in accordance with the specific problem, that would set these values.

Besides the analysis to determine the robustness of the results, the simulation has to be endorsed by experimental analysis.

4 Experimental Work

A crucial part of this study is the experimental work, which allows the validation of the data obtained from the simulation, and the test of the TFM in a real set-up. This chapter presents the experimental work performed during this project. At first the set-up of the test is described and finally the data extracted are presented.

4.1 Experimental set-up

For the experiments a CR 10 pump with 4 stages is used and placed in *Grundfos* test bench to simulate the real working environment for the pump. Inlet and outlet pipe lines are connected to the pump and different measurement devices are installed to analyse the pump behaviour. In Figure 4.1 the set-up used during the experiments is shown.

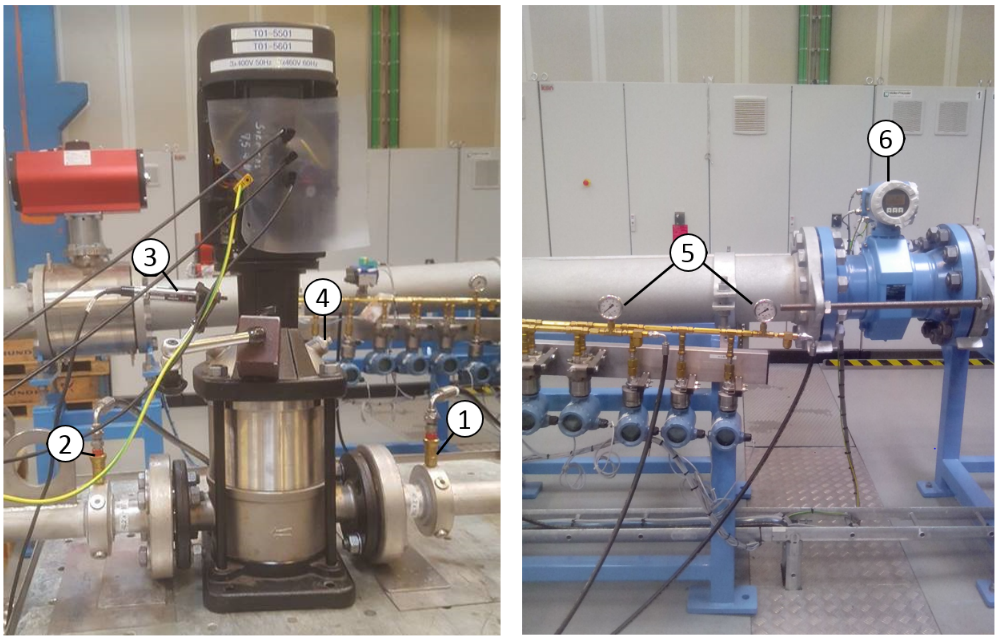

Figure 4.1. Experimental set-up for the TFM test.

The measurement devices employed during the test and depicted in Figure 4.1 are:

1. Inlet pressure connection.
2. Outlet pressure connection.
3. Photoelectric pump shaft tachometer.
4. Socket for turbine angular velocity magnetic sensor.
5. Bourdon pressure gauges.

6. External flow meter

The values provided by the experiments include: flow rate pressure, pump power, water temperature and rotational speed of the pump and the turbine. The test conditions are controlled from a central unit which is also in charge of collecting the experimental values, except the turbine rotational speed which is logged separately on a secondary computer.

4.2 Test description

This section describes the steps followed during the experimental work and the test conditions. All The tests were performed at *Grundfos'* facilities using the same equipments. The capacity and precision of the equipment used is not presented in this study

Prior to the test, the measurement equipments are evaluated to confirm their condition. The central unit scans the flow capacity of the pump and creates a 20 value scale. Using this scale the operator is able to control the flow provided to the pump. Two different tests are performed using the set-up described before. First, a test without the turbine is carried out. This test will describe the standard operation conditions of the pump and is used as the basis to analyse any change in the set-up. The second test maintain the general set-up, but the turbine is included in the pump. In Figure 4.2 the installation of the turbine into the pump is shown. The turbine is marked with the number 7 and is already mounted on the shaft.

Figure 4.2. Turbine position in the pump.

Once the turbine is in place the upper part of the pump casing is tightened. Trough the empty socket of the magnetic sensor the turbine free spinning is checked. Finally the magnetic sensor is installed.

During the experiments, the flow rate in the system was increased in steps of around 1 m^3/hr within values that ranges between 2 and 17 m^3/hr. The first value represents the minor flow that the magnetic sensor is able to register accurately. The pump has the capacity of running at different rpm, but for the measurements collected it was maintained at around 2915 rpm.

Since the turbine angular velocities are not registered at the same computer with the other variables, the experimental time is used as the linking variable. The central unit collects 10 measurements for each flow. Meanwhile, the secondary computer collects 60 measurements from the turbine sensor . Averages of these set of values are used during the data analysis. These tests allow to determine the differences between running the pump with and without the flow sensor.

4.3 Experimental data

As stated in the previous section, the results obtained from the experimental work are sets of values measured at different flows. In order to use this results, the average values and the standard deviation of the relevant parameters are calculated. As an example, Figures 4.3 and 4.4 depict the values of pump head and turbine rpm obtained during the testing of the set-up for the 8 bladed turbine. The efficiency data was also plotted earlier in Figure 1.4.

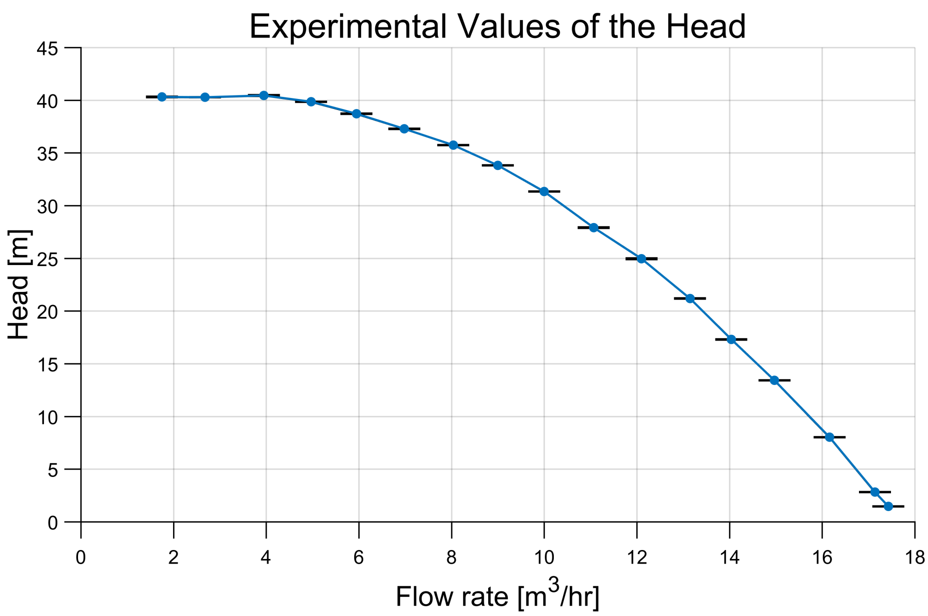

Figure 4.3. Experimental values of the head in the set-up with the 8 bladed turbine.

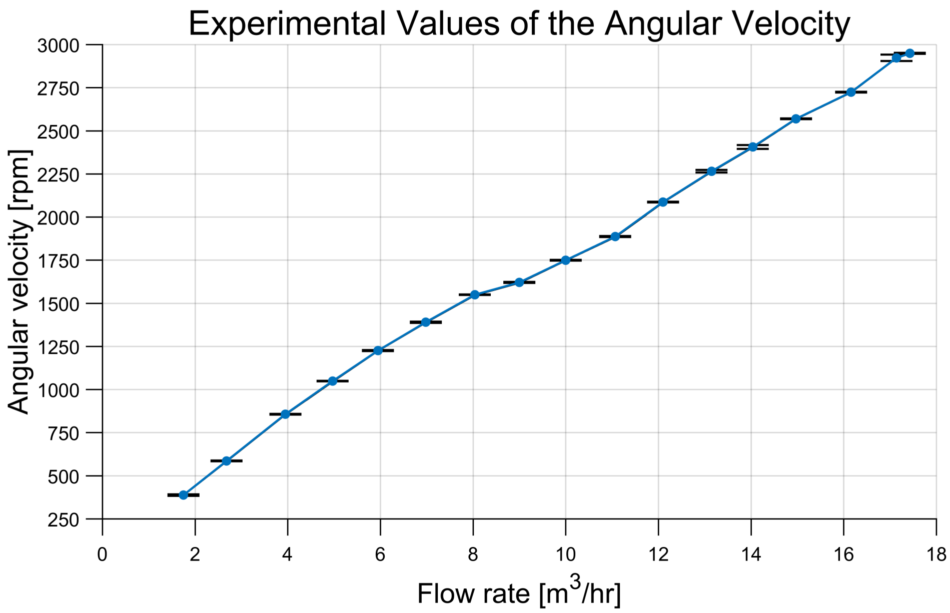

Figure 4.4. Experimental values of the angular velocity in the set-up with 8 bladed turbine.

Other tests including different prototypes are performed with the same set-up, and they all follow the same structure described in this section.

5 Model development

The following section describes the development and verification of the fluid flow and the frictional bearing model. The accuracy of the model is important as the results give the basis of the pressure losses in the system that will be used for the optimisation of the turbine. Furthermore, the torque generated in the flow meter depends on the flow velocity and angle at the moment of impact, thus the torque calculations is also dependent on the model accuracy.

5.1 The modelled flow domains

The domain of the CFD model contains the flow meter and the upper part of the CR 10-4 pump casing. The pump sections before the system is not modelled due to the limited time frame of the thesis.

Figure 5.1 illustrates the geometry used for the CFD model containing the flow meter marked with green and the top part of the CR 10 which is marked gray. The hollow areas in and around the flow meter represents the blades and the flow meter walls. The flow domain have been simplified by taking out the magnetic sensor and smoothing the outer wall for any protrusions. As reference, the real geometry of the pump can be seen in Figure 1.2.

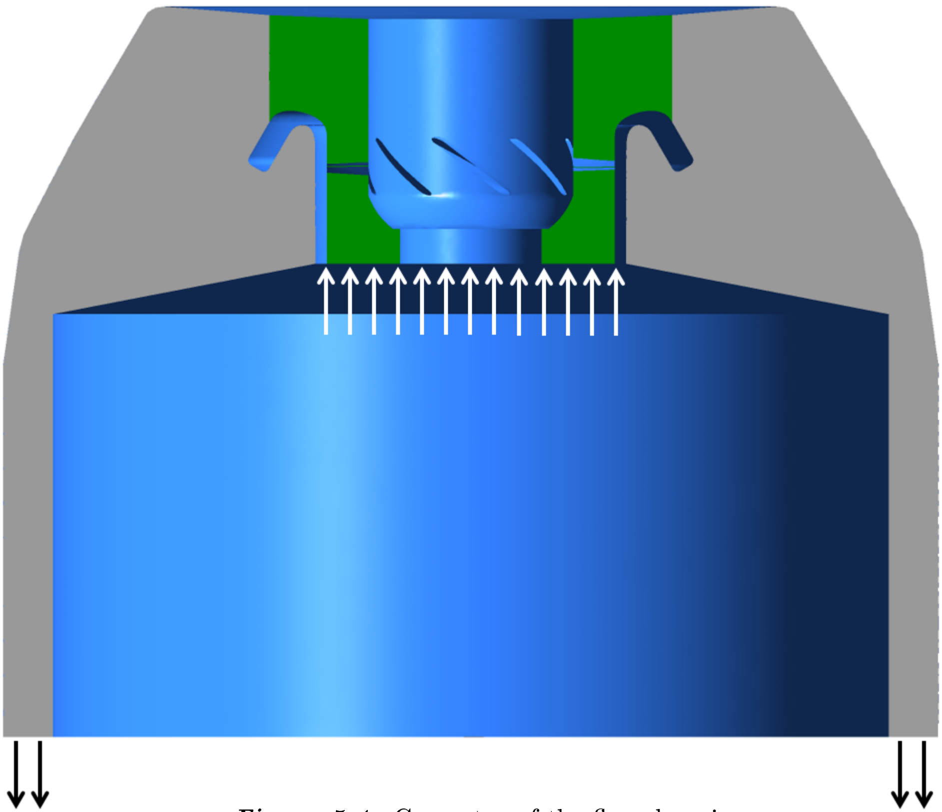

Figure 5.1. Geometry of the flow domain.

5.2 Input data for CFX

This section describes the input values for the CFX model. The data used for the model were provided by *Grundfos* and were used after a consistency check.

5.2.1 Mass flow data

The experimental data presented in chapter 3 are the input for the CR 10-4 pump simulation. The following Figure 5.2 show the experimental mass flow and the corresponding turbine rotational speed. All the values presented are averages of the data sets collected during the experimental work.

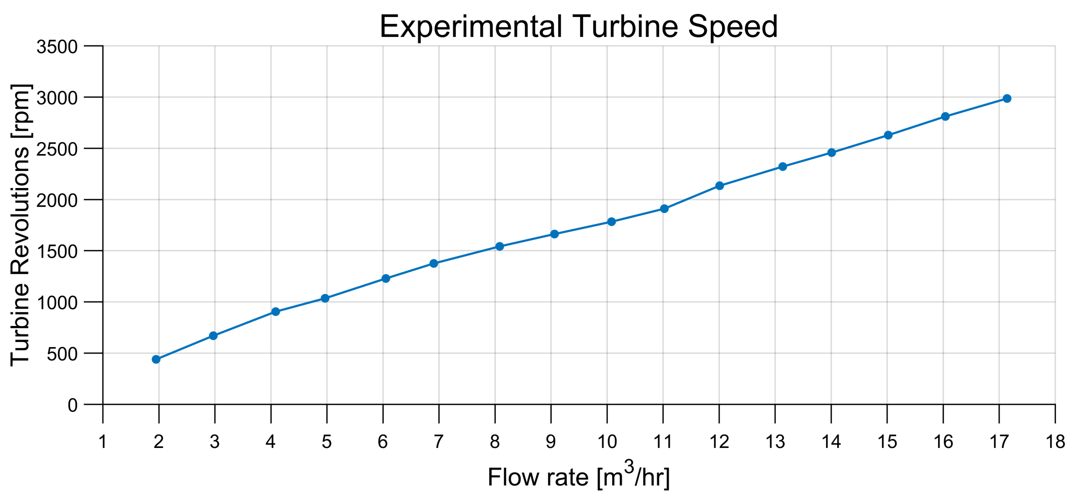

Figure 5.2. Experimental turbine rotational speed at different flow rates.

Figure 5.2 shows a linear relation between the flow rate and the turbine revolutions as stated in introduction. For the following simulations, flow rates of 6, 10 and 14 m^3/hr have been chosen. The corresponding turbine speed will be used as the starting point to determine the rotational speed for the simulation.

5.2.2 Inlet boundary

In the introduction it was stated that the inlet boundary has a large importance for the rotor design, flow characteristics and the calibration of the pump, thereby emphasising the importance of finding the correct inlet boundary. In this case, there are two applicable ways to generate the inlet boundary without the use of experiments: an predefined inlet adjustable to the flow rate, or a simulated inlet conditions from an existing CFD model as it was made for this study, where the last stage of the CR 10 pump was modelled. To select the best inlet boundary, it is necessary to investigate the outlet conditions from an existing CFD model from *Grundfos*. Figure 5.3 illustrates the existing CFD model containing the flow meter inlet marked in green. The four inlet lines marked in yellow represent the location from where sample velocities are taken.

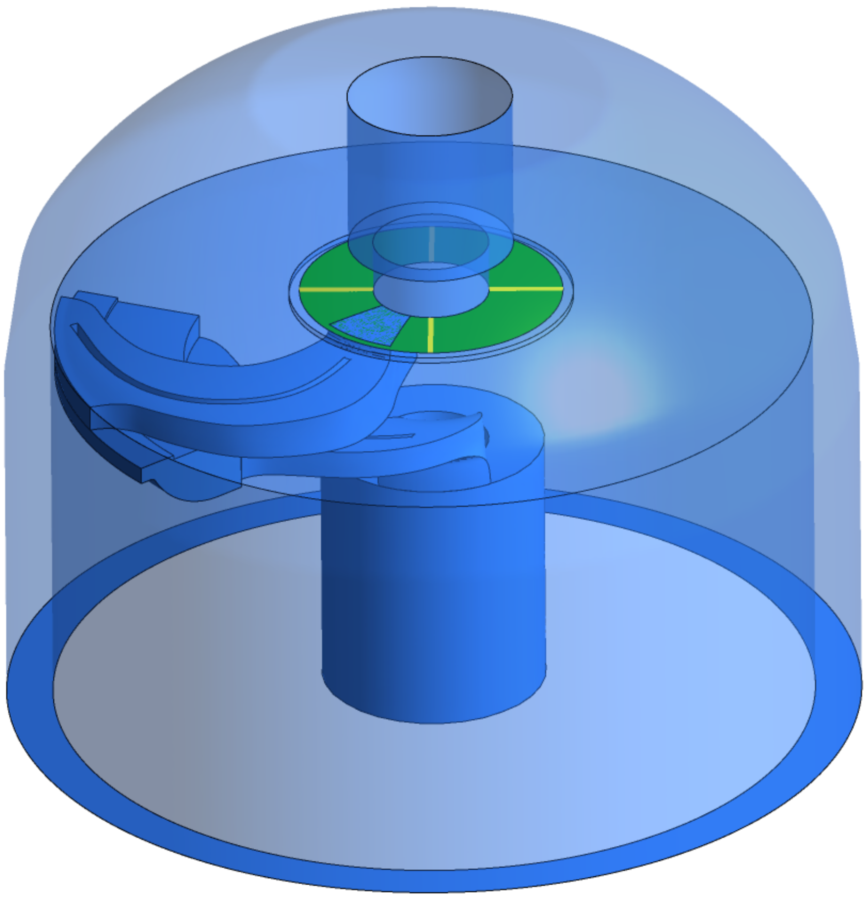

Figure 5.3. Geometry of CR 10 pump without flow meter seen from above.

The velocity data from the inlet lines seen in Figure 5.3 are used to generate a mean velocity profile for the different flow inlets. Figure 5.4 (A) and (B) illustrates the variation of the tangential and axial speed for the four inlet lines.

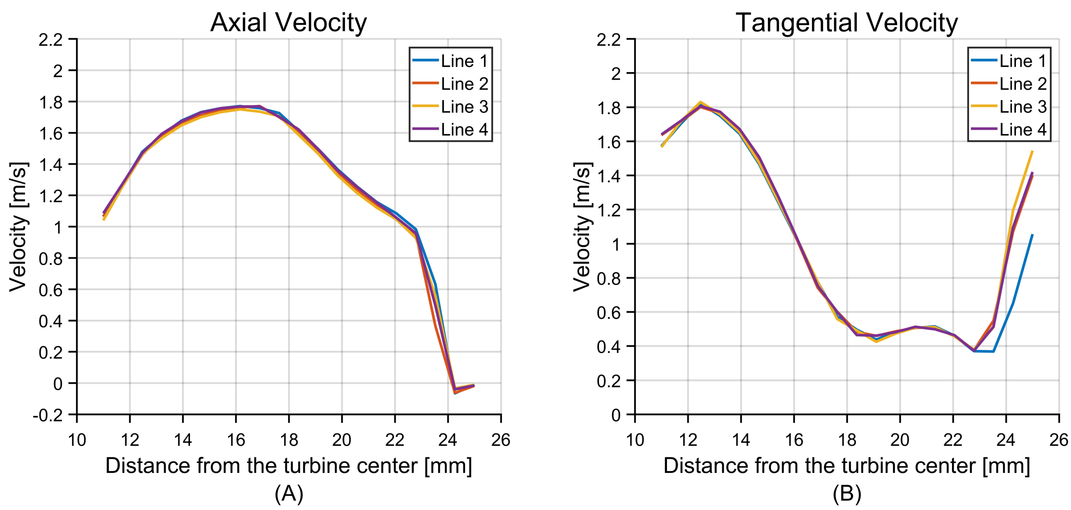

Figure 5.4. Illustration of the axial velocity variations (A) and the tangential velocity variations (B) simulated with an inlet flow of 6.84 m^3/hr.

Figure 5.4 (A) and (B) shows a small variation over the profile. The small variations occurs at all inlet profiles generated from the existing CFD model. It is concluded that the mean velocity profile generated from the four inlet lines can be used as an overall inlet profile. Afterword, the variation of the inlet profile generated by the mass flow will be investigated. The variation generated by different mass flows is illustrated in Figure 5.5.

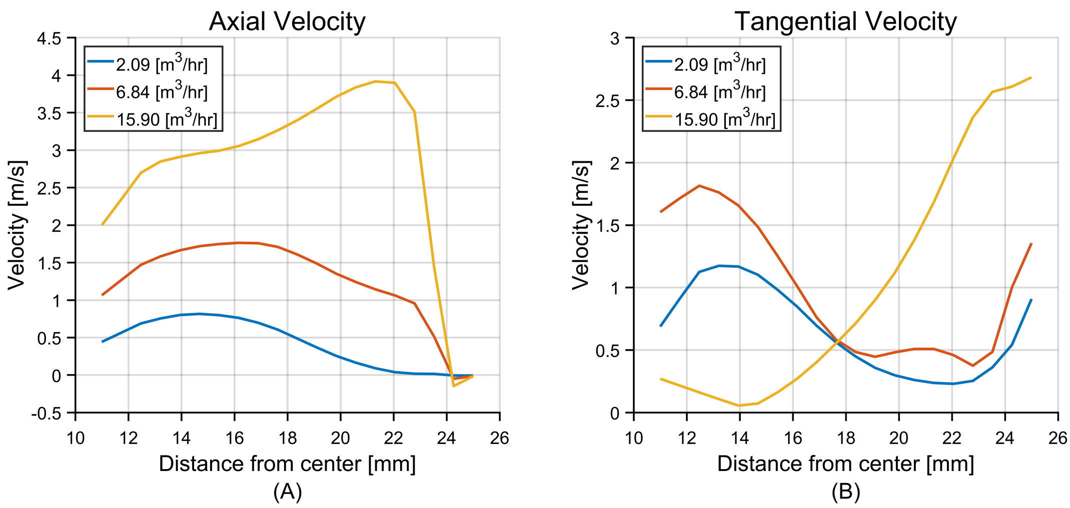

Figure 5.5. Illustration of the axial velocity variations (A) and the tangential velocity variations (B) between 2.09, 6.84 and 15.90 m^3/hr.

Figure 5.5 (A) shows an increasing axial velocity at higher flows. Furthermore, the shape has been changed due to higher deviations at larger distances from the center of the turbine. Figure 5.5 (B) illustrates the deviation in the tangential velocity. In this case, the inlet profile change dramatically from 6.84 to 15.90 m^3/hr, almost following an opposite trend. From analysing the axial and tangential velocity it is concluded that an unique inlet profile can not represent all the flow rates. Therefore, the flow profiles used as input for the model are generated from the existing pump model, and they are specific for each flow rate.

5.3 General CFX settings

The important settings used in CFX are given in the following table:

Overall settings for CFX	
Analysis time	Steady state
Timescale control	Physical timescale
Turbulence model	SST k-ω
Scheme	High resolution

Table 5.1. Settings defined for the CFX simulations.

The settings presented in Table 5.2 are elaborated in the following points:

- **Analysis time**: Due to the small deviations in the system a steady state simulation can be used. The steady state simulation is also used due to its small computational time compared to a transient model.
- **Timescale control**: To provide a sufficient relaxation of the non-linearised equations and information of the transient behaviour in the simulation, the physical timescale is chosen. Furthermore, it improves the converting of the simulation by enabling a fixed time scale[ANSYS, Inc, 2016].
- **Turbulence model**: The CFD model needs to be able to handle both the free stream and near wall effects. This is required, because the torque calculations at the flow meter needs a proper near wall modelling to achieve accurate results. Furthermore, the head loss needs accurate results at both the near wall and free stream areas to achieve good results. On this basis the SST k-ω has been chosen due to its accuracy at both the near wall and free stream areas.
- **Scheme**: The simulation systems needs to be able to handle shocks and discontinuities. The hight resolution scheme is therefore chosen for its ability to model and achieve accurate results when shocks and discontinuities are present in the system.

5.4 Verification of the model

The model has to comply with certain characteristics to ensure that the results provided represent the physical phenomena evaluated. This section describes the chosen setting for the model, the grid independence study, and the analyse of the first cell hight.

5.4.1 Chosen convergence criteria

An evidence of the convergence is when the calculations of an iterative process approaches a certain value. One way to ensure convergence is to monitor the residuals. When the residuals are lower than a defined value, the simulation are said to be converged. The convergence criteria for the CFX simulation are given in Table 5.2.

Residual	**Absolute Criteria**	**Residual**	**Absolute Criteria**
Continuity	1e-05	P-Mass	1e-05
U-Momentum	1e-05	k	1e-05
V-Momentum	1e-05	ω	1e-05
W-Momentum	1e-05		

Table 5.2. Convergence criteria defined for the CFX simulation.

The chosen values for the convergence criteria are determined on the basis of common practice guide lines found in [ANSYS, 2017]. Where it is stated that 1e-05 is a good convergence and is usually sufficient for most applications in the engineering world. The selected convergence criteria will be used in the follow verification of the model.

5.4.2 Grid independence

The turbine and top pump geometry generated at Grundfos are modelled with Catia and a mesh is created in ANSYS Meshing. A grid independence study is done to ensure that the simulation results are not affected by the mesh. Five different meshes were generated with its number of cells ranging from 1.4 up to 2.4 million. For the simulations, a steady state CFD model using: the high resolution scheme, the SST k-ω turbulence model, a turbine surface roughness of 40 microns and a convergence criteria of $1e^{-5}$, as stated in Table 5.2, was used for the grid independence study. The results generated by the study can be seen in Figure 5.6.

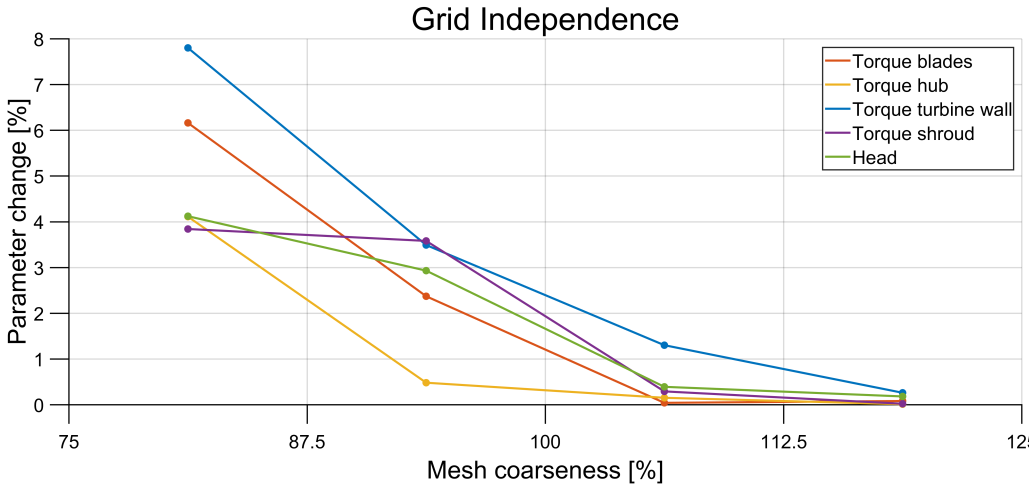

Figure 5.6. Change in key parameters between different coarseness of the mesh with a change of 12.5%. Each point on the curves illustrates a percentage difference between the two nearby mesh coarsenesses.

As expected, the difference decreases when the mesh is refined with more cells and increases drastically when a smaller amount of cells is used. Figure 5.6 shows a minimal deviation between a coarseness of 100 and 112.5. The only larger deviation is generated by the Torque Turbine Wall with a value of 1.30 %. The percentage deviation between the grids only describes the change between two grid qualities, but does not ensure that a correct tendency is being reached. To see how specific parameters change with different cell densities, the torque on the blades and on the outer turbine wall have been plotted in Figure 5.7.

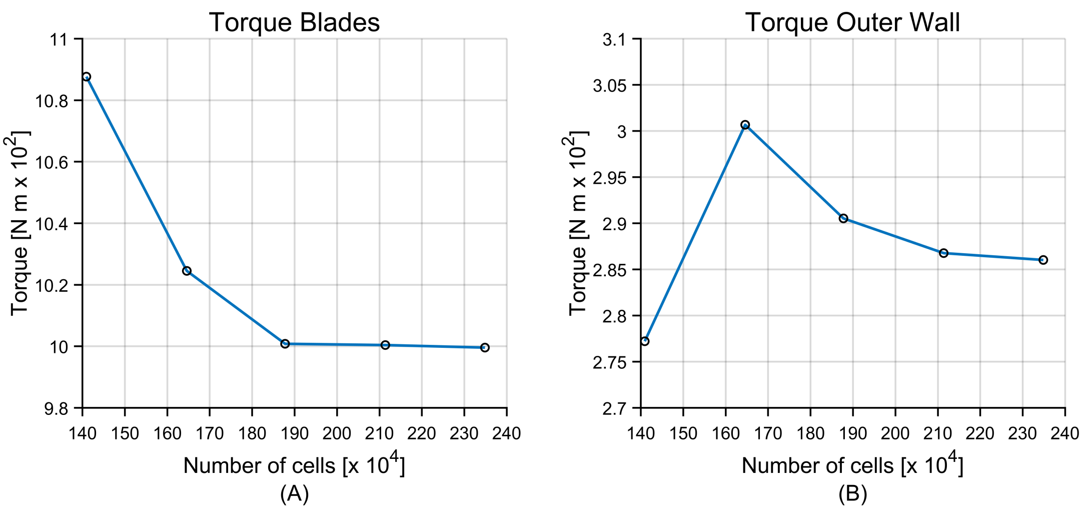

Figure 5.7. Torque on the blades (A) and torque on the outer turbine wall (B) for different grid sizes.

It is noticeable that a constant torque is reached around 1.9 million cells for the blades and around 2.1 million for the outer wall. On the basis of the gathered data from the 5 grids, it is concluded that a mesh of 2.1 million cells is suitable for the simulation. The main reason for selecting this grid lies in the deviation of the torque on the outer turbine wall. Which has not been stabilized before the selected grid.

5.4.3 First layer thickness

When modelling the near wall area with SST $k-\omega$ the near wall mesh needs a very high cell density to achieve accurate results. While performing the grid independence study the first cell height was held constant. To see the first cell height effect on the key parameters, investigations have been performed with 4 cell heights, ranging from 100 to 8%. The 100% stands for the cell height used during the grid independence study. The results from the change in cell height can be seen in Table 5.3.

First Layer Height [%]	**Number of Cells**	**Force Z [%]**	**Torque Blades [%]**	**Torque Hub [%]**	**Torque Turbine Wall [%]**	**Torque Shroud [%]**	**Head [%]**
8	3.524.585						
		1.02	0.58	1.94	0.85	1.82	0.03
10	3.370.645						
		2.10	1.46	8.60	10.60	3.38	0.15
25	2.490.201						
		5.47	7.18	15.15	2.43	3.97	6.16
100	2.114.030						

Table 5.3. Comparison of results from simulations with different cell heights.

The results shows a stabilization tendency with lower cell heights. Moreover, the results for the torque turbine wall generates a large deviation between a cell height of 25 and 10%. But then, decreases to 0.85% when going from a height of 10 to 8%. For further investigations the tendency of the total torque (all torques combined) and the head have been studied. The results of this study can be seen in Figure 5.8.

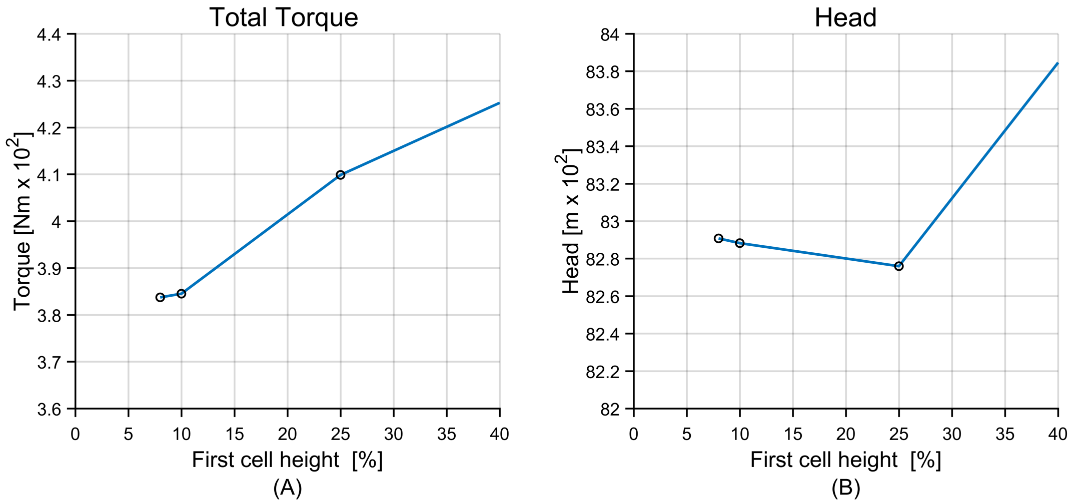

Figure 5.8. Total Torque (A) and Head (B) for different cell heights.

The results shows no significant difference between 8 and 10%. Hence, the mesh with 10% height is considered sufficiently refined to simulate the near wall behaviour, as there is only an insignificant improvement obtained by decreasing the height from 10 to 8%. Meanwhile, the number of cells is increased by more than 150 thousand.

5.4.4 Analysis of the convergence criteria

The point at which the simulation is converged is defined by analysing different parameters, giving a good understanding of when the simulation have reached its final result. When assessing the convergence the following three parameters are normaly analysed:

- Residual values
- Mass imbalances
- Variables of interest

In the following section, the convergence analysis will be described. As example the final simulation of the 8 bladed turbine at a flow rate of 10 m^3/hr and a rotational speed of 1782 rpm has been used.

Convergence of residuals

The residual is one of the main parameters when investigating a simulations convergence. Hence, the residuals directly describes the error in the solution for the chosen system. The following analysis is based on the criteria stated earlier in section 5.4.1. Figure 5.9 shows the residuels for the chosen simulation.

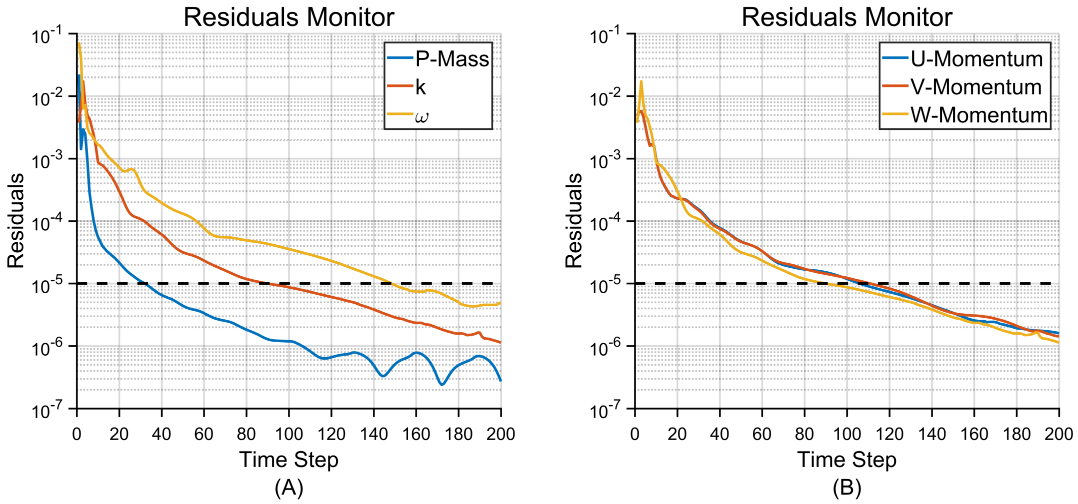

Figure 5.9. Mass imbalance in the top part of the pump (A) and the flow meter domain (B).

In Figure 5.9, the upper boundary chosen for convergence can be seen as a dashed line with a value of 10^{-5}. All the plotted residuals shows a clear convergence going even lower then 10^{-5}. Hence, the simulation is concluded to be converged in relation to the residuals.

Convergence of mass imbalance

The next parameter of interest is the mass imbalance generated in the system. As stated in Section 3.4, the mass imbalance for the different domains need to be less than 1%. Figure 5.10 shows the imbalance for the top part of the pump and the flow meter.

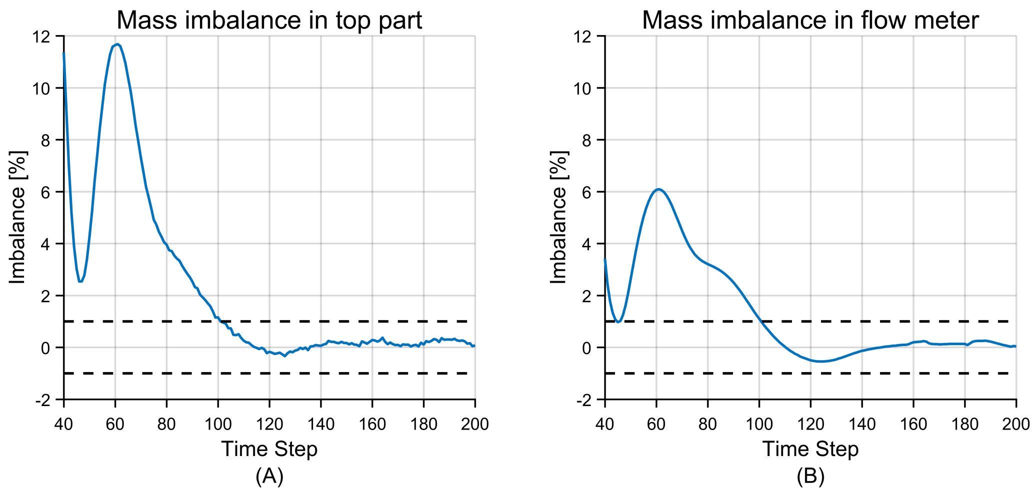

Figure 5.10. Mass imbalance in the top part of the pump (A) and the flow meter domain (B).

In Figure 5.10, the upper and lower boundary of 1% is defined with two dashed lines. Figure 5.10 (A) and (B) shows a small mass imbalances far below the border of 1% and can therefore be defined as converged with respect to the mass imbalance.

Convergence of variables of interest

When looking at convergence the residuals is only describing the difference between two iterations or time steps. The residuals are not describing if the simulation is converged to the right value. For at better understanding the variables of interest, different torques and head losses, are investigated. Figure 5.11 show the behavier of the head loss and the torque on the blades.

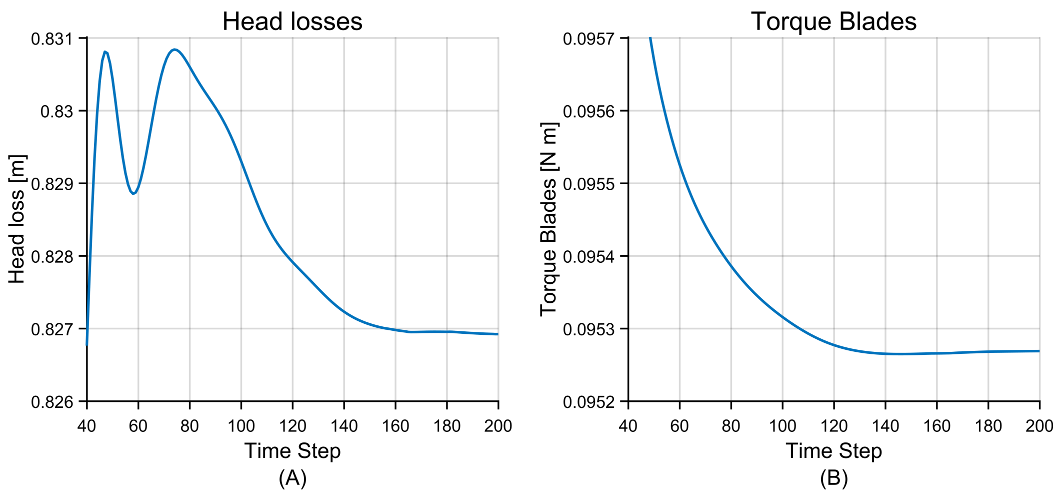

Figure 5.11. Convergence behaviour of head loss (A) and torque on the blades (B).

The measurement of head loss and torque on the blades shows a clear stabilisation around 160 and 130 time steps. The positions of the stabilisations shows the importance of looking at the variables of interest. Hence, the stabilisation of one parameter is not an indications for all parameters convergence.

5.4.5 Observed phenomena around the blades in the CFD simulation

In this section the flow behaviour around the turbine blades are analysed. The investigation is based on what can be observed in the CFD model and physical parameters as pressure and velocity. Furthermore, the results are compared with the angle of attack extracted from the model. Therefore, the angle of attack will first be investigated.

Angle of attack

The angle of attack α is closely related to the performance of the turbine. As stated in Section 3.3.1, this parameter influences the drag and the lift of the blade. Three elements affect directly the value of α: the angle of the blade, the flow velocity and the radial distance of the blade. A fourth parameter could be mentioned, the turbine angular velocity, which depends on the parameters already stated. Figure 5.12 show the angle of attack at 10 m^3/hr and a rotational speed of 1782 rpm. The angular velocity used for the calculation corresponds to the steady state value found in the CFD model.

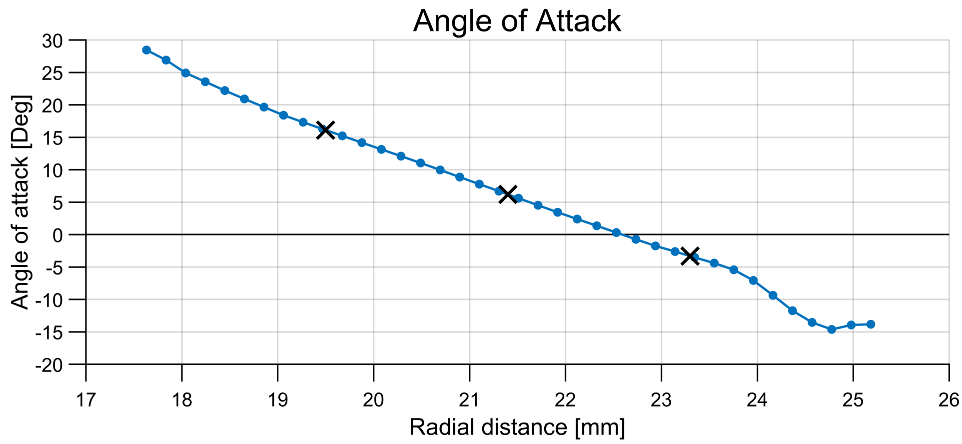

Figure 5.12. Angle of attack for the 8-bladed turbine at a flow rate of 10 m^3/hr and with a rotational speed of 1782 rpm.

The figure shows high angles of attack at small radial distances. The angle decreases with the radial distance generating a negative angle at the last third of the blade. To investigate how the angle of attack affects the interaction between the flow and the turbine, the velocity and the total pressure around the blades are investigated at the following three positions:

- Near the hub (at 25% of the blade).
- The middle (at 50% of the blade)
- Near the shroud (at 75% of the blade)

The three positions are also depicted with crosses in Figure 5.12. Next, the flow around the blade is shown with the help of contour plots displaying the velocity and pressure magnitudes, overlapped with a velocity vector map. These vectors, represented by equally distributed arrows, depict only the velocity direction. The magnitude is expressed by the colors of the contoured areas. In Figure 5.12 the three blade positions where the analysis is carried out can be seen, accompanied by their corresponding angles of attack.

Flow near the hub

In the following investigations of the three positions on the blade, all the contour plots have the same scale for an easier comparison. First, the flow behaviour near the hub is analysed. The contours is described in Figure 5.13 and 5.14.

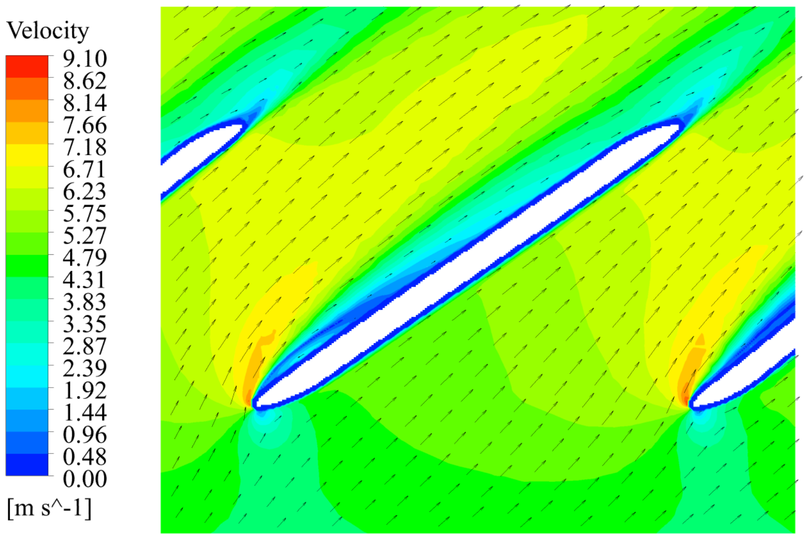

Figure 5.13. Velocity distribution near the hub with a flow rate of 10 m^3/hr and an angular velocity of 1782 rpm.

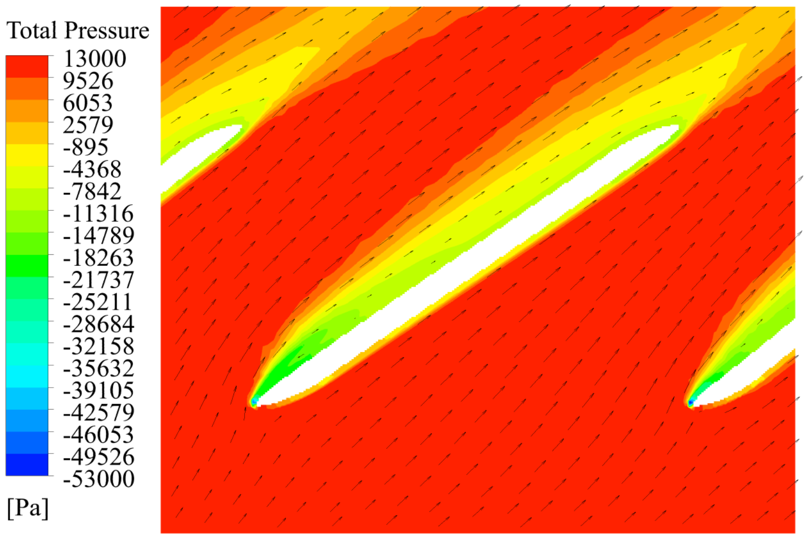

Figure 5.14. Pressure distribution near the hub with a flow rate of 10 m^3/hr and an angular velocity of 1782 rpm

Figure 5.13 shows a small bubble separation near the leading edge. At the chosen location the angle of attack is 16.1°, as seen from Figure 5.12. At the leading edge of the blade the stagnation point is marked as a low velocity area. This is the point which divides the low pressure area over the blade from the high pressure area beneath the blade as it can be seen in Figure 5.14.

Flow at the middle of the blade

The flow behaviour at the middle section of the blade is illustrated in Figure 5.15 and 5.16 for the velocity and pressure distributions respectively.

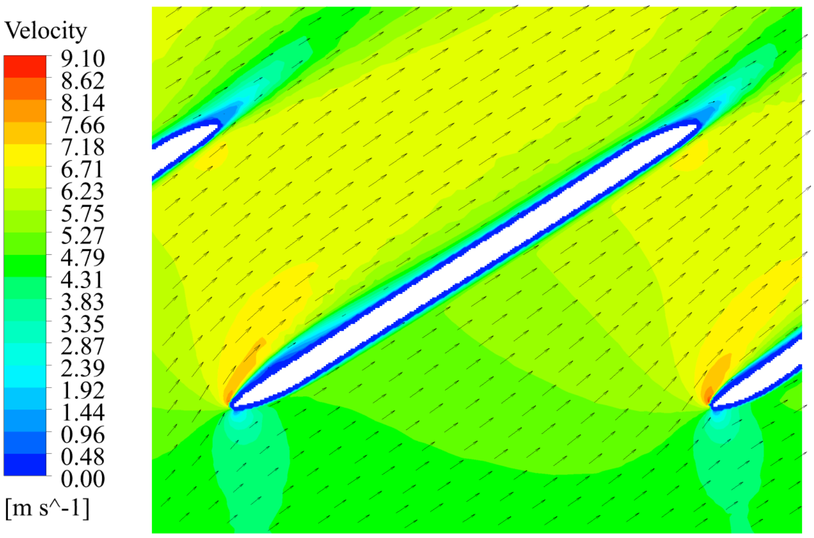

Figure 5.15. Velocity distribution at the blade middle with a flow rate of 10 m^3/hr and an angular velocity of 1782 rpm.

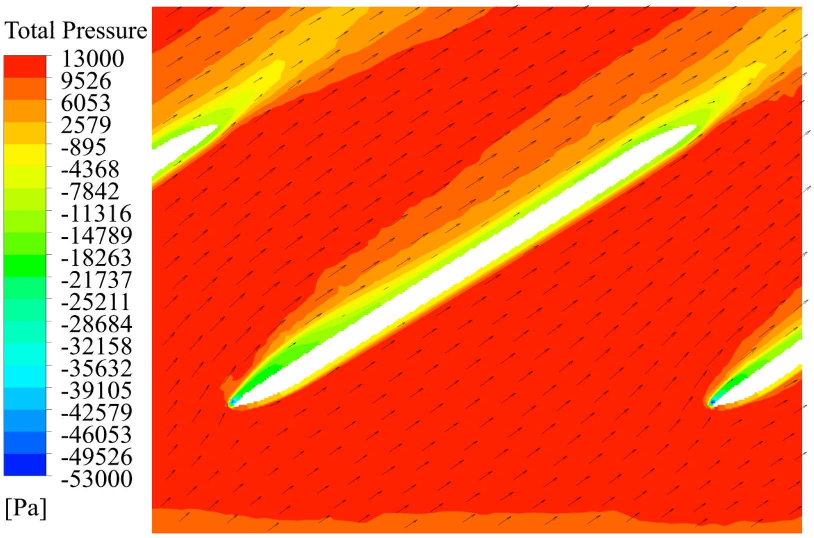

Figure 5.16. Pressure distribution at the blade middle with a flow rate of 10 m^3/hr and an angular velocity of 1782 rpm.

In Figure 5.15 the separation bubble at the front of the blade has almost disappeared. The reduction in separation is an effect of the smaller angle of attack, which is 6.2°. The pressure contour shows a smaller low pressure zone above the turbine compared with the investigation at the hub.

Flow near the shroud

The last analysis will be near the shroud. Figure 5.17 and 5.18 depicts the behaviours.

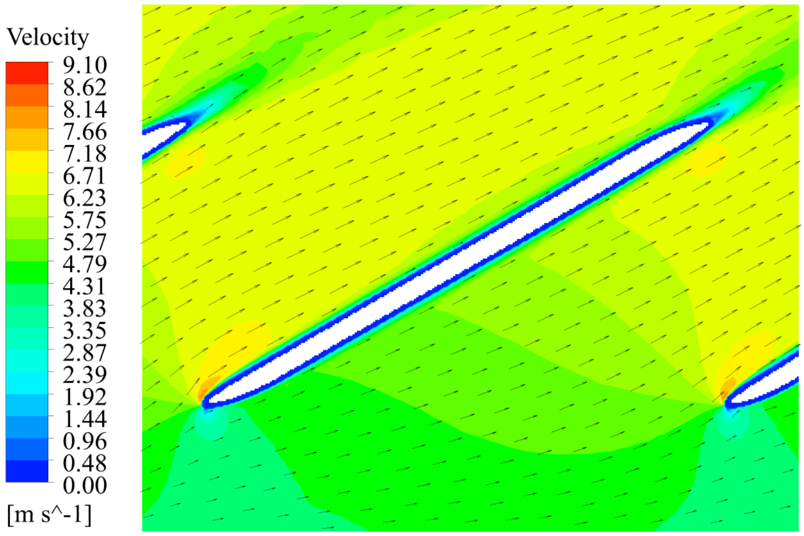

Figure 5.17. Velocity distribution near the shroud with a flow rate of 10 m^3/hr and an angular velocity of 1782 rpm.

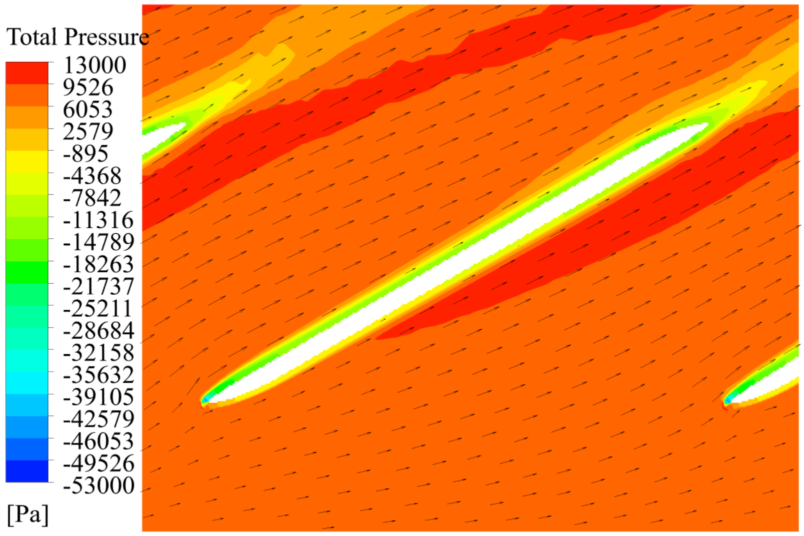

Figure 5.18. Pressure distribution near the shroud with a flow rate of 10 m^3/hr and an angular velocity of 1782 rpm.

At this location of the blade the angle of attack is around -3.3°. With a negative angle of attack there is only a small flow separation at the trailing edge as seen in Figure 5.17. The negative angle has changed the pressure distribution. Near the leading edge the pressure magnitude is the same above and beneath the blade. With the negative angle of attack a negative lift is normally expected, as described in Section 3.3.1. However, this can not be confirmed from the contour plots. From the investigation of the velocities and pressures, it can be concluded that the model behaves as expected. To be able to analyse the behaviour further, compared to stalling point and overall behaviours, an experimental investigating of the lift and drag coefficient for the specific blade is needed.

5.4.6 Bearing counter torque model

In the following section the bearing counter torque model will be described and investigated. The bearing counter torque is the only counter torque calculated independently from the CFD model. In section 3.2, the method selected to calculate the friction on the bearing was presented. Figure 5.19 shows a cross section of the turbine and an enlargement of the bearing zone, where the geometry of the interacting surfaces can be seen. The grey element is the turbine itself, it is adjoined to the bearing which is represented in blue. There is no relative motion between these two elements. On the contrary, the dark green element depicted is part of the mechanical shaft seal of the pump and it rotates with the shaft. Thus the surfaces in relative motion are the blue and green elements. There are two contact areas between them, an axial plane where the contact is lubricated by water and a radial plane where the contact is not lubricated. The contact zones are highlighted and numbered in Figure 5.19. The lubricated zone is marked as 1 and the direct contact zone is marked as 2.

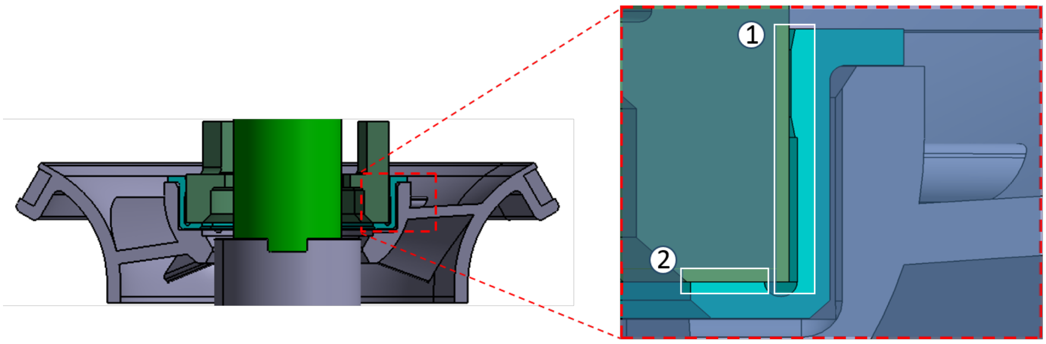

Figure 5.19. Contact surfaces of the turbine bearing.

The magnitude of the torque produced on this bearing can be seen in Figure 5.20. The main friction is produced in the axial plane, corresponding to the inner surface of the bearing. This lubricated friction is calculated using Petroff´s equation 3.4. In this case the torque increases with the rotational speed of the turbine, as the dashed orange line shows. On the other hand, the friction produced on the radial plane diminish when the rotational speed increases. The total torque follows this last trend.

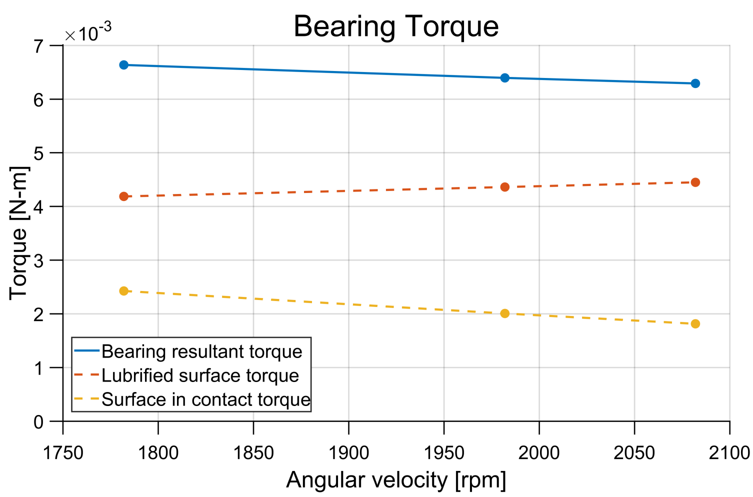

Figure 5.20. Bearing torque for 10 m^3/hr at different rotational speeds.

5.4.7 Torque and null torque calculations

It is considered that for a stable flow the turbine would reach a constant angular velocity. At this condition all the torques acting on the turbine should equilibrate and as shown in Equation 3.1 from Section 3.1. The previous sections have described the CFD and the bearing friction model. These models simulate the different torques generated in the system. The CFD simulation describes the torques generated on the blades, the hub, the shroud and the outer wall of the turbine, and the friction model describes the torque generated on the bearing.
It is considered that for each flow rate the turbine rotational speed is constant, meaning that the resultant torque acting on the turbine must be zero. Therefore, at this condition all the torques acting on the turbine have to cancel-out.
The different steps followed to determine the angular velocity at the null torque condition are described in Figure 5.21.

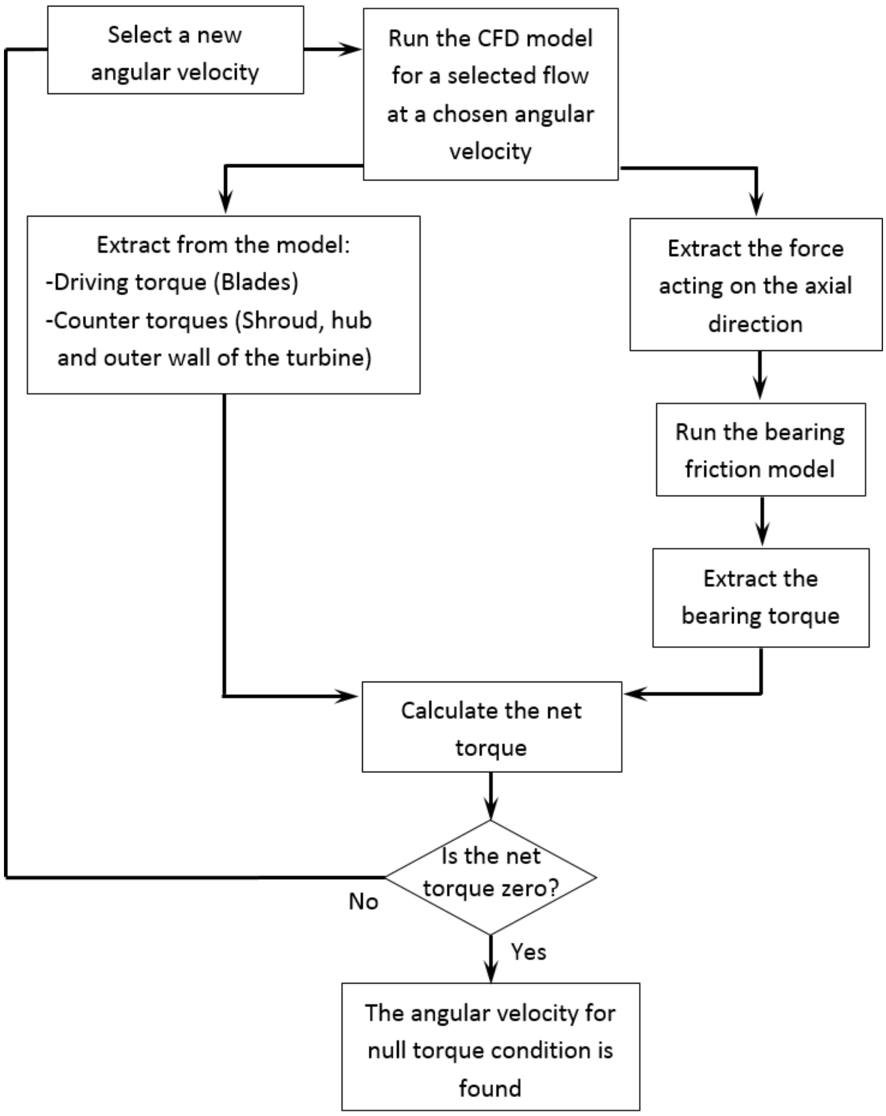

Figure 5.21. Steps to determine the angular velocity at null torque condition.

The procedure described in Figure 5.21 is applied for all the studied flow rates.
Next, a thorough investigation of the different torques on the turbine will be carried out. Figure 5.22 shows the different components of the torque, obtained from the CFD model and from the friction calculations. The torques are calculated at flow rates of 6, 10 and 14 m^3/hr. The corresponding experimental angular velocities are used for this calculation.

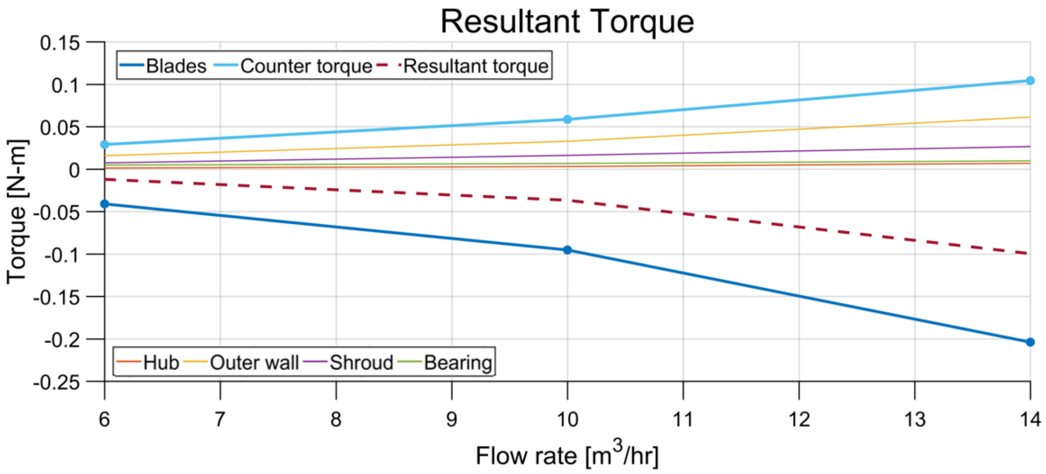

Figure 5.22. Resultant torque evaluated at the experimental angular velocities.

The driving torque, generated by the fluid on the blades, is considered negative. On the other hand, the counter torque is positive and represents the summation of all the torques depicted with thinner lines in Figure 5.22. This components of the counter torque are listed in a separate legend located at the bottom of the figure. If the model has the same outcome as the experiments, the resultant torque (dashed line) would be zero. Instead, there is a negative resultant torque, meaning that the simulated driving torque is too high, or that the counter torques are underestimated. The main contribution to the resistant torque comes from the internal and external parts of the shroud, yellow and purple line respectively. A marginal contribution is observed from the bearing and the hub marked with green and red respectively. In order to reach the null torque condition the rotational speed needs to be modified. This is done and investigated in the following part.

Modifications of the rotational speed and calculation of the null torque

By using the obtained rotational speed from the experiments the null torque condition was not reached. To find the null torque, simulations at different rpm are needed. Figure 5.23 shows the torque tendency at a flow rate of 10 m^3/hr for different angular velocities.

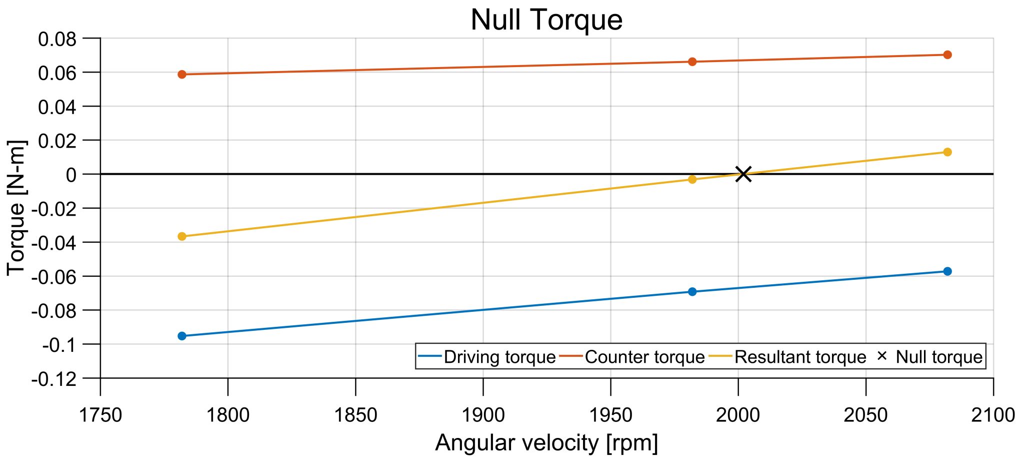

Figure 5.23. Null torque condition at a flow rate of 10 $[m^3/hr]$.

In Figure 5.23, it can be noticed that the driving torque produced on the turbine blades increases with the rotational speed. The resistance torques increases as well but more slowly. In this particular case, the resultant torque is annulled at a rotational speed of 2002 rpm, this speed is marked with a cross.

In the next section the simulated speed at which null torque is achieved will be compared with the experimental results to investigate the overestimation in the rotational speed.

5.5 Comparison of modelled results and experimental results

Once the simulated rotational speeds are generated, the results are compared with experimental data from *Grundfos*. Afterword, the simulated and the experimental head losses are also compared.
The angular velocities calculated in the simulation are compared with the results from the experiments at flow rates of 6, 10 and 14 m^3/hr, Figure 5.24 shows this comparison.

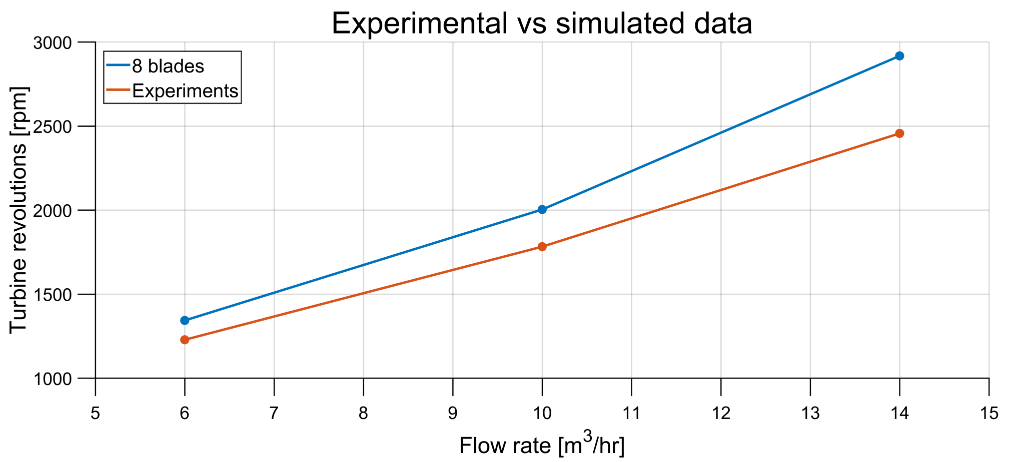

Figure 5.24. Comparison between the simulation and the experimental angular velocities.

It is noticeable that the two lines roughly follows the same tendency. It is also visible that there is a gap between the curves, which increases with the flow. At 6 m^3/hr the gap is 8.4%, and rises to 11.0 and 15.8% for flows of 10 and 14 m^3/hr respectively. The percentage deviation is calculated with respect to the simulated data. In the following, the simulated head loss will be compared with experimental results.

Investigation of head losses

The following section describes the experimental head measurements, head losses, and the deviation between experimental and modelled data. First, the experimental head curves can be seen in Figure 5.25. The curves are smoothed by a second order polynomial in order have a more stable tendency. The two polynomials have the same R value of 0.9997.

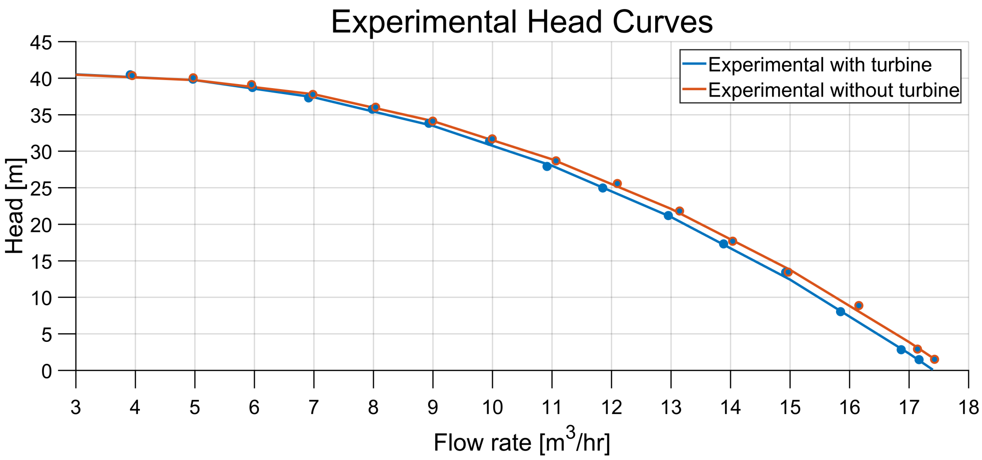

Figure 5.25. Pump head curves with and without the turbine.

It can be seen in Figure 5.25 that the head curves follow a very similar trend. In fact, the curves are undistinguishable until 6 m^3/hr where a certain separation starts. The difference between the two curves increasing with the flow rate, becoming more important for high flows. The increasing error could be due to a higher loss generated in the top part of the pump.

Next, the calculated head loss in the CFD model will be described. In the CFD simulation only the head loss generated by the turbine was needed. For accurate head results two models are needed; one with and another without the turbine. Nevertheless, due to the time frame of the project, it was chosen not to make a second model without a turbine. Hence, the head loss is generated from the pressure difference between the inlet and the outlet in the model. In Figure 5.26 the inlet and the outlet can be seen marked in red and green respectively.

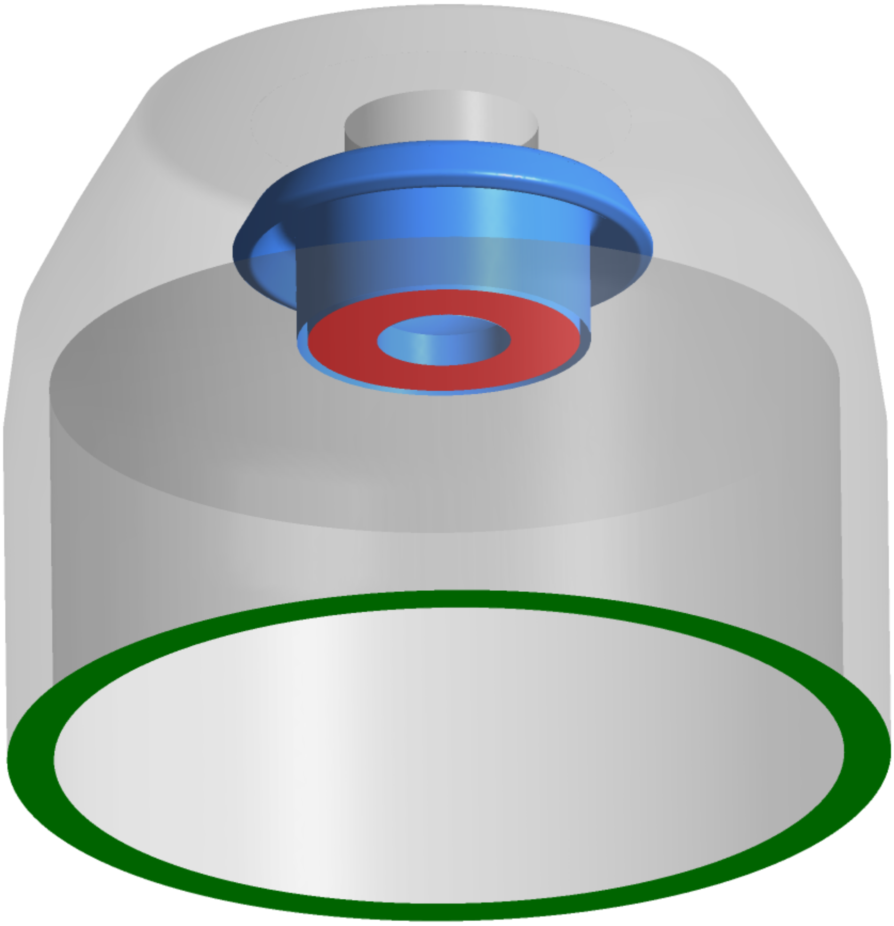

Figure 5.26. Pump geometry showing the turbine, the inlet and the outlet marked with blue, red and green respectively.

If the head loss is calculated from the variation in pressure between the inlet and outlet, the losses produced at the top part of the pump will be included. In the upper part of the pump the losses are created due to changes in flow direction . To investigate the effect of the pump sealing on the head loss, a plane has been placed just above the turbine to measure the loss through the inner part of the turbine. This plane can be seen in red in Figure 5.27

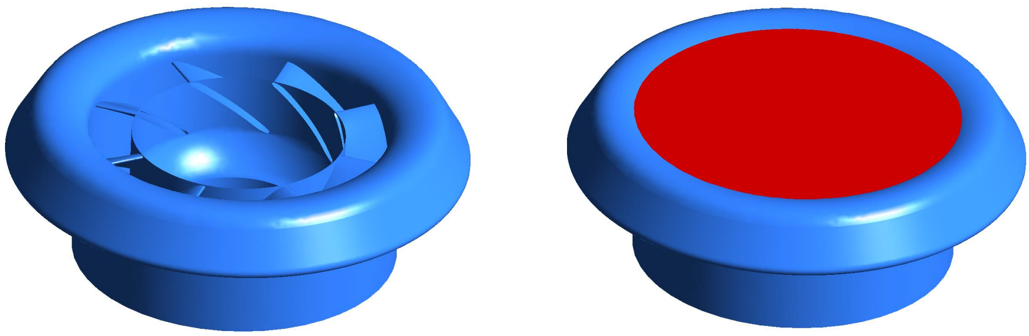

Figure 5.27. Plane just above the turbine for head calculation through the inner part of the turbine.

The loss though the turbine corresponds to 78.4% of the total head loss generated in the model. This percentage only considers the inner part of the turbine. Thereby, not taking the outer part of the turbine into consideration. On the base of this, the final head loss is calculated between the inlet and the outlet of the CFD simulation, to be able to see the variations generated by the outer part of the turbine.

The simulated head loss is compared with the experimental results as seen in Figure 5.28. The experimental head loss corresponds to the deviation between the two curves in Figure 5.25.

Figure 5.28. Comparison of head losses from experimental and the simulated results.

As it can be seen in Figure 5.28, the two head losses increase linearly with the flow rate. The slope of the simulated curve is steeper. At low flows it shows slightly smaller losses but for most of the flows, it present higher losses than the experimental results.

5.5.1 Conclusion of the verification process

In the process of validating the CFD model, it has not been possible to accurately simulate the rotational speed measured from experiments. However, for further analysis, it is assumed that the tendency of the deviation at different flow rates is maintained despite the turbine geometry. Hence, the rotational speed can be estimated down to an acceptable range of rpm. This will be investigated further in Chapter 6 where results from geometry modifications are shown.

The next essential parameter of validation is the simulated head losses. The simulated results shows a small error until 10 m^3/hr. At higher flow the simulated results develops a larger head loss.

On the basic of these investigations, the model is considered to be verified and able to determine; the rotational speed and the head losses in the system. However, for accurate head losses at flows above 10 m^3/hr experimental data are needed.

5.6 Model uncertainties

In this section possible variants in the models and the experiments will be investigated to see their effect on the rotational speed. Furthermore, the assumptions used in the modelling parts will be described to discuss possible deviations. The most relevant among these are analysed in the following paragraphs.

Bearing friction uncertainties

Some of the parameters contained in the friction calculation includes some uncertainties. First, the water viscosity that lubricates the bearing, depends on the temperature. The fluid contained between the surfaces could experience an increase in temperature, reducing its viscosity and thus the friction. Also, it is assumed that the whole space between the surfaces is fully occupied by water. Another uncertainty is the friction coefficient implemented between the non lubricated surfaces in contact. Finally, the distance between the lubricated surfaces could have a variation of $\pm 0.02mm$ from the value used during calculations. Depending on this variations, the friction value will oscillate within a certain range. A sensitivity analysis is required to define the effect of this variation on the turbine behaviour. Table 5.4 demonstrates the variation in angular velocity due to changes in the distance between surfaces, friction coefficient and temperature. The value termed “Base case” was calculated with a friction coefficient of 0.01, a clearance between lubricated surfaces of 0.05 mm and at a temperature of 25°C.

Exp. angular velocity	**Variations simulated**									
	Base case		**Friction Fr=0.02**		**Clearance distance 30μm**		**Clearance distance 70μm**		**Temp. 35°C**	
[rpm]	**[rpm]**	**[%]**	**[rpm]**	**[%]**	**[rpm]**	**[%]**	**[rpm]**	**[%]**	**[rpm]**	**[%]**
1228	1341	8.43	1335	-0.45	1327	-1.04	1350	0.67	1350	0.67
1782	2002	11.03	1991	-0.55	1992	-0.50	2008	0.30	2008	0.30
2456	2917	15.80	2899	-0.62	2907	-0.34	2922	0.17	2921	0.14

Table 5.4. Sensitivity of the angular velocity to different parameters.

The new friction coefficient is the double of the one used on the base case. By applying this coefficient, the change in angular velocity is around 0.5% of the base case. The change in the clearance produces a larger variation corresponding to 1.04%. Finally, a 10°C change in temperature is investigated, generating a variation below 1%. A more radical change in temperature will increase further the turbine revolutions, but as it can be seen in Figure 5.29, the viscosity slope is less steep at higher temperatures. Consequently, the viscosity is less dependent of temperature.

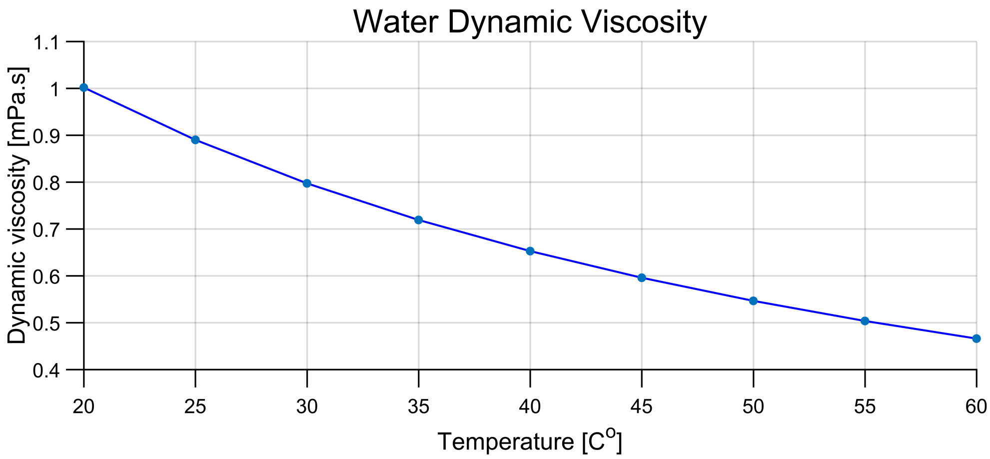

Figure 5.29. Water viscosity at different temperatures [Wagner and Kretzschmar, 2008].

Next, two opposite cases are considered. The first where the variations reducing the friction torque meaning high temperature, larger clearance and low friction coefficient. The second case displays the opposite behaviour. The results for this scenarios are presented in Table 5.5.

Flow rate	**Base case**	**Minimum torque**		**Maximum torque**	
[m³/hr]	**[rpm]**	**[rpm]**	**[%]**	**[rpm]**	**[%]**
6	1341	1356	1.12	1319	-1.64
10	2002	2012	0.50	1979	-1.15
14	2917	2925	0.27	2889	-0.96

Table 5.5. Maximum and minimum values for the frictional torque.

Under the premise that the counter torques calculated on the base case were underestimated, the torque should be adjusted to a higher value. The difference between the experimental and the simulation results would be reduced to 6.79, 9.88 and 14.84% for the three flows, 6, 10, and 14 m^3/hr respectively.

Surface roughness

The surface roughness of the turbine prototype used for experiments plays an important role in the interaction between the turbine and the flow. The prototypes are produced by additive manufacturing allowing the creation of complex shapes in a relative short time. In this technique, layers of polymer are placed successively on the top of previous layers until the designed shape is completed, thus it is also known as 3D printing. Although this is an optimal technique for prototype production, grooves are formed between two adjacent layer, creating a certain roughness on the prototype surface. According to studies this roughness is in the order of 10 to 40 μm [DEZS and KOSA, 2012], [Garcia et al., 2013], [Dubey et al., 2014]. This range, a higher value of 60 μm and a case 0 μm have been used to analyse the effects of the surface roughness in the model. The results from this study can be seen in Table 5.6.

Roughness [μm]	Force Blades [N]	Torque Blades [N-m]	Torque Hub [N-m]	Torque Turbine Wall [N-m]	Torque Shroud [N-m]	Head [m]
0	14.928	-0.0981	0.0022	0.028	0.011	-0.827
20	14.992	-0.0962	0.0027	0.030	0.014	-0.829
40	15.134	-0.0953	0.0030	0.033	0.016	-0.829
60	15.232	-0.0939	0.0034	0.036	0.018	-0.828

Table 5.6. Roughness influence on the turbine performance.

The results shows an increase in all counter torques and a decrease in the driving torque generated by the blades. This phenomenon is due to the increase in surface roughness, which in turbulent flow entails the roughness elements to extend further into the boundary layer. This expansion into the boundary layer generates a larger drag and thereby slows down the rotation of the blades [Cengel and Cimbala, 2006]. Under the validation of the CFD model a surface roughness of 40 μm was used. To see the variation when the roughness is increased to 60 μm or decreased to 20 μm. These two variations have been simulated to see the deviation in the rotational speed. The deviation can be seen in Figure 5.30.

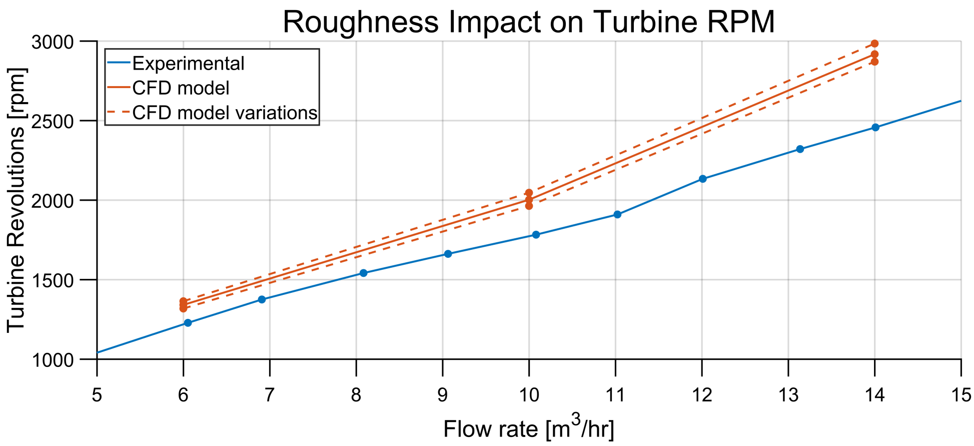

Figure 5.30. Simulation results of different roughness's compared to experimental results.

It can be seen in Figure 5.30 that the simulation results change with the flow rate. Hence, a larger flow rate generates higher deviations. The exact deviation in rpm can be seen in Table 5.7.

Roughness [μm]	6 [m^3/hr]	10 [m^3/hr]	14 [m^3/hr]
20	23	44	67
60	23	39	47

Table 5.7. Roughness influence on the turbine performance.

Leakage effect on the turbine rpm

The following section will investigate the effect that a leakage would have on the turbine angular velocity. The investigation is performed by decreasing the inlet profiles by 1, 5 and 10%. Thereby, simulating a leakage before the turbine. The results can be seen in Figure 5.31.

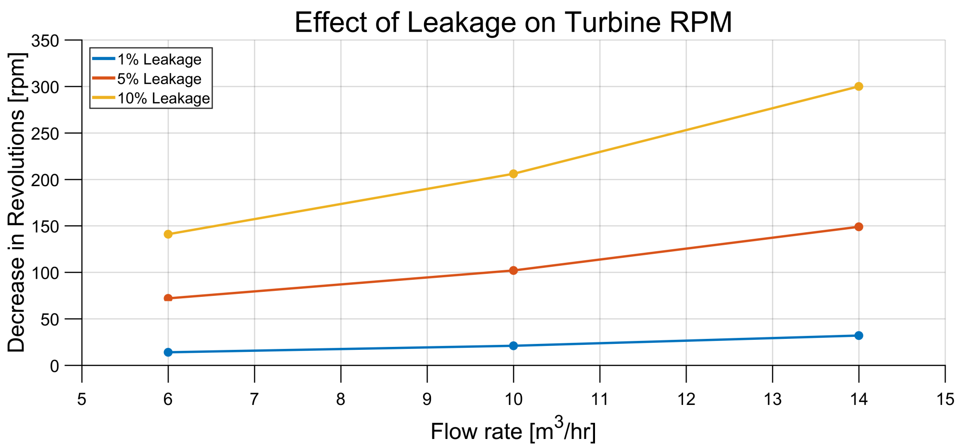

Figure 5.31. Simulation results for a decrease in turbine rpm produced by a leakage of 1, 5 and 10%.

It can be seen in Figure 5.31 that a higher leakage increases the slope of the curves. From 6 to 14 m^3/hr the deviation in rotary speed increases. To see the change compared with the experiment results a leakage of 1 and 5% can be seen in Figure 5.32 (A) and 5.32 (B) respectively.

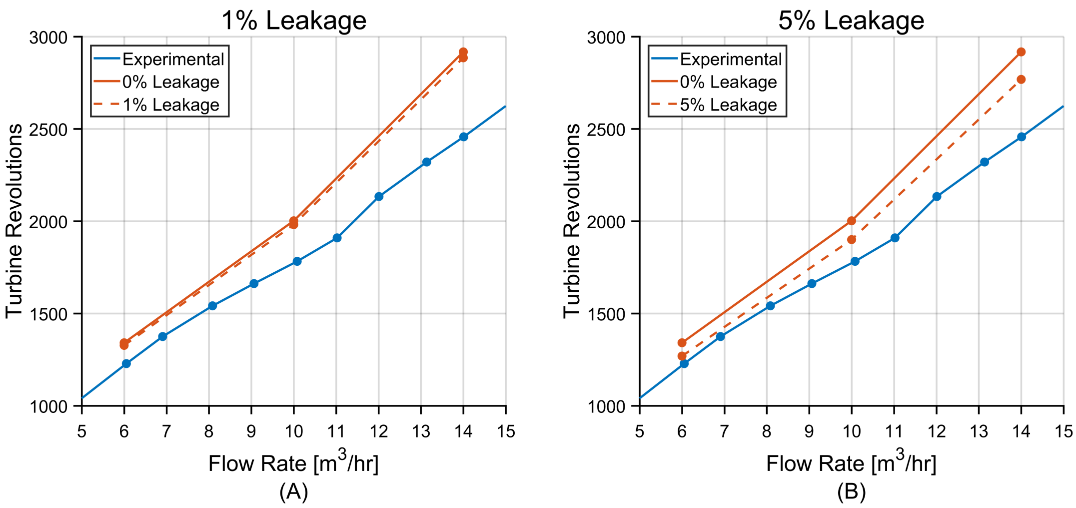

Figure 5.32. Simulation results of a leakage of 1% (A) and 5% (B).

Figure 5.32 shows how the curve is moved down when a leakage is incorporated in the system. Furthermore, the slope of the simulated rotational speed have been decreased.

The slope changes can be investigated by making a linear regression. The slopes change can be seen in Table 5.8.

	Experimental	0% Leakage	1% Leakage	5% Leakage	10% Leakage
Slope	153.5	197.0	194.8	187.4	177.1

Table 5.8. Slope change for different leakage values

It can be seen in Table 5.8 that the slope change is small with the leakage. Hence, it is still improving the tendency to come closer to the experimental results.

5.6.1 Experimental variations

The last variation investigated is generated by the experimental results. These results are mean values representing sets of measurements collected at different flow rates. As for every system, the pump set-up has some fluctuations among the values collected. These fluctuations will be analysed in this section.

In order to determine the dispersion of the experimental results, the average of each set of 10 values was calculated. Moreover, the maximum and minimum values for every flow rate were used to determine the percentage deviation from the average.
For every flow value used, an angular velocity is allocated and analysed as well. The variations of the experimental results are determined shown in Figure 5.33.

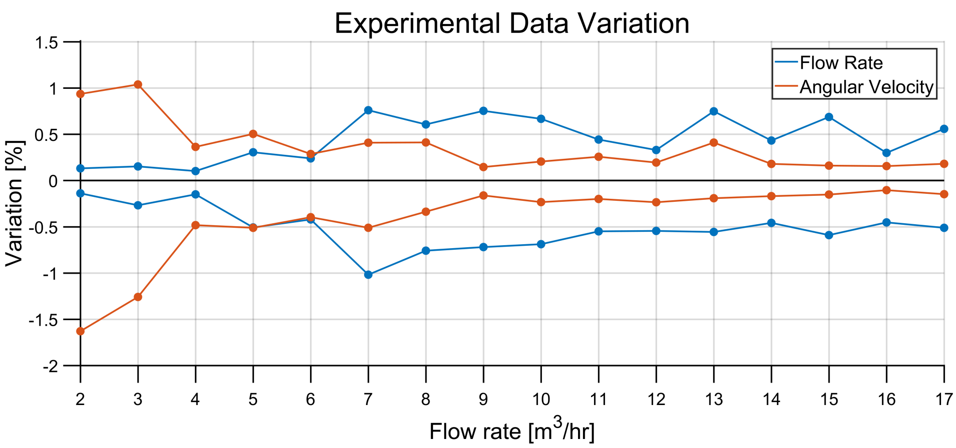

Figure 5.33. Experimental data variation for the flow rate and the angular velocity.

It can be seen that for small flow rates, the angular velocity is erratic compared with the rates obtained at higher flows. Beside this first data, the deviation is maintained within ±0.5 and ±1% for the angular velocity and the flow rate respectively.

5.6.2 Overall Variation

This section describes the overall rpm variation collecting the previously mentioned deviations. The following variations is used in the overview:

- Friction coefficient of 0.02.
- Clearance distance of 30 and 70μm.
- Roughness of 20 and 60μm
- 2% leakage.
- Rotational speed variation from experiments.
- Flow rate variation from experiments.

The summation of all the above mentioned variations can be seen on Figure 5.34.

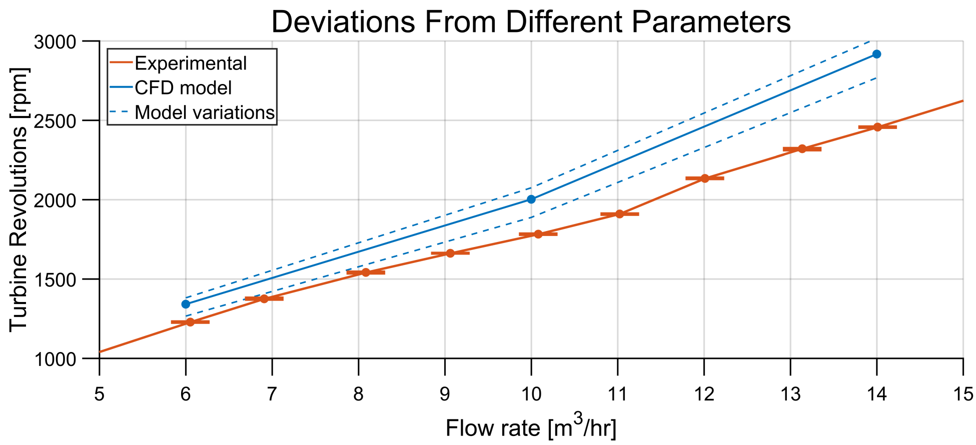

Figure 5.34. Notarial deviation from different parameters.

In Figure 5.34, it can be seen that the variation from the experiments is relatively small. The only variation affecting the experiments is the rotational speed, generating a difference from 2.4 up to 8.4 rpm. The rpm values extracted from the model before and after the variations can be seen in Table 5.9.

Flow Rate $[m^3/hr]$	**Rotational speed measured from experiments** $[rpm]$	**Rotational speed before variations** $[rpm]$	**Rotational speed after variations** $[rpm]$
6	1228	1380	1256
10	1782	2075	1888
14	2456	3016	2768

Table 5.9. Comparison of the rotational speed before and after incorporating the parameter variations.

The results in Table 5.9 show a larger rpm variation at higher flows. After incorporating the deviations decreasing the rpm, a new difference of 2.2, 5.6 and 11.3% for a 6, 10 and 14 m^3/hr respectively.

6 Analysis of Geometrical Modifications.

This chapter presents the analysis of the geometrical changes performed on the CFD model. It presents both, a change in blades number, as well as a change in blade angle. The main focus is on the change in head loss and flow behaviour around the blades. Furthermore, the results from the simulation needs to be assessed in order to decide, whether the investigated geometrical changes are beneficial or not.

The geometrical changes are analysed by investigating the change in head and flow properties around the blades. During the simulation to determine the effects of reducing the amount of blades, an estimated rpm value is used for the simulation. Afterword, experiments will be performed with the new prototype built with the blade number that has shown the best results. Furthermore, the experiments will provide the real turbine rpm results used in the final simulation. For the simulations that studies the change in blade angle, the angular velocity will be estimated, due to lack of experimental results.

6.1 Blade number

To investigate the blade numbers effect on the head loss in the system, some blades are removed from the CFD model. Hence, two new turbines are generated with three and four blades. Figure 6.1 shows the two new turbines.

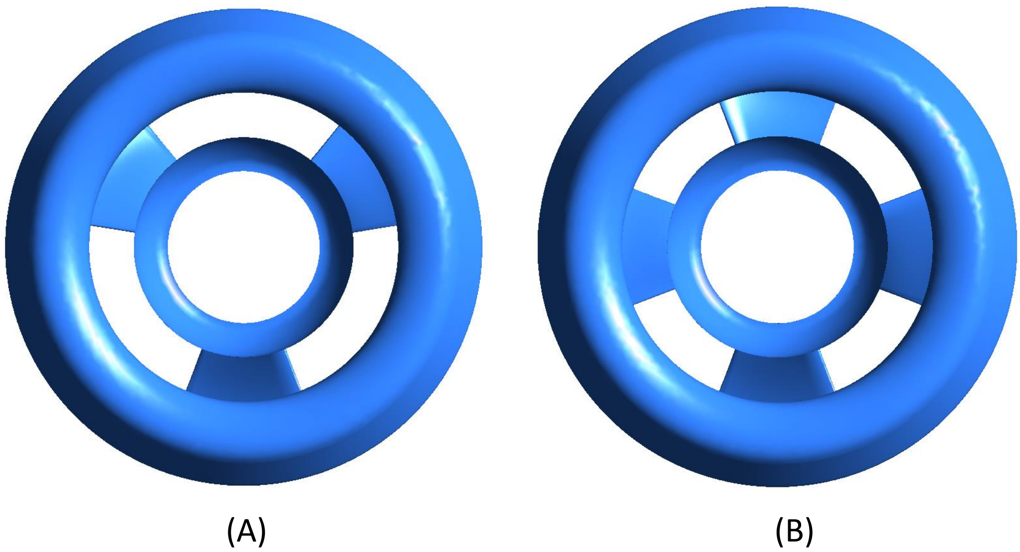

Figure 6.1. Illustration of the turbine design with 3 blades (A) and 4 blades (B).

To determine the best number of blades, the simulated head loss of the three designs has been investigated. Figure 6.2 shows the head loss for the three designs.

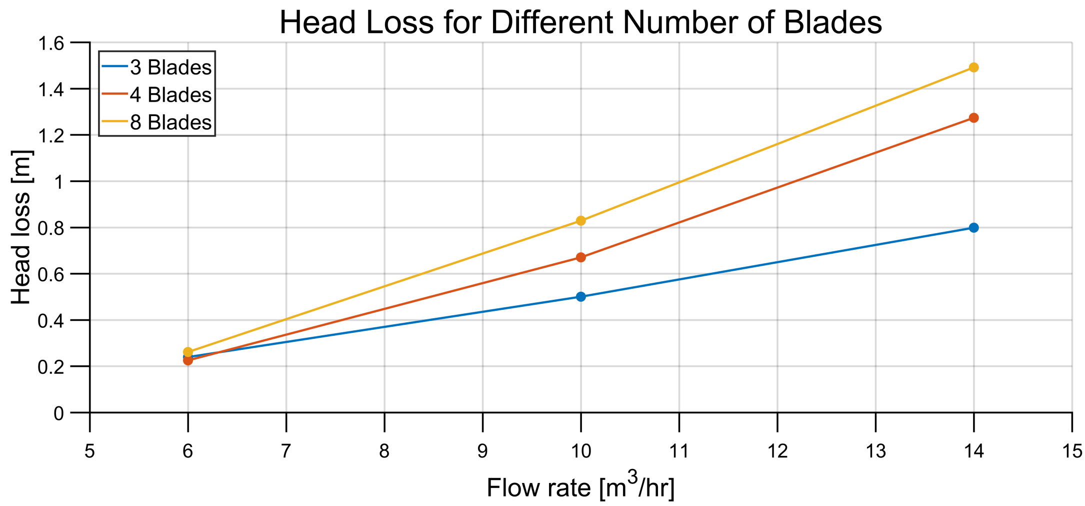

Figure 6.2. Comparison of the head losses in the system with 3, 4 and, 8 blades.

As it can be seen in Figure 6.2, the head losses increases at higher flow rates and decreases with a reduction in blade number. Furthermore, the losses of the 3 bladed design has a less steep slope than the other two designs.

A separate calculation was made by using the Zweifel criteria, Equation , and assuming an angle of attack between 10° and 15°. The results shown a turbine solidity that oscillated between 2 and 3 blades. The usage of a 2 bladed turbine could affect the low range detection, thus it was not considered as an option.

On the basic of the results presented in this section, it is concluded that the 3 blades turbine generates the smallest head loss, thereby being the best design for further investigations.

6.2 The influence generated by the change of blades

To investigate the difference generated by the change in blade number, the flow behaviour around the blades is analysed. The flow around the blades is mainly dependent on two parameters: The angle of attack and the velocity. Figure 6.3 shows the angle of attack for the 8 and 3 bladed turbine for 10 m^3/hr (A) and 14 m^3/hr (B).

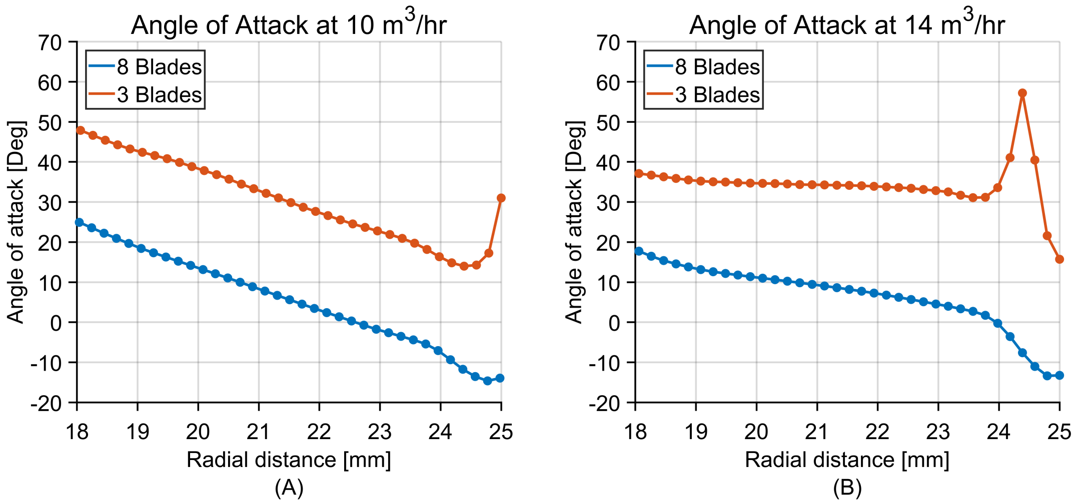

Figure 6.3. Angle of attack for the turbine with 3 and 8 blades at 10 m^3/hr (A) and 14 m^3/hr (B).

The figures shows an increasing angle of attack for both flows when blades are removed from the turbine. The reason for the increase lies in the number of blades used to guide the flow. A smaller number of blades have more difficulties guiding the flow as seen in Section 3.3.2. Thus, the angle of attack moves closer to the angle from the inlet conditions.

In the following section, the change in velocity between the 8 and the 3 bladed turbines will be investigated. The investigation will be performed at the center of the blade and at a flow rate of 10 m^3/hr and 14 m^3/hr.

Flow behaviours at 10 m^3/hr

In the following, the velocity behaviour around the blades will be investigated at a flow rate of 10 m^3/hr to show the effects of decreasing the number of blades. Figure 6.4 shows the velocity distribution around the middle part of the blades for the 8 bladed (A) and the 3 bladed turbine (B) with a flow rate of 10 m^3/hr.

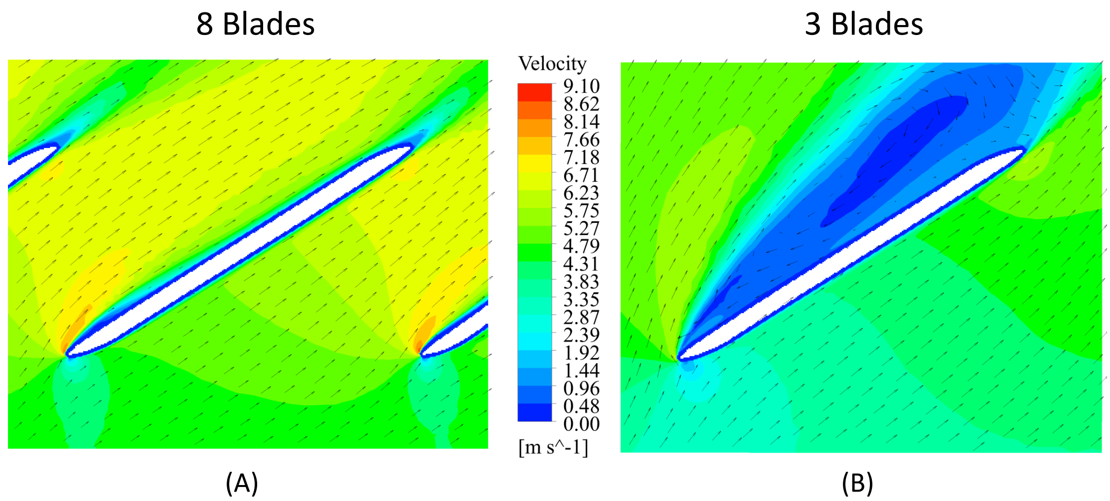

Figure 6.4. Comparison of velocity at the middle of the blade with a flow rate of 10 m^3/hr for the turbine with 8 blades (A) and 3 blades (B).

In the figures, it can be seen how a larger separation is formed when going from 8 to 3 blades. The increased separation is due to the wider spacing between blades. The guidance of the fluid is no longer performed by the neighbouring blades. The angle for the 8 bladed is 6.2°, while the angle for the 3 bladed is 32.8°.

Flow behaviours at 14 $\mathbf{m^3/hr}$

In this section, the velocity behaviour around the blades will be investigated at a flow rate of 14 m^3/hr. This is done to see whether the tendency from a flow rate of 10 m^3/hr is repeated at 14 m^3/hr. Figure 6.5 shows the velocity distribution around the middle part of the 8 bladed (A) and the 3 bladed turbine (B) with a flow rate of 14 m^3/hr.

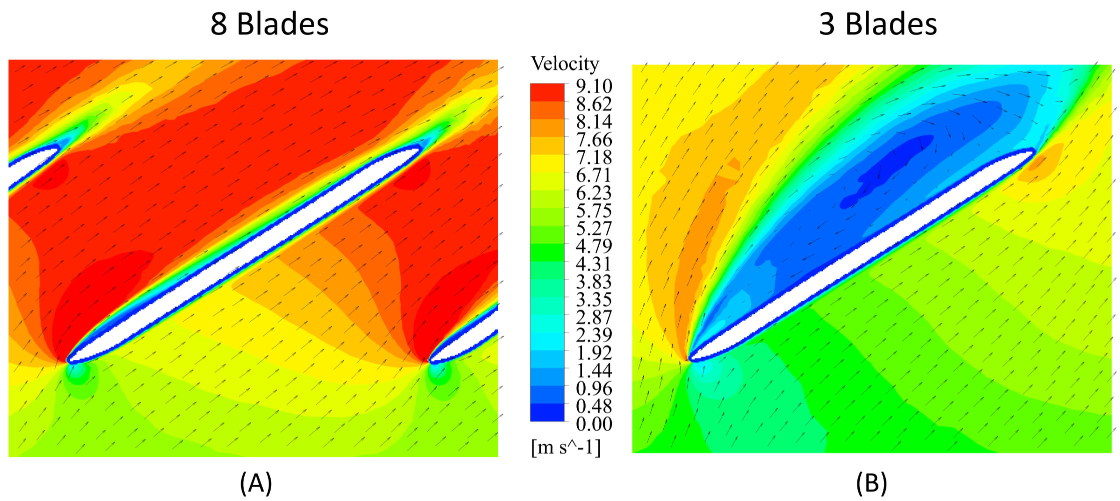

Figure 6.5. Comparison of velocity at the middle of the blade with a flow rate of 14 m^3/hr for 8 bladed (A) and 3 bladed turbine (B).

The figures shows the same tendency as seen in Figure 6.4 where a clear separation is generated between the 8 and 3 bladed turbine. In this case the angle of attack changes from 8.4° to 25.3° exhibiting a smaller deviation in angle of attack. At 10 m^3/hr the difference in angle was 26.6° while the deviation at 14 m^3/hr represents a difference of 16.9°. For more images depicting the flow behaviour around the blades see Appendix B. The change in blades generates an overall increase in the angle of attack and thereby develops a separation around the blades. It is concluded that the 3 bladed performance, in comparison with the flow field and separation around the blades, is worse than the 8 bladed. On the contrary the models shows a smaller head loss in the system with 3 blades. To further investigate the deviation between the 3 and the 8 bladed turbines, a prototype of the 3 bladed turbine is 3D printed to analyse its performance experimentally. The data from the new design is investigated in the next section.

6.3 Analysis of the experimental data

This section present some of the data collected from the experimental work performed at Grundfos facilities. The differences between the data from the 3 and the 8 bladed turbine are discussed.

During the experimental work, different data were collected from three set-ups. The first experiment was for the pump without the flow meter, the second and third experiments included the 8 and the 3 bladed turbine respectively. As it was described in section 4.2, sets of data are logged both for the water flow and the turbine angular velocity. The linear relation between the flow and the turbines rotational speeds was demonstrated during the experimental work. This relation is presented in Figure 6.6.

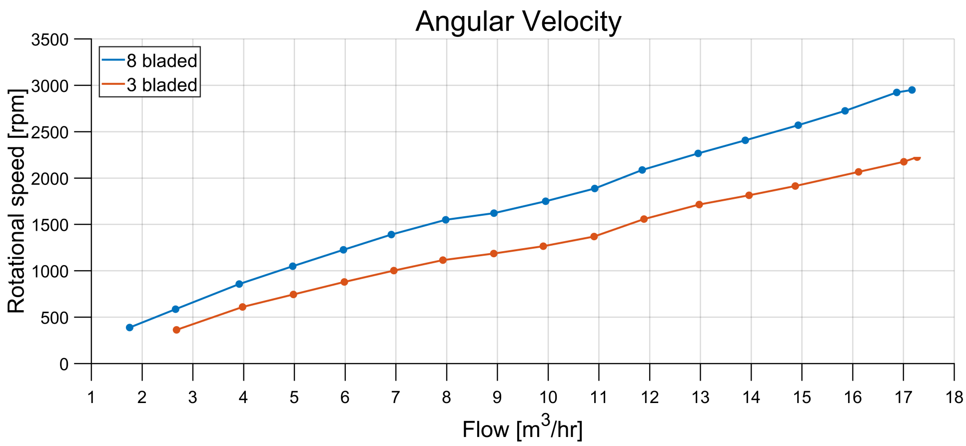

Figure 6.6. Experimental data for the system flow and the turbine angular velocity.

As expected, the turbine with more blades has a higher angular velocity. Besides, the slope of the 3 bladed turbine is less steep. The first flow detected for the 8 bladed turbine was at 1.75 m^3/hr while the first flow reported from the 3 bladed prototype was at 2.68 m^3/hr. This difference is related with the fact that at low flows the 3 bladed turbine rotates at an angular velocity which is below the magnetic sensor detection range. Next, an analysis will be performed on the dispersion of the collected experimental data. The flow data obtained experimentally does not show any substantial difference for the three experiments, meaning that the TFM does not affect the flow stability of the system. This was expected considering the good performances that the TFM has presented. On the contrary some differences can be found by analysing the standard deviation of the angular velocities that are presented in Figure 6.7

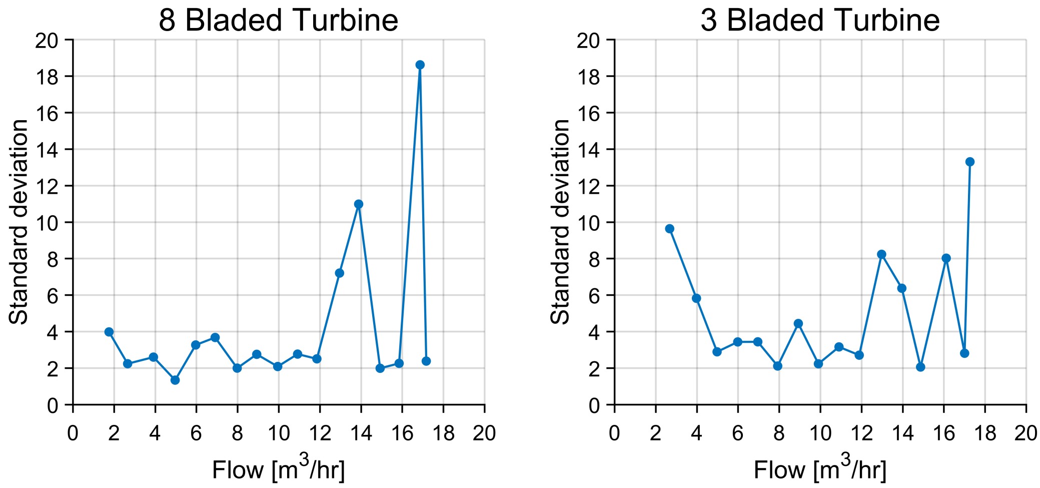

Figure 6.7. Comparison of the angular velocity standard deviation for the 3 an 8 bladed experimental values.

Different behaviours are depicted by this curves. At high flows values appear more erratic while at the rest of the graph they look more stable. The 8 bladed turbine presents more stable values for low flows than the 3 bladed turbine. This could be related to the lower rotational speed reported by the 3 bladed prototype. Above 12 m^3/hr a more spread standard deviation shows that the values are less compact. Nevertheless, at high flows the rotational speed is also higher, and these variations are less important in proportion to the mean value reported for the set. The data deviation between 5 and 12 m^3/hr is quite alike for both designs.

6.4 Comparison with experimental data

In the following section, the simulated speed and head loss will be compared with the experimental data generated at Grundfos. The first parameter to be investigated is the rotational speed. Figure 6.8 shows the comparison between the results from the simulation of the 3 bladed turbine and from the experiments.

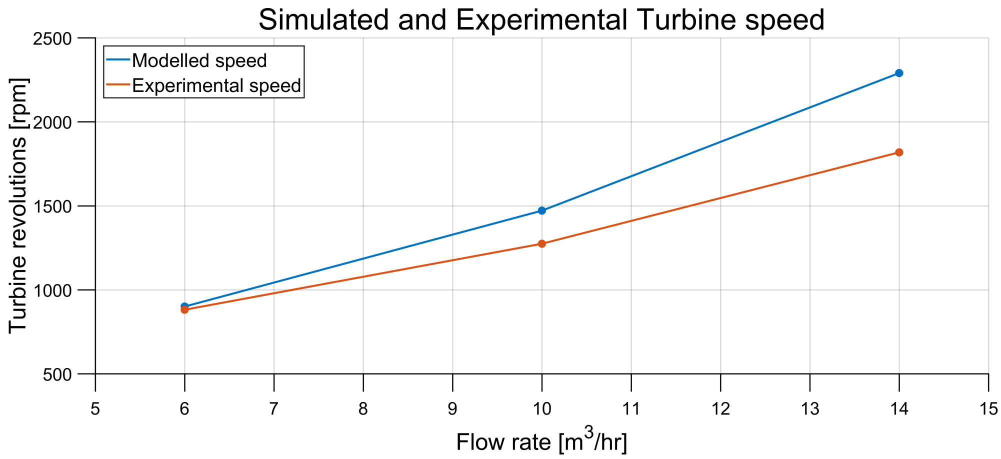

Figure 6.8. Comparison between experimental and simulated data.

The simulated results show a steeper tendency than the experimental data. The model simulates a deviation of 2.1% at a flow rate of 6 m^3/hr, 13.4% deviation at a flow rate of 10 m^3/hr, and a 20.6% deviation when simulation at 14 m^3/hr. To investigate the change in deviation between the 8 and 3 bladed turbine a comparison can be seen in Table 6.1.

Flow rate [m^3/hr]	8 blades deviation [%]	3 blades deviation [%]	Deviation between 8 and 3 blades [%]
6	8.4	2.1	-6.5
10	11.0	18.6	2.4
14	18.8	20.6	4.8

Table 6.1. Experimental flow rate and corresponding turbine rotational speed.

In Table 6.1 it can be seen that the deviation between 8 and 3 blades have a maximum change of 6.5%. Using the model deviation measured from the 8 bladed turbine, the maximum difference in rpm is calculated and an error of 6,5% is predicted for the simulation of the 3 bladed turbine. The error produced is considered within an acceptable range.

Comparison of head losses

The head losses have been used to select the best solution. In the following section the head losses from the three scenarios will be investigated. To have a stable tendency, the experimental results are smoothed by a second order polynomial. The three polynomials have the same R value of 0.9997. Figure 6.9 shows the experimental results from the three turbines.

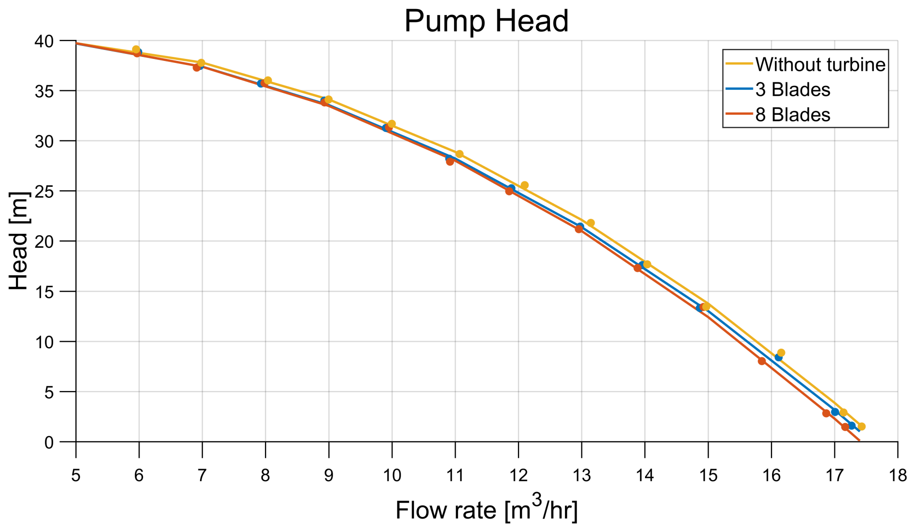

Figure 6.9. Comparison of the head losses from the three turbines with a second order polynomial to describe their tendency.

In Figure 6.9, the experimental results shows a deviance between the 3 and the 8 bladed turbine that starts around 10 m^3/hr and increases with higher flow rates. Next, the simulated results will be compared with the experimental head loss. Figure 6.10 shows this comparison. The experimental head loss is calculated from the difference between the 3 bladed turbine and the experiments performed without turbine.

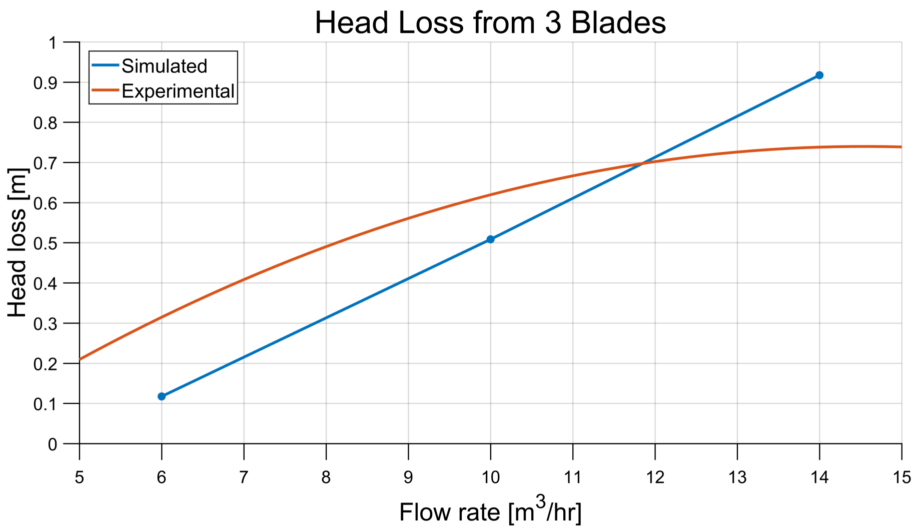

Figure 6.10. Comparison of the simulated and experimental head loss generated by the 3 bladed turbine.

In the figure, it can be seen that the simulated results follows a linear tendency, while the experimental results generates a logarithmic tendency. If the simulated results continue with the same tendency at higher flows, the error will increase with the flow rate due to the rising head loss from the simulation.

Comparison of the efficiency

In the industry, the efficiency is the key parameter when evaluating the performance of a pump. Hence, by comparing the pump efficiency for the three cases analysed, the impact of using different turbines is determined. Figure 6.11 depicts the efficiency for the different turbines used.

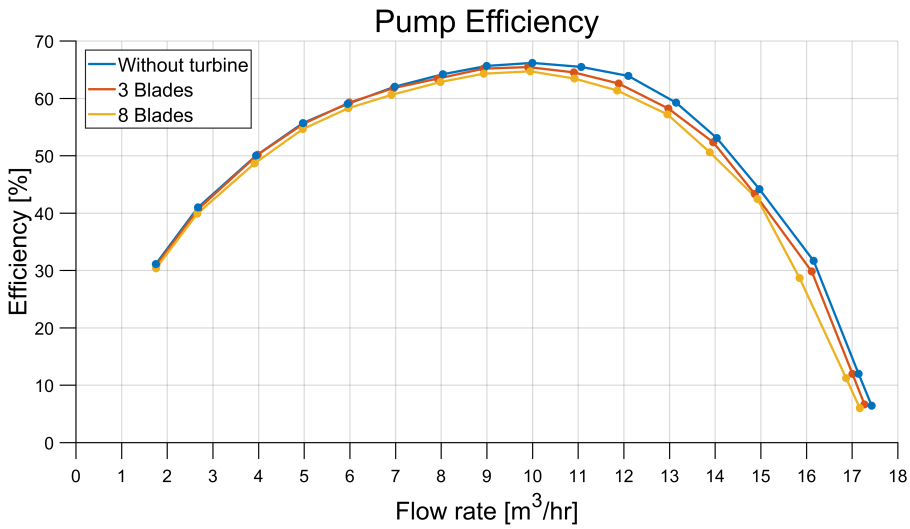

Figure 6.11. Efficiency for the CR 10 pump without and with the two turbines.

In Figure 6.11 the experimental results show an improvement in efficiency when going from 8 to 3 blades in the turbine. In fact, the efficiency of the 3 bladed turbine is almost identical to the pump efficiency without turbine until 7 m^3/hr. For a closer look, the efficiency drop generated by the two turbines is compared in Figure 6.12.

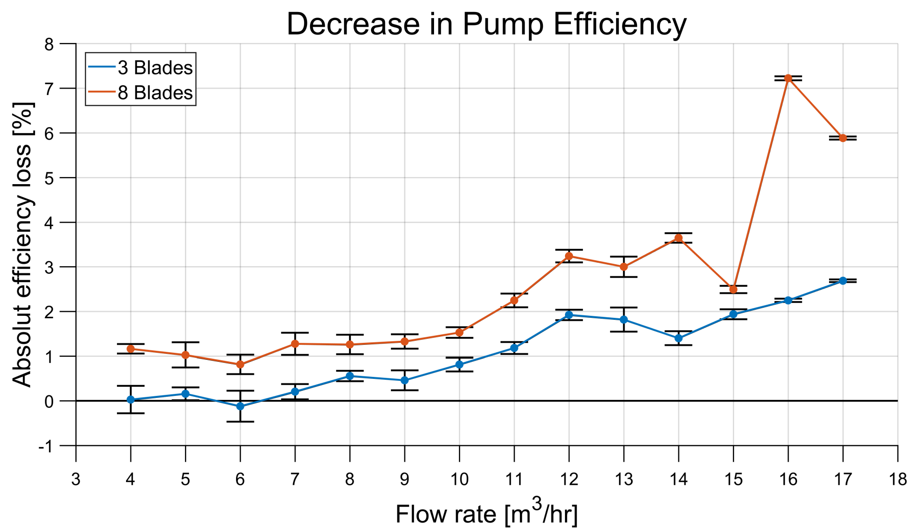

Figure 6.12. Efficiency drop generated by the 8 and 3 bladed turbine with the standard deviation generated from the experimental results.

It can be seen that the 3 bladed turbine has a better performance at all flow rates. When the performance of the 3 bladed turbine is investigated, it can be seen that efficiency loss below 7 m^3/hr only generates a marginal loss. From 7 to 12 m^3/hr the loss increases with around 2%, where it is stabilized until around 15 m^3/hr where the losses increases again. Looking at the overall range from 4 to 17 m^3/hr the 3 bladed turbine have decreased the efficiency loss with an average of 1.49% compared to the 8 bladed, which corresponds to 57.7% of the efficiency loss generated by the 8 bladed.

From the overall investigation of the turbines, it is concluded that the 3 bladed turbine have a better performance and leads to a higher efficiency of the overall system, but also decreases the range where measurements are possible. On the basis of the investigations, it is concluded that the 3 bladed turbine should be used for further optimisations.

6.5 Change in blade angle

After the investigation of the 3 bladed turbine, it has become clear that the high angle of attack generates large amounts of drag on the blades. On this basis, the following step is to investigate the effects of changing the blade angle with 10°. Figure 6.14 pictures the existing blade and the blade with a 10° change.

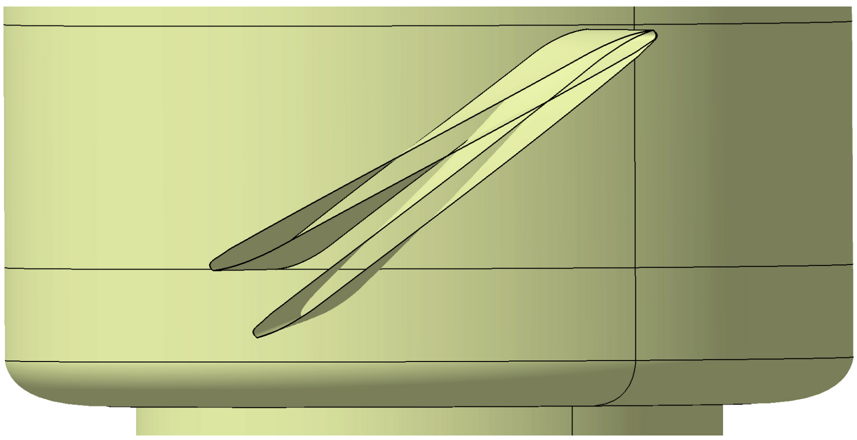

Figure 6.13. Comparison of the existing blade and the blade with a 10 deg change.

After modifying the blade angle, new simulations were made to calculate the new rotational speed. For this purpose, the deviation from the 3 bladed turbine are used due to the lack of experimental data. The deviation can be seen in Table 6.1.
The comparison in rotational speed between the 3 bladed with and without a change in blade angle can be seen in Figure 6.14.

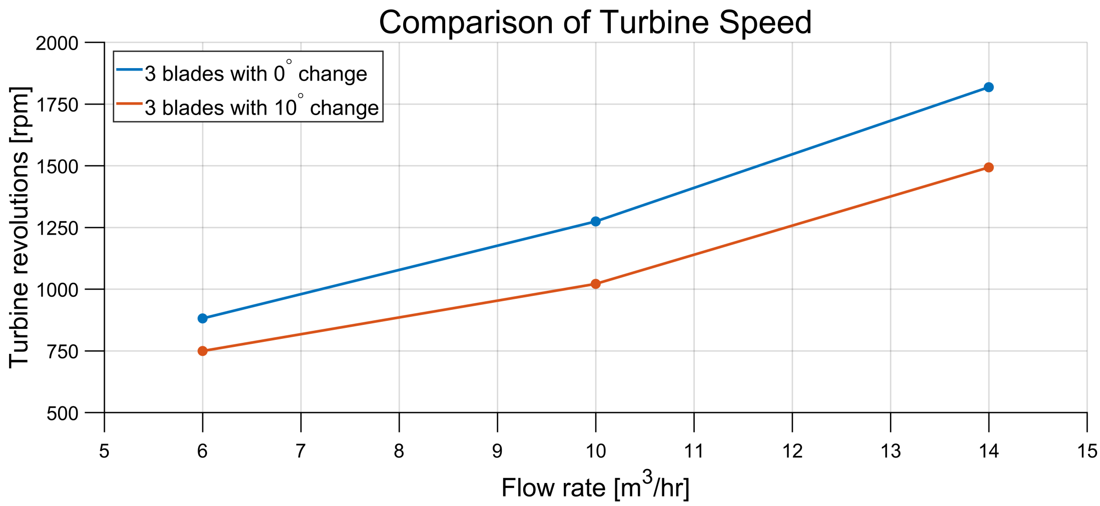

Figure 6.14. Comparison of turbine rotational speed with 0° change and 10° change in blade angle.

After the modification of the blade angle, it can be seen that the turbine speed decreases. Thus, the flow uses less energy to rotate the turbine. Next, the angle of attack is investigated to see its change after the modification of the blade angle. The angle of attacks can be seen in Figure 6.15.

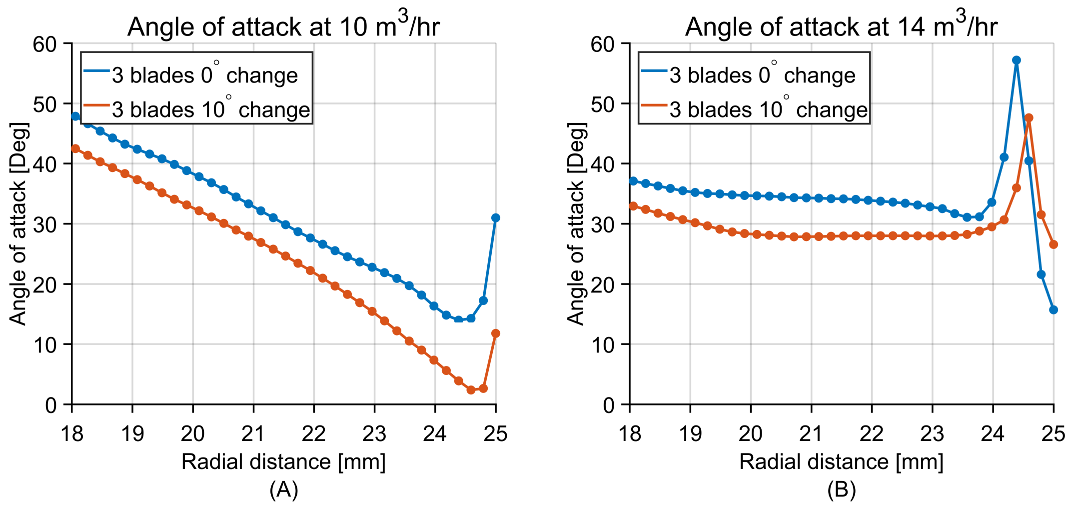

Figure 6.15. Angle of attack for the 3 bladed turbine with a 0 and 10 deg change in blade angle at a flow rate of 10 m^3/hr (A) and 14 m^3/hr (B).

Figure 6.15 shows a decrease of around 5° for the two flow rates. The reason for the small change in angle of attacks is the decreased rotational speed which increases the angle. In the following section the velocity around the blades will be investigated.

Change in velocity around the blades

The investigation of velocity is made at the middle of the blade as earlier comparisons. Figure 6.16 shows the velocities at 10 m^3/hr.

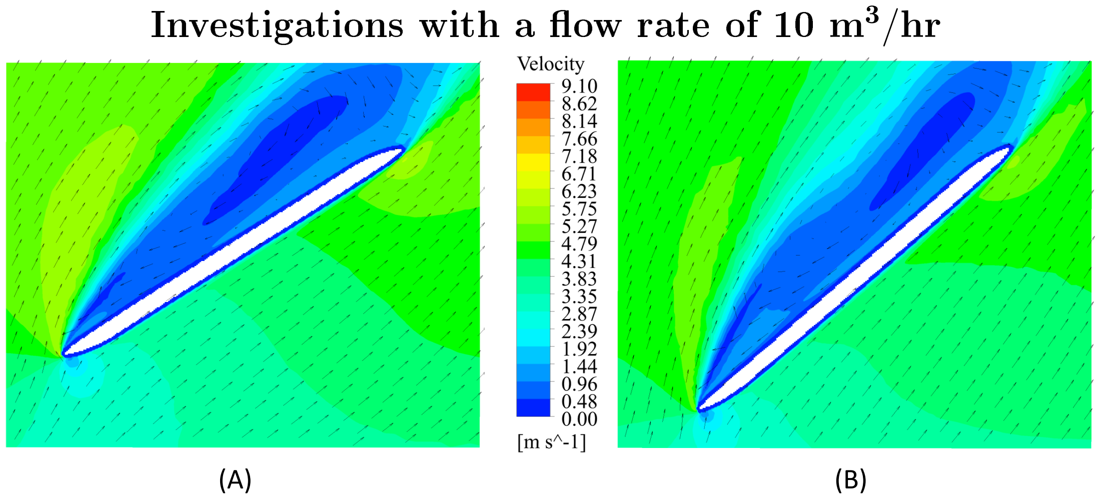

Figure 6.16. Comparison of velocity at the middle of the blade with a flow rate of 10 m^3/hr for 3 blades with 0° change (A) and 3 blades with 10^o change (B).

The figures shows similar behaviours with a small change in thickness and length of the separation. To see if the same behaviour occurs at 14 m^3/hr, this flow rate is investigated in Figure 6.17.

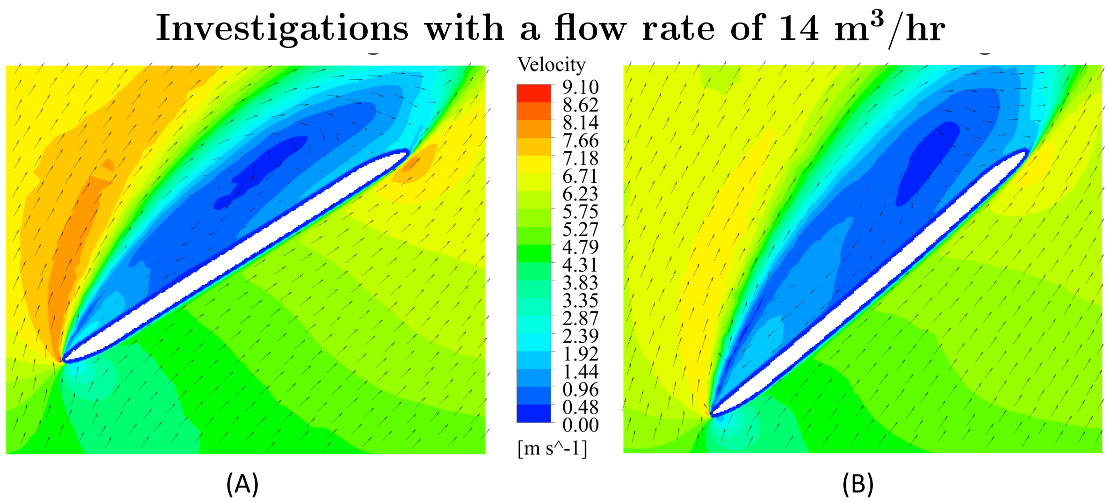

Figure 6.17. Comparison of velocity at the middle of the blade with a flow rate of 14 m^3/hr for 3 blades with 0^o change (A) and 3 blades with 10^o change (B).

Figure 6.17 shows similar changes as the ones observed in Figure 6.16. The investigation of the flow around the blades shows no significant change. Therefore, further investigation is needed to verify the best solution. Thus, the head losses in the two systems will be studied in the following section.

6.5.1 Comparison of head losses

To have an understanding of the difference in losses when performing a change in blade angle, the head losses are compared in Figure 6.18.

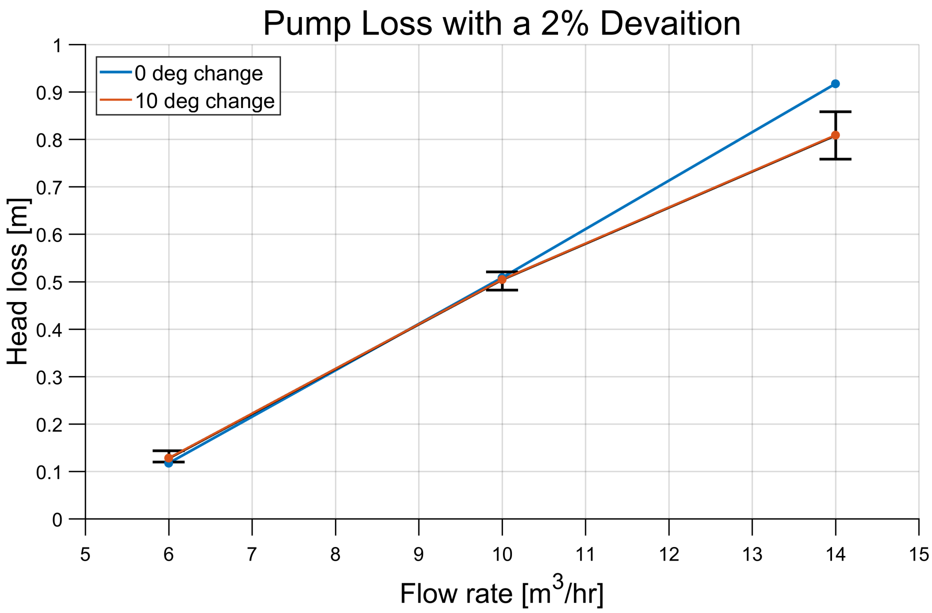

Figure 6.18. Comparison of the head losses with and without a 10° change in blade angle and a 2% rpm deviation in the calculation with a 10° changed blade angle.

The figure illustrates a similar behaviour at flow rates of 6 and 10 m^3/hr. Nevertheless, at 14 m^3/hr the blades with a 10° change generates a smaller loss. Nevertheless, the head loss from the turbine with a changed blade angle is calculated on the assumption that the deviation in rpm is similar to the one without a steeper blade angle. To see the importance of this assumption a 2% deviation in rotational speed has been included in the graph. The deviation shows a large impact at 14 m^3/hr, where half of the distance between the two curves are within the deviation range. If the deviation increases to around 5%, as it was seen between the 8 and 3 bladed (see Table 6.1), it would no longer be possible to decide the best solution. Therefore, experimental data is still needed for validation of the new turbine.

7 Discussion & Conclusion

The following chapter discusses, concludes, and summarises the main results from this project. All results are assessed in order for further understanding and optimisation of the turbine flow meter.

Discussion of the results

In this project, an existing simulation of the CR 10 pump without a turbine provided the inlet boundary conditions for the TFM model. It was considered that this inlet remained invariant despite the usage of a turbine. Usually the incorporation of a new element in a flow would effect the upstream conditions and thereby change the inlet provided by the simulation.

In the construction of the CFD model an unstructured mesh was used, leading to problems in small areas where the inflation layers were not generated according to the chosen setting. Despite this drawback, an unstructured mesh was still chosen based on the time frame of the project and the good convergence of the results. Nevertheless, a more sophisticated mesh could improve the accuracy of the model.

When generating the model the different parameter used were chosen on the basis of the experience of different experts at *Grundfos* and studied literature. In section 5.6 a sensitivity analyses was performed with these parameters to determine their effect on the results. To have an accurate model these parameters need to be further investigated.

As reported in the study, the angle of attack changes along the blade and with the flow rate. Thus, the angle of the blade will not be optimal for every working condition. A blade with a variable angle could improve the behaviour of the turbine in consideration of the angle of attack. Another alternative could be the use of a streamlined profile for the blade shape. Nevertheless, this kind of shapes only have a good performance within a small range of angles of attack reducing their applicability.

The CFD model created and validated with experiments for the 8 bladed turbine showed different deviations in rotational speed with a maximal of 18.8%. Considering these deviations, the predictions for the results of the 3 bladed turbine were within 6.5% from the test results. This deviation in rotational speed will create uncertainties in the calculated parameter since all of them are based on this value. Therefore, experiments may still be needed for further verification of angular velocity.

Key findings

- The investigating of the 8 bladed turbine reveal that it is possible to simulate the rotational speed of the turbine but with an increasing error at higher flows.

- The blade removal study revealed that a smaller number of blades decreases the head loss in the system. The 3 bladed turbine was found the most efficient.
- The reduction in the blade number from 8 to 3 affected only marginally the reading capacity of the flow meter.
- The removal of blades reveal a decrease in angular velocity. Additionally, a smaller flow guidance and higher angle of attack were achieved, leading to flow separation at the blades.
- Experiments with the 3 bladed turbine revealed a decrease in efficiency loss of 57.7% compared to the 8 bladed.
- The change in blade angle revealed a decrease in rotational speed and head loss in the system. However, experiments are still needed for the validation.

A model that can predict the rotational speed has been developed and can be used to investigate further optimisations.
The turbine with 8 blades should be replaced with 3 to minimize the head loss in the system.
An optimisation of the angle of attack for the 3 bladed turbine is required in order to further decrease the head loss.

8 Future Work

Throughout the thesis period, different ideas for further investigations and optimisations have been found. Due to the limited time frame of the master thesis, it has not been possible to make all relevant investigations. Hence, this chapter will give an overview for possible future work in order to improve the CFD model and the turbine flow meter.

In order to validate the results from the change in blade angle, experiments could be done with the new geometry. Furthermore, these experiments would describe the deviation in rotational speed generated from small geometric changes. Thus, minor changes could be validated without experiments.

Instead of validating the existing model, future work could focus on a minimisation of the rotational error. This may be achieved with a structured mesh or by investigating the model parameters further with experiments, to obtain more exact values.

Before making further optimisations on the flow meter the range of operation needs to be specified. With the detailed range it would be possible to enhance the optimisations and overall improve the efficiency of the flow meter.

Additionally, the shape, wide, and length of the blades have impacts on the angle of attack and thereby the main losses in the turbine. Future projects should focus on the adjustment of these parameters to minimise the drag and the lift, to the point where flow measurements is still possible in the whole range of operation.

Finally, future studies could investigate the flow meter's applicability in the whole range of CR pumps. This could be achieved with experimental investigations of the efficiency drop for different pump sizes.

A Basic theory

This chapter deals with some of the basic theory used within this project. First an overview of the momentum equations and the Euler's turbine equation are presented to investigate the momentums affecting the system. Moreover, the rotational forces under ideal and with-slip conditions are investigated. Furthermore, different approaches to determine the losses on the turbine are explored, including the mechanical losses due to the friction on the turbine bearing. As well, the main design parameters related with the turbine performance are described in this chapter.

A.1 The momentum and turbine equation

One of the fundamental relations when studying rotary machines is Newton´s second law, which applied in its momentum form will give information of the interaction between the fluid and the rotor. This expression relates the sum of all external forces working on the fluid to its acceleration. In the field of turbomachinery this approach is important for the analyses of the different energy transfer mechanisms [Dixon and Hall, 2010].

When investigating a system of mass m, the sum of momentums working on the system can be calculated with Equation A.1. This expression provides the change of angular momentum over time.

$$\tau_A = m\frac{d}{dt}(rc_\theta) \tag{A.1}$$

Where r is the distance between the center of mass and the center of rotation, c_θ is the velocity component perpendicular to the radius vector r as seen on Figure A.1.

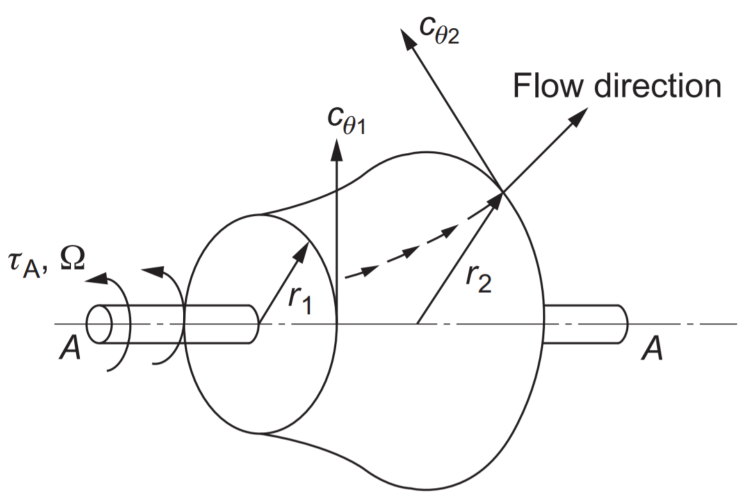

Figure A.1. Control volume for a generalised turbomachine [Dixon and Hall, 2010]

Figure A.1 illustrates a control volume encasing a rotor of a normal turbomachine. Where a swirling flow is entering the domain with a radius r_1, with a tangential velocity $c_{\theta 1}$, and is leaving the domain with a radius r_2, with a tangential velocity $c_{\theta 2}$. For one-dimensional steady flow the torque can be calculated with Equation A.2.

$$\tau_A = \dot{m}(r_2 c_{\theta 2} - r_1 c_{\theta 1}) \tag{A.2}$$

For a turbine running with an angular velocity ω, the work done by the fluid on the turbine can be calculated with Equation A.3.

$$\tau_A \omega = \dot{m}(U_1 c_{\theta 1} - U_2 c_{\theta 2}) \tag{A.3}$$

Where $U = \omega r$ is the blade speed. Then, the work done on the turbine per unit of mass can be specified with Equation A.4.

$$\Delta W_t = \frac{\dot{W}_t}{\dot{m}} = \frac{\tau_A \omega}{\dot{m}} = U_1 c_{\theta 1} - U_2 c_{\theta 2} > 0 \tag{A.4}$$

Equation A.4 is called Euler's turbine equation. Alternatively Equation A.4 can be reformulated as Equation A.5 when adiabatic conditions are assumed.

$$\Delta W_x = (h_{01} - h_{02}) = U_1 c_{\theta 1} - U_2 c_{\theta 2} \tag{A.5}$$

A.2 Rotational forces

This section describes the rotational theory, which is utilised to calculate the rotational speed and the torque generated on the blades by the fluid. The following section is based on [Wadlow, 1998] and is explaining some basic terms and processes.

A.2.1 Ideal rotation conditions

Ideal rotation is defined as a system with a number of simplifications and assumptions. The following assumptions are used for this study:

- The flow is uniform through the turbine.
- The flow is steady and incompressible.
- The rotor is frictionless.
- The rotor is shaped as a perfect helix with infinitesimally thin blades.

Under these ideal conditions the rotational speed is calculated from the pitch of the rotor, s, defined in Equation A.6.

$$s = \frac{2\pi r}{tan\beta} \tag{A.6}$$

Where r is the radius of the rotor and β is the angle of the rotor blades with respect to the axial direction, as seen in Figure A.2.

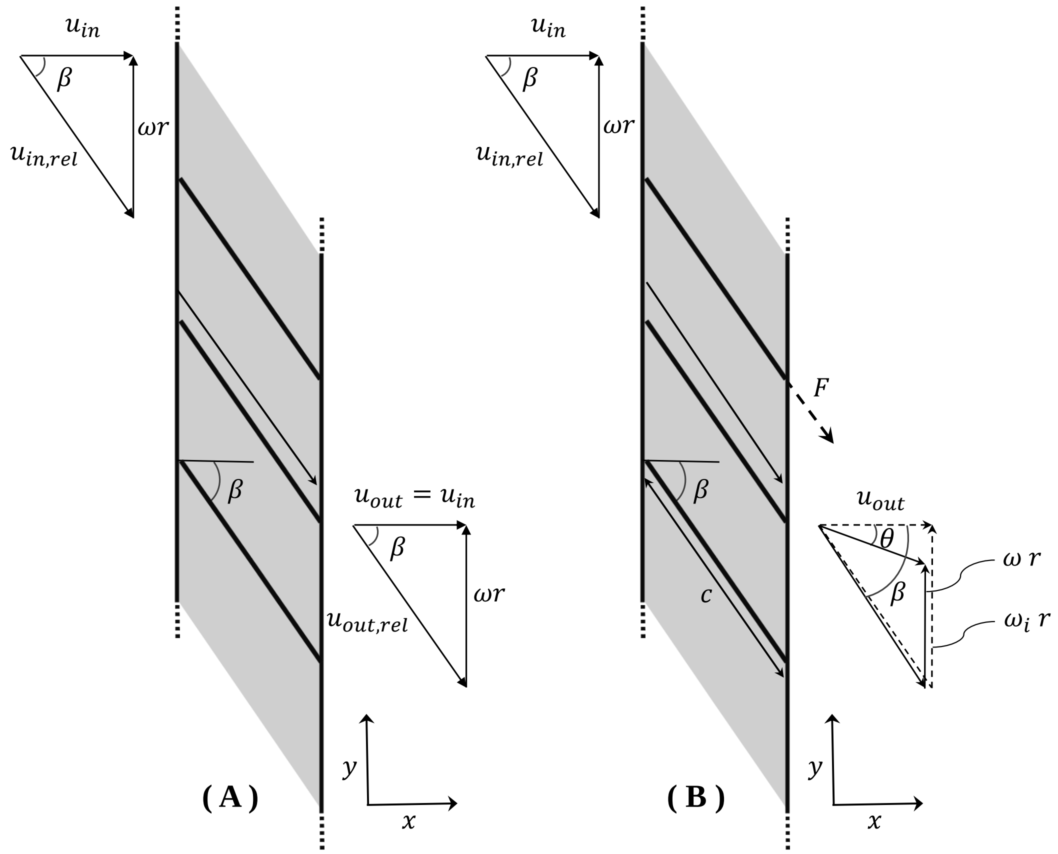

Figure A.2. **(A)** Illustration of steady flow entering and leaving an ideal frictionless rotor with infinitely thin rotor blades with an angle β. **(B)** Vector diagram for a flat blade axial turbine rotor, with the difference between ideal (subscribed i) and the actual tangential velocity which is the rotor slip velocity generated due to the effect of the rotor retarding torques.

As stated earlier, friction is not considered in the ideal case leading to the flow leaving the rotor parallel to the blades. Hence, the inlet velocity and the rotational velocity are related through β as defined in Equation A.7

$$tan\beta = \frac{\omega_i r}{U_{in}} \tag{A.7}$$

Where ω_i is the angular velocity of the rotor for the ideal case and U_{in} is the velocity of the flow entering the rotor. For ideal conditions the angular velocity is defined as in Equation A.8.

$$\omega_i = \frac{U_{in} tan\beta}{r} = \frac{2\pi U_{in}}{s} \tag{A.8}$$

The volumetric flow Q entering the rotor is equal to the velocity of the fluid multiplied by the area as seen in Equation A.9.

$$Q = U_{in} A \tag{A.9}$$

From combining Equation A.8 and A.9 the following relationship between the volumetric flow and the rotational speed can be found:

$$Q = \frac{As}{2\pi}\omega_i \tag{A.10}$$

The relationship in Equation A.10 is used in an actual turbine flow meter in the form of:

$$Q = K\omega_i \tag{A.11}$$

Where K is the meter factor, which normally are found from calibrations. In ideal cases K should remain constant for different operation conditions.

A.2.2 Rotational speed with slip conditions

In the ideal situation the meter response is perfectly linear and only determined by the geometry of the rotor. In reality, there are numerous torques of different importance that oppose the driving torque. At steady flows, the rotor speed is assumed to satisfy the equilibrium stated as seen in Equation A.12.

$$\begin{aligned} Fluid\ driving\ torque = {} & rotor\ blade\ surfaces\ fluid\ drag\ torque + rotor\ hub \\ & and\ tip\ clearance\ fluid\ drag\ torque + rotation\ sensor \\ & drag\ torque + bearing\ friction\ retarding\ torque \end{aligned} \tag{A.12}$$

Referring back to Figure A.2 (B) the actual rotor speed, $r\omega$, and the ideal rotor speed, $r\omega_i$ can be seen. The difference between them comes from the slip velocity created by the counter torques as stated in Equation A.12. This is generated by deflection of the fluid generating swirl, or an exit angle θ. If the radius is denoted by r, and considering that the total change of angular momentum of the fluid passing through the rotor is generated by the overall retarding torque, N_T, Equation A.13 can be obtained [Wadlow, 1998].

$$\int_{r_{in}}^{r_{out}} \frac{\rho Q 2\pi r^2 (r\omega_i - r\omega)}{\pi(r_{in}^2 - r_{out}^2)} dr = N_T \tag{A.13}$$

By integrating Equation A.13 the following equation is formulated:

$$r_d^2 \rho Q(\omega_i - \omega) = N_T \tag{A.14}$$

Where r_d is the difference between the inner and the outer blade radius and ρ is the fluid density. By combining Equation A.13 and A.7 and rewriting, Equation A.15 can be found.

$$\frac{\omega}{Q} = \frac{tan\beta}{r_d A} - \frac{N_T}{r_d^2 \rho Q^2} \tag{A.15}$$

From Equation A.15 it can be seen that the meter response declines with low flow rates and why low friction bearings and other low friction components is needed in gas applications, where the density ρ, is smaller compared with water, and thereby creates a larger decrease in the meter response [Wadlow, 1998].

A.2.3 Torque calculations from airfoil approach

In general there are two methods used for torque calculations; The airfoil approach [Stoltenkamp, 2007] and the momentum approach [Wadlow, 1998]. When using the momentum approach full guidance of the fluid is needed. The airfoil approach, which does not have this constrain, is considered more suitable for this study and will be described in the following section. A TFM is a three dimensional flow device,but for simplification, this three dimensional problem is treated as a two dimensional infinite cascade rotor blades as illustrated in Figure A.3. In the flow meter the flow is calculated between the radius of the hub, r, and $r + dr$ which defines the outer limit of the infinitesimal blades. In the airfoil approach, the driving torque is evaluated by determining lift and drag forces on the rotor blades. The drag force, F_D, acts parallel to the inlet velocity $U_{in,rel}$, and lift force, F_L, acts perpendicular to the inlet velocity. The forces working in the y direction can be expressed in terms of lift and drag forces as seen in Equation A.16

$$F_y = n(-F_L cos\phi + F_D sin\phi) \tag{A.16}$$

where $\phi = \beta - \alpha = arctan\left(\frac{\omega r}{U_{in,x}}\right)$, with β defining the angle between the rotor blade with respect to the x-axis, α is the angle of attack and n is the number of blades. The defined parameters can be seen in Figure A.3.

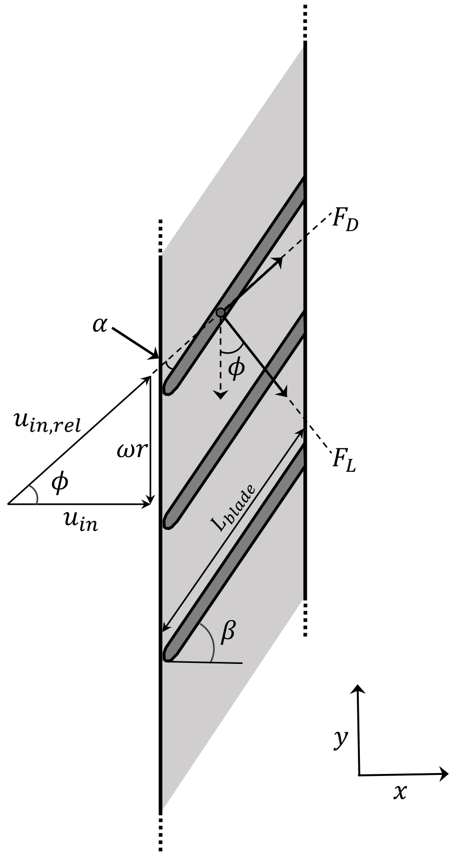

Figure A.3. Lift and drag forces acting on a two dimensional blade.

Figure A.3 illustrates the direction of the lift and drag on a two dimensional blade. The coefficients for the lift and drag are defined in Equations A.17 and A.18 respectively.

$$C_L = \frac{F_L}{\frac{1}{2}\rho U_{in,rel}^2 A_{blade}} \tag{A.17}$$

$$C_D = \frac{F_D}{\frac{1}{2}\rho U_{in,rel}^2 A_{blade}} \tag{A.18}$$

Where A_{blade} is defined by the the chord and the span of the blade. The lift and drag coefficients depends more on the angle of attack and slightly on the Reynolds number. Using Equation A.17 and A.18 the driving torque on the rotor can be defined as:

$$T_d = \int_{r_{hub}}^{r_{tip}} \frac{1}{2} n\rho U_{in,rel}^2 A_{blade} \left(-C_L cos\phi + C_D sin\phi\right) rdr \tag{A.19}$$

A.3 Angle of attack airfoil

Apart from the simple profiles mentioned, more complicated profiles are encountered in literature and each displays different characteristics. The selection of the correct shape profile will depend on the operation condition. As an example, the profiles from the National Advisory Committee for Aeronautics (NACA) can be mentioned. These airfoil profiles have been exhaustively studied and their characteristics are well known. In Figure A.4, lift and drag coefficients are depicted using NACA 2412 as an example, the profile shape is also presented.

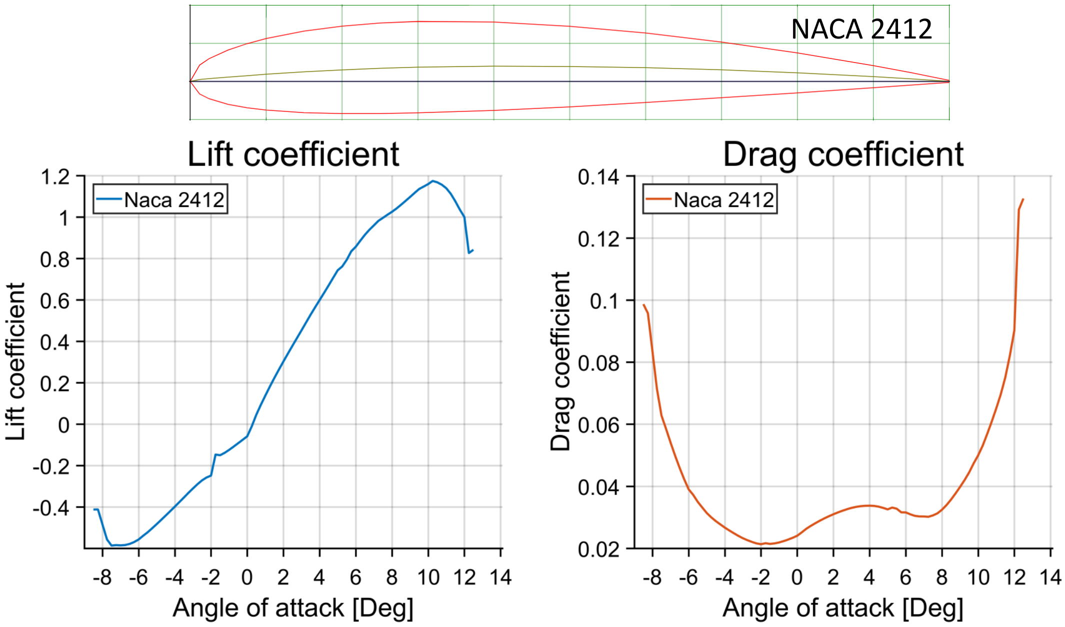

Figure A.4. Lift and Drag coeficients for a NACA 2412 profile with a Reynolds number of 50000 [Tools, 2017].

A.4 Lift coefficient for a flat blade

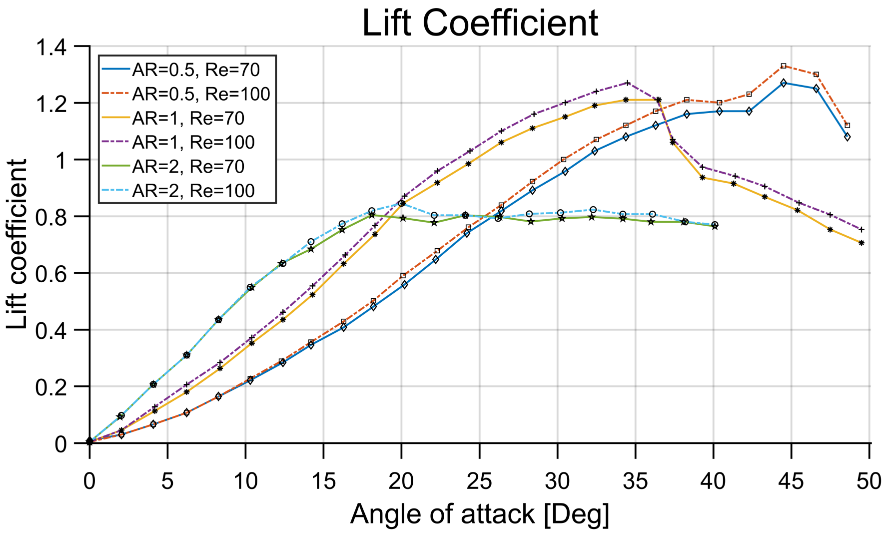

Figure A.5. Lift coefficient at different angles of attack, for different Reynolds number and aspect rations [Torres, 2002].

B Flow Field Around the Blades

In the following some extra pictures illustration the flow velocity around the blades for the 8 and 3 bladed turbine.

Near the hub at 10 m^3/hr

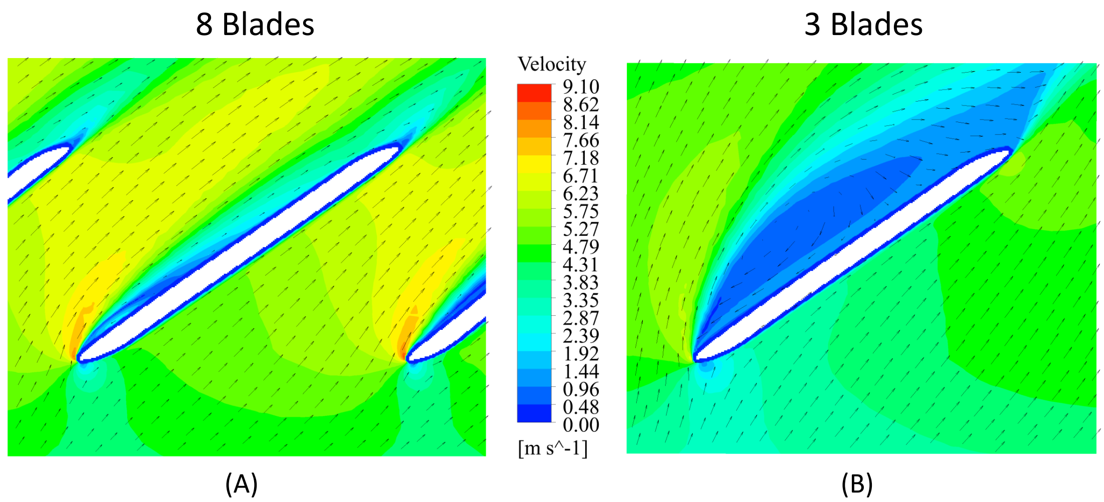

Figure B.1. Comparison of velocity near the hub with a flow rate of 10 m^3/hr for 8 blades (A) and 3 blades (B).

Near the shroud at 10 m^3/hr

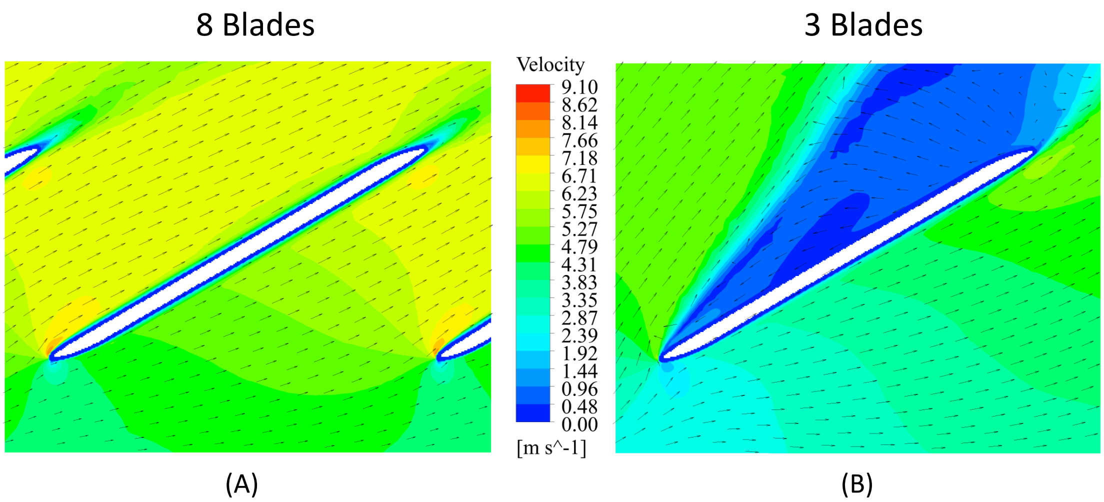

Figure B.2. Comparison of velocity near the shroud with a flow rate of 10 m^3/hr for 8 blades (A) and 3 blades (B).

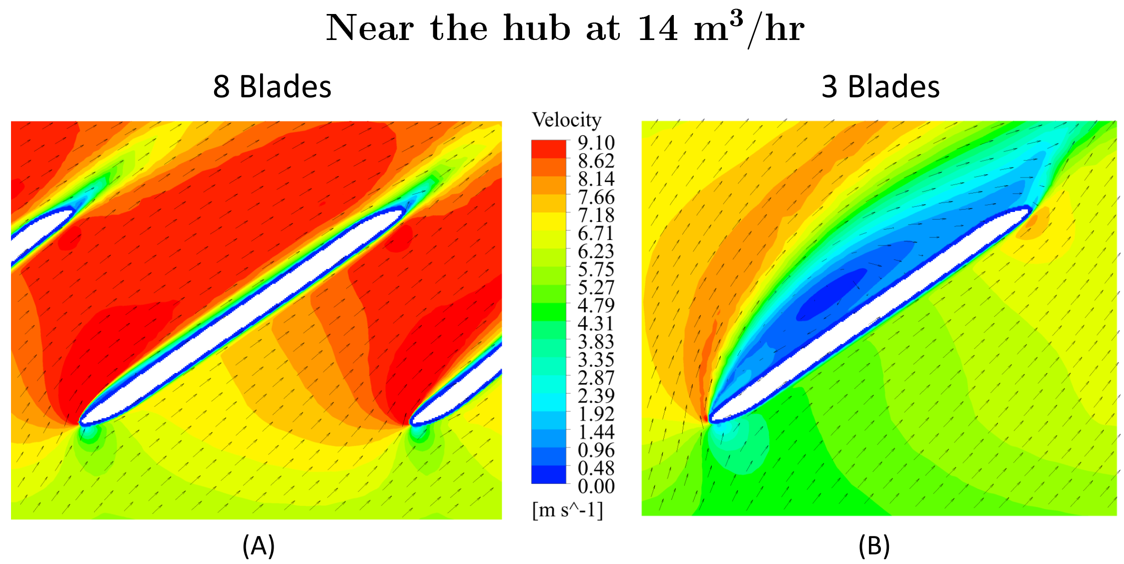

Figure B.3. Comparison of velocity near the hub with a flow rate of 14 m^3/hr for 8 blades (A) and 3 blades (B).

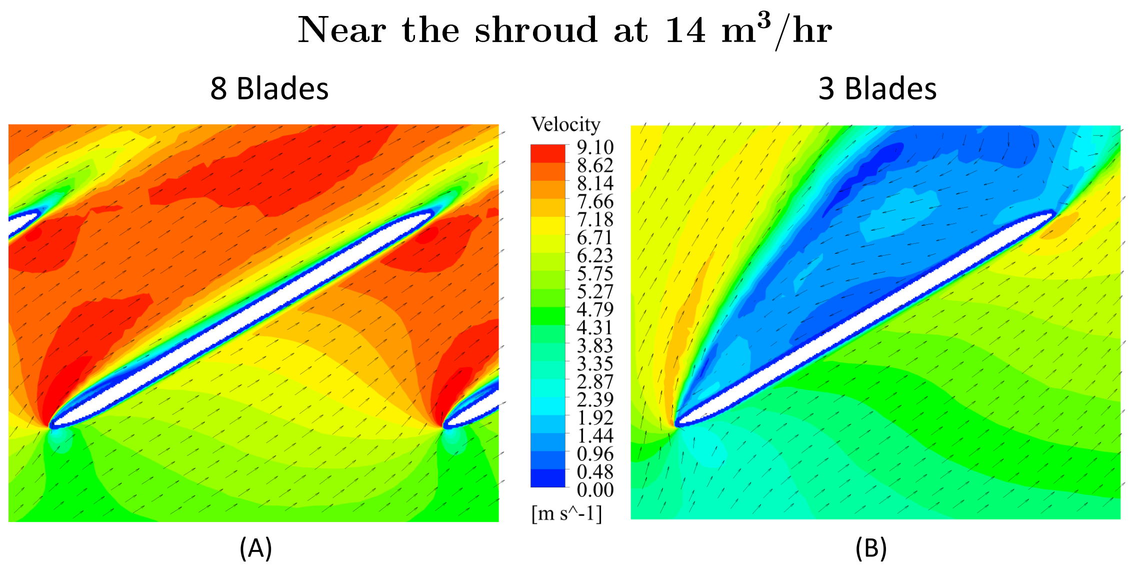

Figure B.4. Comparison of velocity near the shroud with a flow rate of 14 m^3/hr for 8 blades (A) and 3 blades (B).

Bibliography

ANSYS, 2017. ANSYS. *Residuals*, 2017. URL `https://www.sharcnet.ca/Software/Ansys/16.2.3/en-us/help/cfx_mod/i1323887.html`. [Accessed 29-05-2017].

ANSYS, Inc, 2013. ANSYS, Inc. *Ansys fluent theory guide, 2013a.* 2013. URL `https://uiuc-cse.github.io/me498cm-fa15/lessons/fluent/refs/ANSYS%20Fluent%20Theory%20Guide.pdf[Accessed-29-05-2017]`.

ANSYS, Inc, 2016. ANSYS, Inc. *ANSYS Documentation, CFX, Modeling Guide, Turbulence and Near-wall Modeling.* 2016. URL `http://148.204.81.206/Ansys/150/ANSYS%20CFX-Solver%20Modeling%20Guide.pdf[Accessed-29-05-2017]`.

Baker, 1991. R. C. Baker. *Turbine and related flowmeters: I Industrial practice.* 2, 1991. Flow Measurement and Instrumentation Journal, 2,147-160.

Baker, 1993. R. C. Baker. *Turbine and related flowmeters: II. Theoretical and experimental published information.* 4, 1993. Flow Measurement and Instrumentation Journal, 3,123-144.

Cengel and Cimbala, 2006. Y.A Cengel and H. M. Cimbala. *Fluid Mechanics. Fundamentals and Applications. First edition.* Mc Graw Hill, 2006. ISBN 0-07-247236-7.

DEZS and KOSA, 2012. Gergely DEZS and Peter KOSA. *Roughness of Plane Faces Produced by Additive Manufacturing.* 2012. International Journal of Engineering, 2,181-184.

Dixon and Hall, 2010. S.L. Dixon and C.A. Hall. *Fluid Mechanics and Thermodynamics of Turbomachinery Sixth Edition.* 2010. ISBN: 978-1-85617-793-1.

Dubey, Shrivastava, and Singh, 2014. Abhay Kumar Dubey, Ansari Anurag Shrivastava, and Vishnu Pratap Singh. *An Analysis of Surface Roughness Improvement of 3D Printed Material.* 2, 2014. International Journal for Scientific Research & Development, 2,312-314.

Garcia, Rumpf, Tsang, and Barton, 2013. C.R. Garcia, R.C. Rumpf, H.H. Tsang, and J.H. Barton. *Effects of extreme surface roughness on 3D printed horn antenna.* 2013. ELECTRONICS LETTERS, 49, No 12.

Grann, 2017. Helge Grann. *Personal guidance, Grundfos chief engineer, department of Mechanics and Materials.* 2017.

Grundfos, 2013. Grundfos. *Grundfos Pump CR10-04*, 2013. URL `http://www.lenntech.com/uploads/grundfos/96500982/Grundfos_CR-10-4-A-A-A-E-HQQE.pdf`. [Accessed 29-05-2017].

Grundfos, Blueprints, **2016**. *Grundfos, Blueprints*, 2016.

GRUNDFOS Management A/S, **2009**. GRUNDFOS Management A/S. *Mechanical shaft seals for pumps.* 2009. URL http://net.grundfos.com/doc/webnet/mining/_downloads/pump-handbook.pdf [Accessed 29-05-2017].

GRUNDFOS Management A/S, **2017**. GRUNDFOS Management A/S. *Pump Handbook.* 2017. URL http://net.grundfos.com/doc/webnet/mining/_downloads/pump-handbook.pdf [Accessed 29-05-2017].

Hariri, Hashemabadi, Noroozi, and Rostami, **2015**. S. Hariri, S.H. Hashemabadi, S. Noroozi, and A. Rostami. *Analysis of operational parameters, distorted flow and damaged blade effects on accuracy of industrial crude oil turbine flow meter by CFD techniques.* 2015. Journal of Petroleum Science and Engineering. 127, 318-328.

Kagermann, Wahlster, and Helbig, **2013**. Henning Kagermann, Wolfgang Wahlster, and Johannes Helbig. *Recommendations for implementing the strategic initiative INDUSTRIE 4.0*, 2013.

Ortiz, Rival, and Wood, **2015**. Xavier Ortiz, David Rival, and David Wood. *Forces and Moments on Flat Plates of Small Aspect Ratio with Application to PV Wind Loads and Small Wind Turbine Blades.* Energies 8(4), 2438-2453., 2015.

Patel and Ramakrishnan, **2017**. K. Patel and N. Ramakrishnan. *CFD Analysis of Mixed Flow Pump*, 2017. URL `http://www.ansys.com/-/media/Ansys/corporate/resourcelibrary/conference-paper/2006-Int-ANSYS-Conf-255.pdf[Accessed29-05-2017]`.

Salami, **1984**. L.A. Salami. *Effect of upstream velocity profile and integral flow straighteners on turbine flowmeters.* International Journal of Heat and Fluid Flow, 5(3), 155-165., 1984.

Shigley, Mischke, and Budynas, **2006**. Joseph Shigley, Charles Mischke, and Richard Budynas. *Mechanical Engineering Design.* Mc Graw Hill, 2006. ISBN 0-390-76487-6.

Stoltenkamp, **2007**. P. W. Stoltenkamp. *Dynamics of turbine flow meters*, 2007. URL `https://pure.tue.nl/ws/files/2444673/200710208.pdf[Accessed29-05-2017]`. Technische Universiteit Eindhoven DOI.

Tegtmeier, **2015**. Carl Tegtmeier. *CFD Analysis of Viscosity Effect on Turbine Flow Meter Performance and Calibration.* 2015. URL `http://trace.tennessee.edu/cgi/viewcontent.cgi?article=4195&context=utk_gradthes[Accessed29-05-2017]`. Master's thesis. Tennessee Research and Creative Exchange.

Thompson and Grey, **1967**. Richard Thompson and Jerry Grey. *Turbine Flowmeter Performance Model*, 1967. URL `http://www.dtic.mil/dtic/tr/fulltext/u2/825354.pdf[Accessed29-05-2017]`. Greyrad Corporation.

Thorn, **1998**. Richard Thorn. *The Measurement, Instrumentation and Sensors Handbook.* 1998. ISBN 9781439848838. Chapter 28.4 turbine and vane flowmeters.

ToolBox, **2017**. The Engineering ToolBox. *Converting Pump Head to Pressure and Vice Versa*, 2017. URL `http://www.engineeringtoolbox.com/pump-head-pressure-d_663.html[Accessed-29-05-2017]`.

Tools, **2017**. Airfoil Tools. *S1223*, 2017. URL `http://airfoiltools.com/airfoil/details?airfoil=s1223-il[Accessed-29-05-2017]`.

Torres, **2002**. Gabriel Torres. *Aerodynamics of Low Aspect Ratio Wings at Low Reynolds Numbers With Applications to Micro Air Vehicle Design.* 2002. Phd Thesis, University of Notre Dame.

Venkatesa, **2005**. Vasanta Ram Venkatesa. *Fluid Mechanics of Flow Metering.* 2005. ISBN 978-3-540-26725-6.

Wadlow, **1998**. David Wadlow. *The Measurement, Instrumentation and Sensors Handbook.* CRC Press, 1998. ISBN 9780849383472. Chapter 28.4 turbine and vane flowmeters.

Wagner and Kretzschmar, **2008**. Wolfgang Wagner and Hans-Joachim Kretzschmar. *International Steam Tables: Properties of Water and Steam Based on the Industrial Formulation IAPWS-IF97.* 2008.

Xu, **1992a**. Y. Xu. *A model for the prediction of turbine flowmeter performance.* ELSEVIER, 3, 37-43, 1992.

Xu, **1992b**. Y. Xu. *Calculation of the flow around turbine flowmeter blades.* ELSEVIER, 3, 25-35, 1992.

Yin, **2015**. C. Yin. *Computational Fluid Dynamics course, Aalborg University, Lecture slides.* 2015.

Zoheir, Shahrokh, and Hossein, **2014**. Saboohi Zoheir, Sorkhkhah Shahrokh, and Shakeri Hossein. *Developing a model for prediction of helical turbine flowmeter performance using CFD.* 2014. Elsevier. Flow Measurement and Instrumentation 42, 47-57.

List of Figures

List of Tables